The impact of oxygen exothermicity on energy quality of biofuels, and catalytic upgrading

by

Ryan David Merckel

Submitted in partial fulfilment of the requirements for the degree of Philosophiae Doctor in Chemical Engineering in the Faculty of Engineering, Built Environment and Information Technology, University of Pretoria

February 2020

Supervisor: Professor F.J.W.J. Labuschagne

Co-supervisor: Professor M.D. Heydenrych

“Before researchers become researchers, they should become philosophers.”

Masanobu Fukuoka

“Forests precede civilization and deserts follow them.”

François-René de Chateaubriand

Declaration

I declare that the thesis, which I hereby submit for the degree at the University of Pretoria, is my own work and has not previously been submitted by me for a degree at this or any other tertiary institution.

Signed:  14 May 2019

Ryan David Merckel

Abstract

The impact of oxygen exothermicity on energy quality of biofuels, and catalytic upgrading

Energy systems and products have always focused heavily on the fuel rather than the oxidant. That oxygen is the definitive factor in the exothermicity of combustion reactions rather than the fuel is demonstrated through the application of the principles governing classical thermodynamics. Through a rigorous analysis of the changes in bond (dissociation) energies undergone by each element during combustion for 359 fuels, it is observed that oxygen contributes more than $100\ \%$ towards the (net) higher heating value (HHV), with only a few exceptions. Hydrogen present in the fuel contributes only weakly to the HHV (with a maximum contribution of $\sim 16\ \%$). The oxidation of carbon typically consumes energy evolved during combustion, thereby contributing negatively to the HHV, and in a rare case has a maximum contribution of just $\sim 18\ \%$. These results suggest that the reduction half-reaction, rather than the oxidation half-reaction (concerning the fuel elements), is responsible for the exothermicity of the combustion reaction. An accurate one-parameter correlation for estimating the HHV as a function of the mass of oxygen consumed during combustion is derived from an approximation of the general thermodynamic relation, as $\Delta_c h^\circ|_{\mathrm{HHV}} = -13.87\ m_{\mathrm{O}_2} (\mathrm{MJ\ kg^{-1}})$. The constant is obtained from the simplification of a modifier function $\mu_{D_H} = -13.87\ e^{-0.092\omega_{\mathrm{O}_2}}\ (\mathrm{MJ\ kg^{-1}})$ in the equation $\Delta_c h^\circ|_{\mathrm{HHV}} = \mu_{D_H} m_{\mathrm{O}_2} - \Delta h_{\mathrm{vap}}\ (\mathrm{MJ\ kg^{-1}})$, which is a function of the mass fraction of oxygen consumed, ω_{O_2}. The resulting correlation of $\Delta_c h^\circ|_{\mathrm{HHV}} = -13.87\ m_{\mathrm{O}_2}$ performs well statistically when evaluated against $1\ 087$ fuel combustion data of wide chemical composition with a chemical formula of $\mathrm{C}_{\nu_\mathrm{C}}\mathrm{H}_{\nu_\mathrm{H}}\mathrm{O}_{\nu_\mathrm{O}}\mathrm{N}_{\nu_\mathrm{N}}\mathrm{S}_{\nu_\mathrm{S}}\mathrm{P}_{\nu_\mathrm{P}}$. For this correlation, a coefficient of determination of $R^2 = 0.981$, a root-mean-squared error of $\mathrm{RMSE} = 1.5\ \mathrm{MJ\ kg^{-1}}$ and a mean bias error of $\mathrm{MBE} = 1.8\ \%$ are achieved.

This pivotal contribution of oxygen to combustion exothermicity and the possibility that reduction half-reactions are, in general, exothermic may have serious repercussions for the biofuel arena, but also for electrochemical cell technologies and energy systems overall. As energy products, biofuels may be evaluated in terms of energy quality, in both their synthesis and upgradation. An expression for the change in energy quality, ΔE_Q, which occurs as a result

of the synthesis of biofuel from biomass or by the upgradation of biofuel, is derived mathematically as a function of the ratio of the mass of oxygen consumed for the product over the feed, as $\Delta E_{\mathrm{Q}} = \left(m_{\mathrm{O}_2}\big|_{\mathrm{product}}\right)/\left(m_{\mathrm{O}_2}\big|_{\mathrm{feed}}\right) - 1$. This equation implies that any improvement to energy quality must accompany an increase in the consumption of oxygen. This improvement is, however, limited as it has been found that the ΔE_{Q} of any system is bounded according to the expression $\Delta E_{\mathrm{Q}} = m_i/m_f - 1$, where m_i and m_f are the initial and final masses of combustible material. As a consequence, if $m_f = m_i$ (i.e. no change in m_i occurs), then no change in energy quality occurs, while $\Delta E_{\mathrm{Q}} \to \infty$ when $m_f \to 0$ in cases where the oxidation potential of m_i is increased. That is to say, reductions to mass yields that accompany improved oxidation potential result in increases in energy quality. Furthermore, an analysis of more than 16 million generated fuel data shows that maximising carbon mass yields limits the change in energy quality that is possible to $116\ \%$—a much higher value of ΔE_{Q} may be achieved if this metric is not adopted. These results contradict the *prima facie* objectives of increasing total and carbon-specific mass yields, which are applied to biofuel synthesis and upgradation, and especially with regard to the manufacture of pyrolysis oil.

Together with these aforementioned results, a novel technique of analysis comprising three methods is developed for use with the analytical technique of pyrolysis-GC/MS (py-GC/MS) which is well suited to the study of pyrolysis and catalytic upgradation of fast pyrolysis oils. These three methods use a graphically based approach whereby cumulative atomic ratios, calorific values and elemental masses are plotted against the cumulative masses for compounds characterized via py-GC/MS. This technique allows the accurate estimation of the atomic ratios, elemental compositions and calorific values of pyrolysis oils via linear extrapolation. Following the demonstration and validation of these three methods with the use of 19 sets of data from the literature, this technique is used in the evaluation of four catalysts, namely bentonite, zsm-5 zeolite, the oxide C2013 and the oxide M1213. The comparisons between uncatalyzed (neat) pyrolysis oil and catalysed pyrolysis oils are based on their ability to increase the calorific value and decrease the oxygen content of pyrolysis oil. These objectives were achieved (for *Eucalyptus grandis* as the feedstock) in the following order: neat pyrolysis oil ($-27.6\ \mathrm{MJ\ kg^{-1}}$ and $30.4\ \%$ oxygen) < zsm-5-catalyzed pyrolysis oil at $500\ ^{\circ}\mathrm{C}$ ($-29.1\ \mathrm{MJ\ kg^{-1}}$ and $28.2\ \%$ oxygen) < bentonite-catalysed pyrolysis oil ($-30.1\ \mathrm{MJ\ kg^{-1}}$ and $28.1\ \%$ oxygen) < C2013-catalysed pyrolysis oil ($-31.3\ \mathrm{MJ\ kg^{-1}}$ and

$24.9\ \%$ oxygen) < zsm-5-catalysed pyrolysis oil at $300\ °C$ ($-32.5\ MJ\ kg^{-1}$ and $23.5\ \%$ oxygen) < M1213-catalysed pyrolysis oil ($-39.1\ MJ\ kg^{-1}$ and $14.2\ \%$ oxygen).

The results presented in this thesis rely strongly on the revelation that oxygen contributes significantly to the chemistry of combustion, but this does not appear to be applicable solely to oxygen. Fluorine, too, seems to demonstrate a similar exothermicity when undergoing reduction. When combusted with methane, ethane, propane and butane, it is found to contribute $110.6\ \%$, $108.5\ \%$, $107.6\ \%$ and $107.2\ \%$ towards to the HHV, respectively. This finding warrants further investigations of other energy systems that follow similar chemical changes relating to redox chemistry.

Acknowledgements

I owe much gratitude to both my supervisors for their continued support and the significant contributions they have made, giving up much of their time and effort towards our research endeavours. Mike Heydenrych has been indispensable as a mentor throughout this research, and has played a crucial role in the contributions presented in this thesis. Johan Labuschagne has provided a strong foundation and much-needed guidance for this research, and his assistance in wrestling with the many difficulties encountered during this research is highly appreciated.

I thank Xandra van Heerden for her support and inspiration. She has taught me endurance and encouraged me to finish what I've started, and for this I am most grateful.

Many thanks are due to Dr Chu Watanabe and Professor Bruce Sithole for their assistance with the py-GC/MS data used in this thesis.

I am also grateful for the financial support provided by the Paper Manufacturers Association of South Africa.

I am most grateful to the Mälardalen Högskola for supplementing my academics. If it were not for my 3-month visit to the University, I doubt I would have come to some of the major breakthroughs presented in this thesis.

I am exceedingly blessed to have the love and support of Eduard Horak and his family. Their continued encouragement has helped me to accomplish what I would not have done alone.

I thank my mother for her continued support and guidance throughout my academic studies. Her love for me is ever enduring and never withheld. Even in the absence of my late father, she has maintained the drive in me to keep on pushing through.

My gratitude also extends to A. Shlain and K. Vettikatus who have brought me much joy and laughter. Their love and meaningful contributions have not gone unnoticed.

Contents

List of figures

List of figures appearing in the appendix

List of tables

Nomenclature

Symbol	Description	Units
A	Entity of matter	1
C-i	Stoichiometric carbon number	
$\Delta_{\mathrm{c}} D_H$	Massic bond dissociation combustion enthalpy	$\mathrm{MJ\ kg^{-1}}$
$\Delta_{\mathrm{c}} D_H^{\circ}$	Massic bond dissociation combustion enthalpy	$\mathrm{MJ\ kg^{-1}}$
$\Delta_{\mathrm{c}} H^{\circ}{}_m$	Standard molar combustion enthalpy	$\mathrm{MJ\ kmol^{-1}}$
$\Delta_{\mathrm{c}} h^{\circ}$	Standard massic combustion enthalpy	$\mathrm{MJ\ kg^{-1}}$
$\Delta_{\mathrm{c}} \bar{h}^{\circ}$	Mean standard massic combustion enthalpy	$\mathrm{MJ\ kg^{-1}}$
ΔE_{Q}	Change in energy quality	%
$D_{H,m}$	Molar bond dissociation enthalpy	$\mathrm{MJ\ kmol^{-1}}$
$\bar{D}^{\circ}{}_{H,m}$	Mean standard molar bond dissociation enthalpy	$\mathrm{MJ\ kmol^{-1}}$
$\Delta_r h^{\circ}$	Standard massic reaction enthalpy	$\mathrm{MJ\ kg^{-1}}$
$\Delta_{RS} h^{\circ}$	Standard massic resonance enthalpy	$\mathrm{MJ\ kg^{-1}}$
$\Delta_{\chi r} H_m^{\circ}$	Molar standard molar electronegativity enthalpy	$\mathrm{MJ\ kmol^{-1}}$
Δh_{vap}	Massic vaporisation enthalpy	$\mathrm{MJ\ kg^{-1}}$
$\Delta_{\mathrm{r}} U^{\circ}$	Standard internal energy	J
ϵ	Differential error	
e^-	Electron	
E_{Y}	Energy yield	%
f	Subscript denoting a final entity	
$\mathrm{H \cdots O}$	Intermolecular hydrogen bond	
i	(Lower) index of summation or an entity	
j	(Upper) index of summation or an entity	
k_i	Reaction rate coefficient for reaction of order n and m	$\mathrm{mol^{1-(m+n)}\ L^{(m+n)-1}\ s^{-1}}$
m	Mass quantity	kg
m_A	Mass quantity of entity A	kg
m_f	Final mass quantity	kg
m_{fuel}	Mass quantity of fuel	kg
m_i	Initial mass quantity	kg
M_i	Molar mass of entity i	$\mathrm{kg\ kmol^{-1}}$
$m_{\mathrm{O_2}}$	Mass quantity of diatomic oxygen	kg

Nomenclature continued

Symbol	Description	Units
m_p	Mass quantity of product	kg
m_{pc}	Mass quantity of carbon product	kg
m_v	Mass quantity of upgradation	kg
μ_{D_H}	Oxygenic changes in bond dissociation enthalpy contribution	MJ kg^{-1}
n	Amount of substance (for chemical notation)	mol
n	Upper bound of summation (for summation notation)	
n_{bonds}	Molar bond quantity	mol
n_{O_2}	Molar quantity of diatomic oxygen	mol
v	Stoichiometric entity	1
R^2	Coefficient of determination	
T	Temperature	K
Φ_{c}	Sub-totality of chemical energy associations	MJ kg^{-1}
x	Mole fraction	
x_i	Mole fraction of component i	
x_{fuel}	Mole fraction of fuel	
x_{O_2}	Mole fraction of diatomic oxygen	
χ_r	Electronegativity	J
ω_{i}	Mass fraction of component i	
ω_{fuel}	Mass fraction of fuel	
ω_{O_2}	Mass fraction of diatomic oxygen	
∞	Infinity	

Abbreviations

AE	– Absolute error
AN	– Acid number
BD	– Biodiesel
BM	– Biomass
BM-r	– Biomass region
HC	– Hydrocarbonaceous compounds
HHV	– Higher heating value
LHV	– Lower heating value
MBE	– Mean bias error
N-HC	– Nitrogenous hydrocarbonaceous compounds
RMSE	– Root-mean-square-error
SSE_{res}	– Residual sum of squares
SS_{total}	– Total sum of squares
TAN	– Total acid number

Chapter 1: Introduction

Humanity has depended on combustion processes since antiquity – the chemical process responsible for the release of thermal energy when a fuel burns in an oxidative atmosphere. Reminiscent of all other electrochemical reduction-oxidation half-reactions, combustion takes advantage of the weak bonds of diatomic oxygen, the second most abundant element in the atmosphere, as well as the most abundant element on Earth. Oxygen is crucial not only for combustion reactions, but also for the proper functioning of the biosphere. Oxygen by volume makes up 20.95 % of the air and is released continuously by the metabolic pathways of a plethora of biological entities (Liou, 2002) through the process of photosynthesis. Photosynthesis is a complex process that converts radiative energy to chemical energy, and progresses in two sequential stages, namely via the light-dependent reaction and the light-independent reaction. Van Niel was the first to describe the light-dependent reduction-oxidation half-reaction as (Whitmarsh & Govindjee, 1999)

$$2\mathrm{H_2A} + \mathrm{CO_2} + \mathrm{photons} \rightarrow 2\mathrm{A} + \mathrm{CH_2O} + \mathrm{H_2O} \qquad 1$$

where A is the electron acceptor, with his discovery predicting water to be the proton donor in vascular plants as it is oxidized to diatomic oxygen by the reaction

$$2\mathrm{H_2O} + \mathrm{CO_2} + \mathrm{photons} \rightarrow 2\mathrm{O} + \mathrm{CH_2O} + \mathrm{H_2O} \qquad 2$$

Water is key in capturing solar energy and storing this in the chemical bonds that make up all vascular plants. But less than 5 % of water taken up by the roots of plants is retained, the bulk being transpired into the atmosphere along with oxygen. For every 400 molecules of water transpired only one molecule of $\mathrm{CO_2}$ is gained. In fact, some mature rainforest trees are able to pump almost $1.2\ \mathrm{m^3 day^{-1}}$ of water into the atmosphere (McElrone, et al., 2013)! But the water lost cumulatively by systems of plants to the atmosphere is crucial for maintaining rainfall over the region (Makarieva & Gorshkov, 2010). Based on Equation 2, it may be hypothesized that the reduction of carbon is possible according to the reaction pathway

$$2\mathrm{H_2A} + \mathrm{CH_2O} + [\mathrm{energy}] \rightarrow 2\mathrm{A} + \mathrm{CH_4} + \mathrm{H_2O} \qquad 3$$

with a more general pathway proposed as

$$(n+1)\mathrm{H_2A} + n\mathrm{CH_2O} + n[\mathrm{energy}] \rightarrow 2n\mathrm{A} + \mathrm{C}_n\mathrm{H}_{2n+2} + n\mathrm{H_2O} \quad 4$$

Although there is no known reduction pathway that satisfies Equation 4 precisely, the outcomes of such a reaction nonetheless constitute the ideal goal of fuel manufacturing and refining technologies. One possibility is the oxidation of $\mathrm{H_2S}$ to elemental sulphur, where $\mathrm{A} = \mathrm{S}$ as

$$(n+1)\mathrm{H_2S} + n\mathrm{CH_2O} + n[\mathrm{energy}] \rightarrow (n+1)\mathrm{S} + \mathrm{C}_n\mathrm{H}_{2n+2} + n\mathrm{H_2O} \quad 5$$

An alternative mechanism would be the oxidation of a sulphide to its respective sulphate in an acidic environment according to the reaction

$$4\mathrm{H^+} + \frac{n}{4}\mathrm{S^{2-}} + n\mathrm{CH_2O} + [\mathrm{energy}] \rightarrow \mathrm{C}_n\mathrm{H}_{2n+2} + \frac{n}{4}\mathrm{SO_4^{2-}} + 2\mathrm{H^+} \quad 6$$

May et al. provide strong evidence that the conjugate anion $\mathrm{S^{2-}}$ does not exist in aqueous media (May, et al., 2018) and it is likely that Equation 6 is rather of the form

$$4\mathrm{H^+} + \frac{n}{4}\mathrm{HS^-} + n\mathrm{CH_2O} + [\mathrm{energy}] \rightarrow \mathrm{C}_n\mathrm{H}_{2n+2} + \frac{n}{4}\mathrm{SO_4^{2-}} + \left(\frac{n}{4}+2\right)\mathrm{H^+} \quad 7$$

A chemical looping system may be achieved by combining Equation 7 with an additional reaction of reduction for the sulphate ion, $\mathrm{SO_4^{2-}}$, where residual carbon produced out of the inefficiency of Equation 7 is, for instance, oxidized as

$$\frac{n}{4}\mathrm{SO_4^{2-}} + \frac{n}{4}\mathrm{M^+} + \frac{n}{2}\mathrm{C} \rightarrow \frac{n}{4}\mathrm{MS^-} + \frac{n}{2}\mathrm{CO_2} \quad 8$$

The chemical looping system represented by Equations 7 and 8 allows for the regeneration of the $\mathrm{HS^-}$ to be used once again as an oxidant in the reduction of the $\mathrm{CH_2O}$ species of Equation 7. Such chemical looping systems are in fact already employed in industry today. For example, the Kraft process of pulp and paper mills make use of recovery boilers to regenerate spent pulping chemicals, and simultaneously relies on the combustion of lignin-containing black liquor to provide carbon in a reducing atmosphere for Equation 8 to take place. Here, M represents the element sodium, Na, and facilitates the disintegration of the wood substrate into its fibrous component with black liquor as the by-product (Ek, et al., 2009).

This principle of using regenerative thermochemical looping systems in the manufacture of biofuels utilized in combustion processes mirrors the design of the catalytic systems that are now commonplace in thermochemical processing, and particularly in pyrolysis technologies. Pyrolysis is one of the four main thermochemical routes of biomass conversion and produces many value-adding chemical products and biofuels, as do the other routes of liquefaction, gasification and combustion (Bridgwater & Bridge, 1991). As a sustainable thermochemical conversion process, pyrolysis makes good use of the renewable sources of fixed carbon that biomass is able to capture photosynthetically. But with the aim of pyrolysis technologies to valorise biomass into more useful energy products comes many challenges. Biomass as a feedstock, especially woody biomass, contains a significant portion of oxygen in the form of oxygenated substituents such as carboxylic acids, hydroxyls, ethers and ketones (Bridgwater, 2012). This oxygen content adversely affects the properties of biofuels derived from woody biomass by increasing the corrosivity and instability of the biofuel (de Jong, 2014; Dayton, 2017; Zhang, et al., 2007). The presence of oxygen also reduces the oxidation potential of biofuels and therefore the calorific value is lowered. The ability to measure and predict the calorific value of biofuels plays a crucial part in the design, analysis and control of energy systems, and experimental methods are often the only reliable means of determining the calorific value. As this is not always possible, many indirect methods of approximation have been developed (Basu, 2010), but most correlations are only applicable to coal (Channiwala & Parikh, 2002). The empirical basis of most of these correlations does not provide an in-depth, theoretical understanding of the exothermicity of combustion, and how the energy output of combustion processes might be improved. The contributions of the elemental constituents of the fuel is simply assumed. Similarly, so are the objectives for the synthesis of pyrolysis oils, namely that oxygen presence needs to be reduced and the total mass yield and carbon yield need to be maximized. While the first objective is dealt with in the literature sufficiently, little to no definite validation and/or justification for the last two objectives can be determined following a thorough literature search. To be sure about what the outcomes of the pyrolysis process are (or should be) – specifically in the generation of renewable transportation fuels – more in-depth consideration is needed. Do we really know why the combustion of any typical fuel in oxygen results in the exothermicity we are so reliant on for our energy needs? Chapter 2 of this thesis revisits the fundamental principles that govern

combustion for the thermodynamic point of view, before focus is shifted back to pyrolysis, which is dealt with in further detail in Chapters 3 and 4 (Figure 1). Most conversion technologies utilizing fast pyrolysis as their basis make direct links between process improvements and the mass yields of products. The assumption that process improvement is a proportional function of mass yields is the justification used that results in R&D programmes aiming to achieve these improvements (Bridgwater & Grassi, 1991). But is this association between mass yields and process/product improvements justifiable? Borrowing from the theory developed in Chapter 2 of this thesis, this question is explored in more detail in Chapter 3, and alternatives to the approach currently adopted to enhance fuel are proposed.

The challenge in upgrading biofuels produced from complex biomass feedstocks such as lignocellulosic (i.e. woody) biomass, such as bio-crude and pyrolysis oil, has been met with several potential solutions for improving their modest performance as biofuels. Catalytic fast pyrolysis was already recognized early on as one such solution for bringing about the objectives of upgradation of these fuels: reduce the amount of oxygenates, increase the low calorific values, improve stability and viscosity, and decrease corrosivity (Stoikos, 1991). As the major products produced via pyrolysis and combustion are volatile fragments of their former feedstock, the analytical method of gas chromatography/mass spectrometry (GC/MS) is a powerful tool that can be used in the study of such thermochemical processes (Cizdziel & Chen, 2010). Chapter 4 is used to explore catalytic fast pyrolysis and, with the application of results from Chapters 2 and 3, develops a set of novel methods that enhance py-GC/MS analysis of catalytic pyrolysis processes. Figure 1 summarises the overall layout of this thesis.

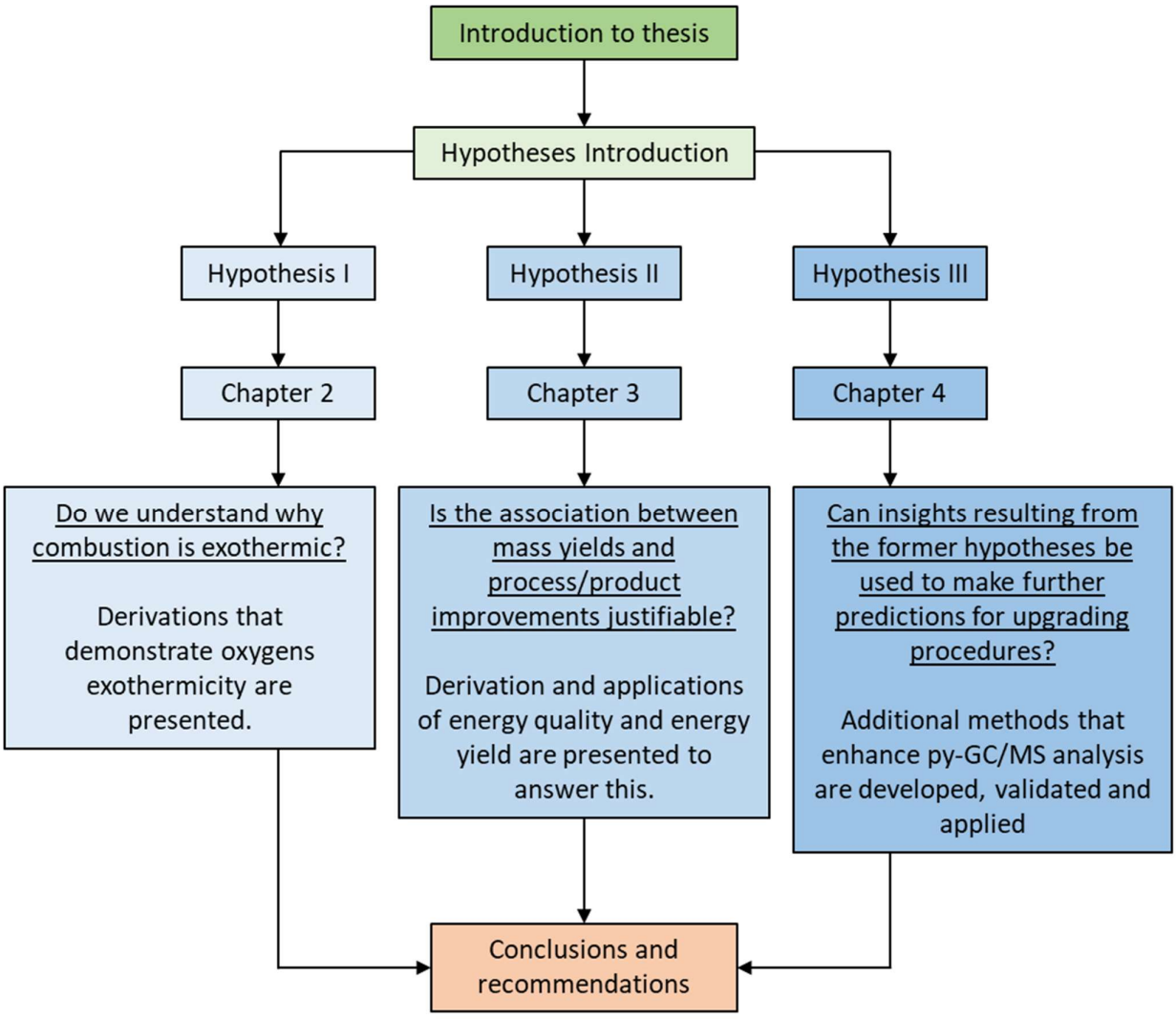

Figure 1: Logic diagram showing the layout of the thesis.

Chapter 2: Revisiting combustion thermodynamics

Oxygen consumption as the definitive factor in predicting heat of combustion

2.1. A brief history of combustion

Energy resources have been an indispensable part of our existence since their earliest discovery. With the onset of the Industrial Revolution in Britain during the 1800s, which subsequently spread to other coal-rich continental European countries (mainly Germany and France) and the United States, energy technologies and products saw vast improvements (Miller, 2004). It was also in the United States where the modern-day inception of the global "oil age" occurred, beginning around 1859 and lasting up until now (Giebelhaus, 2004). More recently the realisation that the abundance of fossil fuel reserves is finite has posed a serious risk to global energy security and has consequently encouraged the progression towards more renewable sources of energy which, in turn, rely on similarly renewable feedstocks such as biomass – the dominant energy form of antiquity (Chakraborty, et al., 2012). Although often cited as non-renewable, fossil fuels nevertheless found their genesis in the incomplete degradation of renewable biomass via reductive reaction pathways (Schobert, 2013). Associated with this is the oxidative pathway of combustion applied to biomass- and fossil fuel-related entities by which their energy potential is redeemed via the reaction with atmospheric oxygen. Combustion reactions are exothermic reduction-oxidation (redox) reactions (Lackner, 2011), and it is via these pathways of oxidation and reduction that we harness the energy from the energy stores that are fossil fuels, biomass, electrochemical fuel cells, and the like. Combustion of fossil fuels, however, also results in the release into and accumulation of CO_2 in the atmosphere, which exacerbates and has become synonymous with climate change; this is yet another reason for the need to adopt more sustainable energy practices.

The adoption of biomass-based energy technologies is not without its challenges. Realising the same degree of technological advancement as achieved with fossil fuels in the past is crucial for the successful implementation of these technologies (Chakraborty, et al., 2012; Yue, et al., 2014; Hassan & Kalam, 2013). Most notable is the high oxygen content present in terrestrial biomass feedstock, as cellulose, hemicellulose and lignin all comprise an

abundance of oxygenated substituents (as carboxylic acids, hydroxyls, ethers and ketones) (Bridgwater, 2012). The adverse effects of oxygenates present in biofuels derived from woody biomass are well documented. For example, the presence of carboxylic acids in pyrolysis oils (such as from the liberation of acetyl groups of xylan during thermochemical processing) increases their corrosivity and instability (de Jong, 2014; Dayton, 2017; Zhang, et al., 2007), and is quantified by either the total acid number (TAN) or the acid number (AN) of the fuel (Oasmaa, et al., 2010; Basu, 2010). Similarly, the oxygenates in biofuels impact negatively on their heating value by reducing the oxidation potential. Measurement and estimation of the higher heating value (HHV) of fuels are crucial during the first stages of fuel utilization and valorisation, in the design, analysis and control of energy systems, and in the efficient generation of heat and power on an industrial scale. Although experimental methods are the most reliable means of determining HHV, this is not always possible, and often requires indirect methods of approximation (Basu, 2010).

There have been many past attempts at correlating the heat of combustion of fuels with either the physical properties and composition of the fuel and/or the oxygen required for combustion, with most of these attempts being applicable to coal combustion. Dulong's correlation of 1880 (first published by Mott & Spooner in 1940) was perhaps one of the first empirical correlations available for estimating the HHV of coal (Mott & Spooner, 1940); it correlates HHV with the mass percentages of carbon, hydrogen, oxygen and sulphur in coal by means of correlation coefficients. Modified versions of this correlation were subsequently proposed (Strache & Lant, 1924; D'Huart, 1930), with the association of oxygen with carbon and hydrogen being considered (Steuer, 1926; Sumegi, 1939), and the effect of nitrogen being introduced (Dulong-Berthelot, in (Channiwala & Parikh, 2002)). Several more empirically derived correlations are available in the literature which make use of elemental analyses. These include nitrogen effects for coal (Gumz, 1938), assume specific associations of oxygen with carbon and hydrogen in coal (Mott & Spooner, 1940), and have more general applications such as for hydrocarbons (Boie, 1953), solid municipal waste (Khan & Abu-Gharah, 1991), wastewater sludges (Niessen, 2010) and pure organic compounds (Chang, 1979). Grabosky and Bain (1981) assumed that all elements constituting fuels are responsible for the HHV and came up with a correlation based on the elemental composition of C, H, S, and N (Mott & Spooner, 1940). Demirbaş *et al.* similarly propose a correlation for use with

lignocellulosic materials and make use of correlation coefficients close to the HHV for carbon and hydrogen, as well as the average bond dissociation enthalpy of oxygen (although it is unclear whether this was intended) and include nitrogen (Demirbas, et al., 1997), while the correlation by Beckman *et al.* (1990) is intended for use with biomass-derived oils (Channiwala & Parikh, 2002). There are further correlations that include thermodynamic considerations and heating values for various elements (Wilson, 1972) and bond dissociation enthalpies with respect to carbon (Vondracek, 1934). Channiwala and Parikh offer a more general correlation applicable over a wide range of gaseous, liquid and solid fuels, and provide an in-depth background on the development of most correlations discussed here (Channiwala & Parikh, 2002). A less popular approach is to correlate HHV proportional to oxygen consumed with combustion, while also considering the oxygen content of the fuel, but few correlations based on this approach are available in the literature (Channiwala & Parikh, 2002; Schmidt-Rohr, 2015).

The commonality of the aforementioned correlations, being mostly empirical, is in that they all fail to explain adequately the thermodynamic fundamentals of the combustion process. Attempts at applying certain concepts are made, such as using heats of formation (which are themselves mostly derived from heats of combustion), bond dissociation enthalpies and the association of atoms with each other. The matter is discussed in much detail by Schmidt-Rohr (Schmidt-Rohr, 2015), who demonstrates semi-quantitatively that the exothermicity of the combustion reaction is due to the weaker bonds in diatomic oxygen forming much stronger bonds in the combustion products of water and $\mathrm{CO_2}$, while bond changes of the fuels play only a minor role. Schmidt-Rohr further demonstrates the proportionality between HHV and oxygen consumed by correlating the lower heating value (LHV) of fuels on a mole basis (the linear relationship between the HHV and LHV is discussed later in Chapter 3), as $\Delta_c H^\circ_m\big|_{\mathrm{LHV}} = -418\, n_{\mathrm{O_2}}$ ($\mathrm{MJ\,kmol^{-1}}$) where $n_{\mathrm{O_2}}$ is the moles of oxygen required for combustion. The complexity of most fuel oils and the feedstock from which they are derived does not easily allow for the determination of these quantities on a molar basis. Nonetheless, the implication of this relationship is simple: the heat of combustion is directly proportional to the oxygen required by combustion, and the latter depends on the composition of the fuel. From a thermodynamic consideration, this implies that all reactants (i.e. fuel and oxidant) prescribe the thermochemical outcomes of combustion processes and are equivalent to the redox

reactions governing electrochemistry. It is therefore worth considering the mutual inclusiveness of oxygen and fuel with respect to the outcomes of the combustion process, and to consider the respective reduction and oxidation half-reactions. Doing so would provide further guidelines and insight into the development of biofuels to improve and enhance the energy quality required from them. Here, we define the energy quality of combustible substances as the quantity of energy released per unit of matter, on either a mass, mole or volume basis.

2.2. Thermodynamic derivation of heat of combustion

Consider the combustion of a fuel with the chemical formula $\mathrm{C}_{v_\mathrm{C}}\mathrm{H}_{v_\mathrm{H}}\mathrm{O}_{v_\mathrm{O}}\mathrm{N}_{v_\mathrm{N}}\mathrm{S}_{v_\mathrm{S}}\mathrm{P}_{v_\mathrm{P}}$ in oxygen, which is described by the reaction

$$\mathrm{C}_{v_\mathrm{C}}\mathrm{H}_{v_\mathrm{H}}\mathrm{O}_{v_\mathrm{O}}\mathrm{N}_{v_\mathrm{N}}\mathrm{S}_{v_\mathrm{S}}\mathrm{P}_{v_\mathrm{P}} + n_{\mathrm{O}_2}\mathrm{O}_2 \rightarrow v_\mathrm{C}\mathrm{CO}_2 + \frac{v_\mathrm{H}}{2}\mathrm{H}_2\mathrm{O} + \frac{v_\mathrm{N}}{2}\mathrm{N}_2\mathrm{O}_{v_i} + v_\mathrm{S}\mathrm{SO}_2 + \frac{v_\mathrm{P}}{2}\mathrm{P}_2\mathrm{O}_5 \qquad 9$$

where, based on $1\ \mathrm{mol}$ fuel, the oxygen required for combustion is

$$n_{\mathrm{O}_2} = v_\mathrm{C} + \frac{v_\mathrm{H}}{4} + \frac{v_i v_\mathrm{N}}{4} + v_\mathrm{S} + \frac{5v_\mathrm{P}}{4} - \frac{v_\mathrm{O}}{2} \qquad 10$$

The heat liberated by reaction 9 at standard conditions $\Delta_\mathrm{c}H_m^\circ$ may be evaluated with some degree of accuracy as the difference in the sum of bond dissociation enthalpies $D_{H,m}(j,T)$ of reactants and products:

$$\Delta_\mathrm{c}H^\circ{}_m \approx \sum_{i,\mathrm{reactants}} v_i \sum_j D_{H,m}(j,T) - \sum_{i,\mathrm{products}} v_i \sum_j D_{H,m}(j,T) \qquad 11$$

where $\sum_j D_{H,m}(j,T)$ represents all bond cleavages and formation j with respect to component i. In the case of H_2 combusting with O_2 according to the reaction

$$\mathrm{H}_2 + \frac{1}{2}\mathrm{O}_2 \rightarrow \mathrm{H}_2\mathrm{O} \qquad 12$$

$\Delta_\mathrm{c}H_m^\circ$ is calculated as

$$\Delta_{\mathrm{c}}H^{\circ}{}_{m} \approx D_{H,m}(\mathrm{H-H})_{\mathrm{H_2}} + n_{\mathrm{O_2}} D_{H,m}(\mathrm{O=O})_{\mathrm{O_2}} - 2\frac{\nu_{\mathrm{H}}}{2}\frac{2}{3}D_{H,m}(\mathrm{O-H})_{\mathrm{H_2O}} - 2\frac{\nu_{\mathrm{H}}}{2}\frac{1}{3}D_{H,m}(\mathrm{O-H})_{\mathrm{H_2O}} \quad 13$$

which assumes that the bond enthalpies are shared equally as electrostatic potentials between the respective atoms and that the product is in the vapour phase. A more accurate determination of the electrostatic potentials may be obtained by using electronegativity χ_r per atom to weight how the distribution of bond dissociation enthalpies occurs. By rearranging Equation 13, the total change in the bond dissociation energy with respect to the hydrogen species, $\Delta_c D_{H,m}(\mathrm{H})$, may be expressed as:

$$\Delta_{\mathrm{c}}D_{H,m}(\mathrm{H}) = D_{H,m}(\mathrm{H-H})_{\mathrm{H_2}} - 2\frac{\nu_{\mathrm{H}}}{2}\frac{2}{3}D_{H,m}(\mathrm{O-H})_{\mathrm{H_2O}} \quad 14$$

Evaluation of Equation 14 yields $\Delta_{\mathrm{c}}D_{H,m}(\mathrm{H}) = -180.0\ \mathrm{MJ\ kmol^{-1}}$. Similarly, for the oxygen species, $\Delta_{\mathrm{c}}D_{H,m}(\mathrm{O}) = -59.0\ \mathrm{MJ\ kmol^{-1}}$. Summation of $\Delta_c D_{H,m}(\mathrm{H})$ and $\Delta_{\mathrm{c}}D_{H,m}(\mathrm{O})$ yields $\Delta_{\mathrm{c}}H^{\circ}{}_{m}(\mathrm{H_2})\big|_{\mathrm{calc.,LVH}} \approx -239.0\ \mathrm{MJ\ kmol^{-1}}$. This value is close to the measured LHV of $\Delta_{\mathrm{c}}H^{\circ}{}_{m}(\mathrm{H_2})\big|_{\mathrm{meas.,LHV}} = -245.2\ \mathrm{MJ\ kmol^{-1}}$. The hydrogen bonding in the condensed product $(\mathrm{H_2O})$ is significant, being $16.4\ \%$ of the total HHV measured for hydrogen, at $\sim -46.7\ \mathrm{MJ\ kmol^{-1}}$. It just so happens that the difference between LHV and HHV is also $16.4\ \%$. If hydrogen bonding present in the product $n_{\mathrm{bonds}}(\mathrm{H\cdots O})\overline{D}^{\circ}{}_{H,m}(\mathrm{H\cdots O})\frac{\nu_{\mathrm{H}}}{2}$ is included in Equation 13, the HHV may be easily determined as $\Delta_{\mathrm{c}}H^{\circ}{}_{m}(\mathrm{H_2})\big|_{\mathrm{calc.,HHV}} = -285.7\ \mathrm{MJ\ kmol^{-1}}$, which is only $0.4\ \%$ larger than the measured HHV of $\Delta_{\mathrm{c}}H^{\circ}{}_{m}(\mathrm{H_2})\big|_{\mathrm{meas.,HHV}} = -284.6\ \mathrm{MJ\ kmol^{-1}}$. Similarly for the combustion of methane, where $\Delta_{\mathrm{c}}H^{\circ}{}_{m}(\mathrm{CH_4})\big|_{\mathrm{meas.,HHV}} = -890.7\ \mathrm{MJ\ kmol^{-1}}$, $\Delta_{\mathrm{c}}H^{\circ}{}_{m}(\mathrm{CH_4})\big|_{\mathrm{calc.}}$ may be determined by

$$\Delta_{\mathrm{c}}H^{\circ}{}_{m}(\mathrm{CH_4})\big|_{\mathrm{calc.}} = \Delta_{\mathrm{c}}D_{H,m}(\mathrm{C}) + \Delta_{\mathrm{c}}D_{H,m}(\mathrm{H}) + \Delta_{\mathrm{c}}D_{H,m}(\mathrm{O}) - \Delta_{\mathrm{c}}D_{H,m}(\mathrm{H\cdots O}) \quad 15$$

This gives $\Delta_{\mathrm{c}}H^{\circ}{}_{m}(\mathrm{CH_4})\big|_{\mathrm{calc.}} = -895.4\ \mathrm{MJ\ kmol^{-1}}$. When evaluating $\Delta_{\mathrm{c}}H^{\circ}{}_{m}(\mathrm{CH_4})\big|_{\mathrm{calc.}}$, it is realized that $\Delta_{\mathrm{c}}D_{H,m}(\mathrm{O}) = -729.0\ \mathrm{MJ\ kmol^{-1}}$, while $\Delta_{\mathrm{c}}D_{H,m}(\mathrm{fuel}) = -73.0\ \mathrm{MJ\ kmol^{-1}}$ [$\Delta_{\mathrm{c}}D_{H,m}(\mathrm{C}) = 23.0\ \mathrm{MJ\ kmol^{-1}}$ and $\Delta_{\mathrm{c}}D_{H,m}(\mathrm{H}) = -96.0\ \mathrm{MJ\ kmol^{-1}}$]. The heat liberated during methane combustion is therefore primarily due to oxygen being reduced to the combustion products $\mathrm{CO_2}$ and $\mathrm{H_2O}$ and accounts for $101.6\ \%$ of the total heat of combustion of methane on a mass basis. In fact, of the 359 fuels evaluated in this way (Schmidt-Rohr, 2015; Perry &

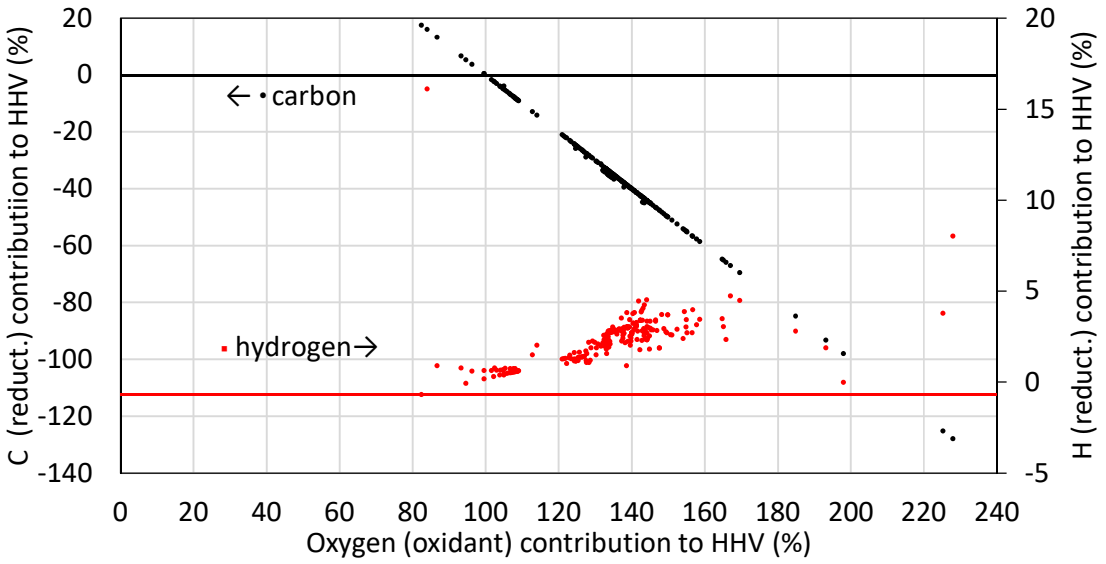

Figure 2: Comparison between the contribution of O_2 required for combustion, and C and H in fuel to $\Delta_\mathrm{c}h^\circ\big|_{\mathrm{calc.}}$.

Green, 2007), only 9 fuels (2.5 %, mass basis) had an oxygen contribution towards $\Delta_c h^\circ\big|_{\mathrm{calc.}}$ of less than 100 % (Figure 2). Some carbonaceous fuels for instance have changes in dissociation enthalpy of carbon that results in a negative contribution towards the heat of combustion of more than 100 %, while the contribution by hydrogen is only modest: from -2 % to 16 %.

By applying the rearrangement of Equation 15 to Equation 11 and dividing by the molar mass of fuel one obtains an expression that describes $\Delta_\mathrm{c}h^\circ$ on a mass basis:

$$\Delta_\mathrm{c}h^\circ\big|_{\mathrm{HHV}} = \Delta_\mathrm{c}D_H(\mathrm{fuel}) + \Delta_\mathrm{c}D_H(\mathrm{O}_2) - \Delta_\mathrm{c}D_H(\mathrm{H}\cdots\mathrm{O}) + \Delta_{RS}h^\circ \qquad 16$$

Here $\Delta_{RS}h^\circ$ represents resonance energies that may be significant depending on the bond configurations. It is helpful to consider the half-reactions related to the changes in bond enthalpies expressed in Equation 16. In the case of methane, the oxidation and reduction half-reactions are, respectively:

i. $\mathrm{C}^{4-} \rightarrow \mathrm{C}^{4+} + 8\mathrm{e}^-$ $\qquad (\Delta_r h^\circ = +23.0\,\mathrm{MJ\ kmol^{-1}})$

ii. $2\mathrm{O}_2 + 8\mathrm{e}^- \rightarrow 4\mathrm{O}^{2-}$ $\qquad (\Delta_r h^\circ = -729.0\ \mathrm{MJ\ kmol^{-1}})$

iii. $4\mathrm{H}^+ \rightarrow 4\mathrm{H}^+$ $\qquad (\Delta_r h^\circ = +91.2\ \mathrm{MJ\ kmol^{-1}})$

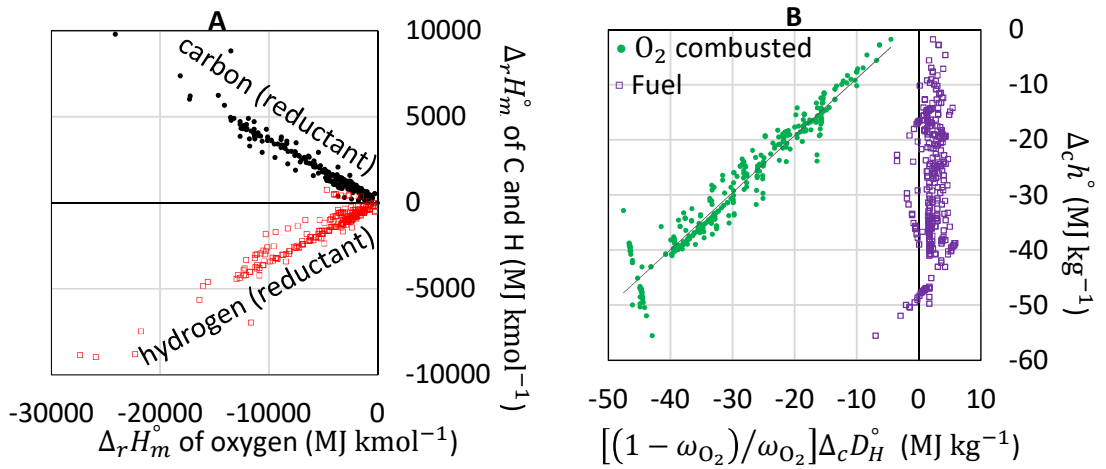

Figure 3: Comparison between the changes in dissociation enthalpies associated with the half-reactions undertaken by oxygen and fuel-based carbon and hydrogen (A), and plot of $\Delta_c h^\circ$ against $\frac{\omega_{O_2}}{\omega_{fuel}}\Delta_c D_H^\circ(O_2)$ and $\frac{\omega_{O_2}}{\omega_{fuel}}\Delta_c D_H^\circ(\text{fuel})$ (B).

Repetition of this exercise for all 359 data points analyzed shows that the reduction of oxygen always results in a negative (exothermic) change in bond dissociation enthalpy, while the oxidation of carbon almost always results in a positive (endothermic) change in bond dissociation enthalpy apart from three data points (Figure 3A).

This suggests that the reduction half-reaction resulting from the evolution of oxygen bonds during combustion is responsible for the liberation of heat during the combustion of fuels, while the oxidation half-reaction of carbon absorbs some of this energy, and thus the apparent gross heat of combustion $\Delta_c h^\circ|_{\text{HHV,gross}}$ would be interpreted mathematically as:

$$\Delta_c h^\circ|_{\text{HHV,gross}} = \left(\Delta_c h^\circ|_{\text{HHV,meas.}} - \Delta_c D_H(\text{fuel})\right) = \Delta_c D_H(O_2) - \Delta_c D_H(\text{H}\cdots\text{O}) + \Delta_{RS} h^\circ \quad 17$$

Although hydrogen does not change the oxidation state during methane combustion, the bond changes that it undergoes still release energy due to the differences in electronegativity χ_r between carbon and oxygen. This change in energy is easily determined from this associated electronegativity difference as $\Delta_{\chi_r} H_m^\circ = -405.5$ MJ kmol^{-1}, which is close to $\Delta_c D_{H,m}(\text{H}) = -402.0$ MJ kmol^{-1}. Because the electronegativity of carbon will always be lower than that of oxygen, the change in dissociation energy associated with this electronegativity difference will almost always be negative (exothermic) for hydrogen.

As combustion reactions are described on both an energy and mass basis, it is useful to rewrite Equation 16 by adding the mass ratio of fuel-to-oxidant in the following way:

$$\Delta_c h^\circ\big|_{\mathrm{HHV}} = \frac{m_{\mathrm{O_2}}}{m_{\mathrm{fuel}}}\left[\frac{m_{\mathrm{fuel}}}{m_{\mathrm{O_2}}}[\Delta_c D_H^*(\mathrm{fuel}) + \Phi_c] + \frac{m_{\mathrm{fuel}}}{m_{\mathrm{O_2}}}\Delta_c D_H(\mathrm{O_2})\right] - \Delta_c D_{H,m}(\mathrm{H\cdots O}) + \Delta_{RS} h^\circ \quad 18$$

or alternatively, if mass fractions are used instead, Equation 18 takes the form of:

$$\Delta_c h^\circ|_{\mathrm{HHV}} = \frac{\omega_{\mathrm{O_2}}}{1-\omega_{\mathrm{O_2}}}\left[\frac{1-\omega_{\mathrm{O_2}}}{\omega_{\mathrm{O_2}}}[\Delta_c D_H^*(\mathrm{fuel}) + \Phi_c] + \frac{1-\omega_{\mathrm{O_2}}}{\omega_{\mathrm{O_2}}}\Delta_c D_H(\mathrm{O_2})\right] - \Delta_c D_{H,m}(\mathrm{H\cdots O}) + \Delta_{RS} h^\circ \quad 19$$

Here additional energy associations such as differences in electronegativity are included in the term Φ_c (i.e. $\Delta_c D_H(\mathrm{fuel}) = \Delta_c D_H^*(\mathrm{fuel}) + \Phi_c$). As a completely theoretical determination of $\Delta_c h^\circ\big|_{\mathrm{meas.,HHV}}$, it is possible to achieve a high level of accuracy using Equation 19, but knowledge of all bond configurations, resonance enthalpies, as well as elemental composition is required with respect to the reactants. The usefulness of Equation 19 is therefore limited to those fuels for which these particulars are fully specified, and immediately disqualifies complex fuels such as coals and biomass-based energy products. A graphical examination of the first two terms on the right-hand side of Equation 19 when applied to 359 fuel data points suggests a strong linear correlation between $\Delta_c h^\circ\big|_{\mathrm{meas.,HHV}}$ and $\left[\left(1-\omega_{\mathrm{O_2}}\right)/\omega_{\mathrm{O_2}}\right]\Delta_c D_H(\mathrm{O_2})$ (Figure 3B). In comparison, the fuel term $\left[\left(1-\omega_{\mathrm{O_2}}\right)/\omega_{\mathrm{O_2}}\right]\Delta_c D_H(\mathrm{fuel})$ of Equation 19 results in an undefined gradient when correlated to $\Delta_c h^\circ\big|_{\mathrm{meas.,HHV}}$, as the former exhibits very little deviation for more or less all values of $\Delta_c h^\circ\big|_{\mathrm{meas.,HHV}}$ (also inferred indirectly from Figure 4B). This insight confirms again the extensive contribution of oxygen towards the heat liberation of combustion reactions (Figure 3B) and may be used in simplifying Equation 19 further. Figure 4A suggests that $\left[\left(1-\omega_{\mathrm{O_2}}\right)/\omega_{\mathrm{O_2}}\right]\Delta_c D_H(\mathrm{O_2})$ may be represented as a function of the mass fraction of oxygen required for combustion as:

$$\frac{1-\omega_{\mathrm{O_2}}}{\omega_{\mathrm{O_2}}}\Delta_c D_H(\mathrm{O_2}) \approx \mu_{D_H}\left(\omega_{\mathrm{O_2}}\right) = -13.87\, e^{-0.092\,\omega_{\mathrm{O_2}}} \quad \mathrm{MJ\ kg^{-1}} \quad 20$$

where the constants have been determined for 1087 fuel data points (Perry & Green, 2007; Domalski, 1972; de Soete, 1975; BCC, 1998; Demirbas, 2008; Demirbas, 1997; Jenkins, et al.,

1998; Garcia, et al., 2014; Grabolski, et al., 2003; Yuan, et al., 2004), (Lin, et al., 2009). Equation 20 is in principle a modifier function and substituted into Equation 19 yields:

$$\Delta_{\mathrm{c}}h^{\circ}\big|_{\mathrm{HHV}} = \frac{\omega_{\mathrm{O}_2}}{1-\omega_{\mathrm{O}_2}}\mu_{D_H} - \Delta h_{\mathrm{vap}} + \Delta_{RS}h^{\circ} = \mu_{D_H}m_{\mathrm{O}_2} - \Delta h_{\mathrm{vap}} + \Delta_{RS}h^{\circ} \qquad 21$$

which assumes $\Delta_{\mathrm{c}}h^{\circ}\big|_{\mathrm{HHV}}$ to be a function of ω_{O_2} only, and where $\Delta_{\mathrm{c}}D_{H,m}(\mathrm{H}\cdots\mathrm{O})$ is approximated by Δh_{vap}. This functionality becomes obvious when plotting $\Delta_{\mathrm{c}}h^{\circ}\big|_{\mathrm{meas.,HHV}}$ against ω_{O_2} (Figure 4A), and an equation similar to Equation 21 could have been obtained based on this observation where μ_{D_H} would take the form of some appropriate constant or variable. Taking the limits of $\Delta_{\mathrm{c}}h^{\circ}\big|_{\mathrm{HHV}}$ as $\omega_{\mathrm{O}_2} \to \{0;1\}$ yields the following results:

1. $\lim_{\omega_{\mathrm{O}_2}\to 0}\Delta_{\mathrm{c}}h^{\circ}\big|_{\mathrm{HHV}} = \lim_{\omega_{\mathrm{O}_2}\to 0}\left[\frac{\langle 0\rangle}{1-\langle 0\rangle}\left(-13.87\, e^{-0.092\langle 0\rangle}\right) - \Delta h_{\mathrm{vap}} + \Delta_{RS}h^{\circ}\right] = -\Delta h_{\mathrm{vap}} + \Delta_{RS}h^{\circ}$
2. $\lim_{\omega_{\mathrm{O}_2}\to 1}\Delta_{\mathrm{c}}h^{\circ}\big|_{\mathrm{HHV}} = \lim_{\omega_{\mathrm{O}_2}\to 1}\left[\frac{\langle 1\rangle}{1-\langle 1\rangle}\left(-13.87\, e^{-0.092\langle 1\rangle}\right) - \Delta h_{\mathrm{vap}} + \Delta_{RS}h^{\circ}\right] \to \infty$

In the first instance the fuel would not be able to participate in a combustion reaction since $\omega_{\mathrm{O}_2} = 0$ and since no reaction would take place without an oxidant $\lim_{\omega_{\mathrm{O}_2}\to 0}\Delta_{\mathrm{c}}h^{\circ}\big|_{\mathrm{HHV}} = 0$. This would be the case for substances that are either fully oxidised or in an inert state. The second limit $\omega_{\mathrm{O}_2} \to 1$ suggests that if an infinite amount of oxygen is required to combust an infinitesimally small quantity of fuel, the energy released would approach some infinite quantity. Between the limits of $0 < \omega_{\mathrm{O}_2} < 1$ the modifier function takes on values with the range $-13.87\ \mathrm{MJ\,kg^{-1}} < \mu_{D_H} < -12.65\ \mathrm{MJ\,kg^{-1}}$, and it is therefore possible to simplify Equation 21 even further through the substitution of μ_{D_H} by a constant value and still approximate $\Delta_{\mathrm{c}}h^{\circ}\big|_{\mathrm{HHV}}$ with some accuracy. This is not necessary, however, since Equation 21 requires only knowledge of the mass-fraction (or percentage) of oxygen consumed during combustion and may be used easily. Regardless, Equation 22 is the proposed simplification of Equation 21 assuming a constant value for μ_{D_H}:

$$\Delta_{\mathrm{c}}h^{\circ}\big|_{\mathrm{HHV}} = \frac{-13.87}{\omega_{\mathrm{O}_2}^{-1} - 1} + \Delta_{RS}h^{\circ} \qquad 22$$

which can be simplified by assuming $\Delta_{RS}h^{\circ}$ to be negligible (especially if this is not known) to:

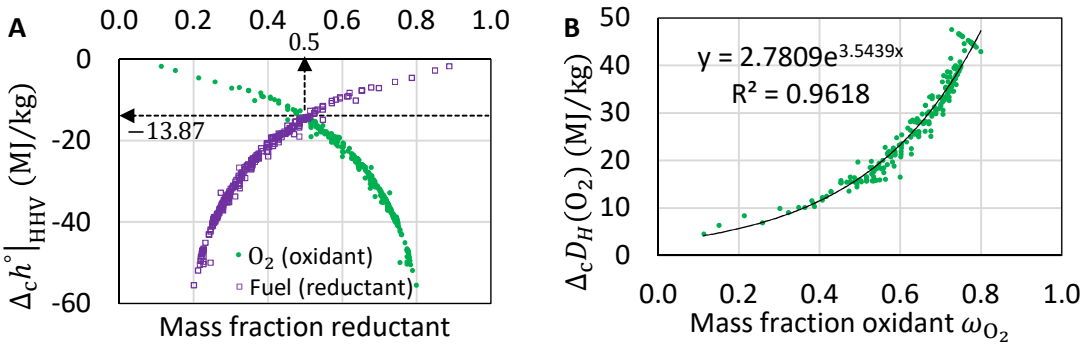

Figure 4: Association of ω_{O_2} with $\Delta_c h^\circ$ (A) and $\Delta_c D_H(O_2)$ (B), with $\Delta_c D_H(O_2) = -13.87$ MJ kg^{-1} at $\omega_{O_2} = \omega_{fuel}$ (A)

$$\Delta_c h^\circ|_{HHV} = \frac{-13.87}{\omega_{O_2}^{-1} - 1} = -13.87\, m_{O_2} \tag{23}$$

where the substitution of μ_{D_H} for -13.87 MJ kg^{-1} is the value obtained for $\Delta_c h^\circ|_{HHV}$ when $\omega_{O_2} = \omega_{fuel}$ as indicated by the dashed lines in Figure 4A.

2.3. Comparisons of correlations

Using conventional statistical methods, the accuracy of Equation 21 and Equation 23 may be validated and compared with previously proposed correlations found in the literature. The coefficient of determination (R^2), the mean bias error (MBE), and the root-mean-square error (RMSE) were used in this case, and computed respectively as follows:

$$R^2 = 1 - \frac{SSE_{res}}{SS_{total}} \tag{24}$$

$$\text{MBE (\%)} = \frac{1}{n}\sum_{i=1}^{n} \frac{\Delta_c h^\circ|_{HHV,calculated} - \Delta_c h^\circ|_{HHV,\ measured}}{\Delta_c h^\circ|_{HHV,\ measured}} \times 100\% \tag{25}$$

$$\text{RMSE} = \sqrt{\frac{1}{n}\sum_{i=1}^{n}\left(\Delta_c h^\circ|_{HHV,\ calculated} - \Delta_c h^\circ|_{HHV,\ measured}\right)^2} \tag{26}$$

where the residual sum of squares SSE_{res} and the total sum of squares SS_{total} are defined respectively as:

$$SSE_{\text{res}} = \sum_{i}^{n} (\Delta_{\text{c}} h^{\circ}\big|_{\text{HHV, calculated}} - \Delta_{\text{c}} h^{\circ}\big|_{\text{HHV, measured}})^2 \quad 27$$

$$SS_{\text{total}} = \sum_{i}^{n} [\Delta_{\text{c}} h^{\circ}\big|_{\text{HHV, calculated}} - \Delta_{\text{c}} \bar{h}^{\circ}\big|_{\text{HHV, measured}})]^2 \quad 28$$

The variances of $\Delta_{\text{c}} h^{\circ}\big|_{\text{HHV, calculated}}$ from $\Delta_{\text{c}} h^{\circ}\big|_{\text{HHV, measured}}$ with respect to Equations 19 and 21 show good replicability of $\Delta_{\text{c}} h^{\circ}\big|_{\text{HHV, measured}}$ based on their respective coefficients of determination, namely $R^2|_{\text{Eq.(9)}} = 0.996$ and $R^2|_{\text{Eq.(11)}} = 0.980$. This variance in $\Delta_{\text{c}} h^{\circ}\big|_{\text{HHV, calculated}}$ increases expectedly with the substitution of $\mu_{D_H} = -13.87\ \text{MJ kg}^{-1}$ of Equation 23, with $R^2|_{\text{Eq.(13)}} = 0.981$. The MBE (i.e. $2.8\ \%$) of Equation 19 is considerably greater in relation to Equation 23 than the other correlations evaluated (Table 1), possibly due to the inadequately defined energy term Φ_{c}. But the impracticality of Equation 19 even without fully defining Φ_c is obvious. Equation 19 only serves to develop the thermodynamic justifications used in the derivation of Equations 21 and 23. Equation 21 performs particularly well as a correlation, based on its MBE of $-0.2\ \%$ and RMSE of $1.5\ \text{MJ kg}^{-1}$ while Equation 23 does reasonably well compared with all other correlations evaluated with an MBE of $-1.8\ \%$ and RMSE of $1.5\ \text{MJ kg}^{-1}$.

The direct comparisons of Equations 19, 21 and 23 with $\Delta_{\text{c}} h^{\circ}\big|_{\text{HHV, measured}}$ are plotted graphically in Figure 5 around the line of symmetry $y = 1.0x$ with dashed trend lines indicating deviation boundaries of $\pm 5.0\ \%$, showing the slight increase in variance with each simplification from Equation 19 to Equation 23 (hydrogen not shown). Overall, Equation 21 offers an acceptable compromise between complexity, by defining the modifier function μ_{D_H}, and simplicity, by eliminating the need for fuel-based parameters such as elemental composition from the correlation. However, Equation 23 is far simpler and, except for the mean bias error, performs statistically as well as Equation 21. It should be mentioned here that the bias relates partly to deviations brought about by not accounting for Φ_{c}-related energies.

Table 1: Summary of statistical data for comparison between various correlations

	Statistical measures			Rank of statistical measures		
Correlation	**|MBE|**	**RMSE**	R^2	**|MBE|**	**RMSE**	R^2
Equation 19[a]	2.8	0.8	0.996	13	1	1
Equation 21[b]	0.2	1.5	0.980	3	3	3
Equation 23	1.8	1.5	0.981	8	2	2
(Boie, 1953)	0.1	1.8	0.972	1	7	7
(Strache & Lant, 1924)	0.9	1.7	0.973	6	5	5
(Mott & Spooner, 1940)	2.5	1.7	0.972	11	6	6
(Channiwala & Parikh, 2002)	0.3	1.9	0.968	4	10	10
(Zhu & Venderbosch, 2005)	0.3	1.9	0.968	4	10	10
(Gumz, 1938)	5.4	1.7	0.974	17	4	4
(D'Huart, 1930)	2.8	1.9	0.969	12	8	8
(Schuster, 1934)	2.2	2.0	0.964	9	11	11
(Demirbas, et al., 1997)	3.1	2.1	0.961	14	12	12
Dulong-Berthelot (Channiwala & Parikh, 2002)	1.6	3.1	0.915	7	17	17
(Vondracek, 1934)	5.0	2.2	0.954	15	13	14
(Schmidt-Rohr, 2015)	6.5	2.4	0.959	19	14	13
(Tillman, 1978)	0.1	6.9	0.574	2	22	22
(Beckman, et al., 1990)	5.6	2.8	0.931	18	15	15
(Grummel & Davis, 1933)	2.3	3.9	0.860	10	19	19
(IGT, 1978)	5.1	3.2	0.905	16	18	18
(Sumegi, 1939)	10.9	2.8	0.930	23	16	16
(Grabosky & Bain, 1981)	6.9	6.2	0.646	20	21	21
(Seyler, 1938)	7.9	4.7	0.798	22	20	20
(Jenkins & Ebeling, 1985)	7.9	7.6	0.481	21	23	23
(Niessen, 2010)	35.8	10.0	0.084	24	24	24

[a]The term Φ_c in this case was tedious to specify fully and was therefore not used here.

[b]Calculated using $\Delta_c D_{H,m}(\mathrm{H\cdots O})$ instead of Δh_{vap}.

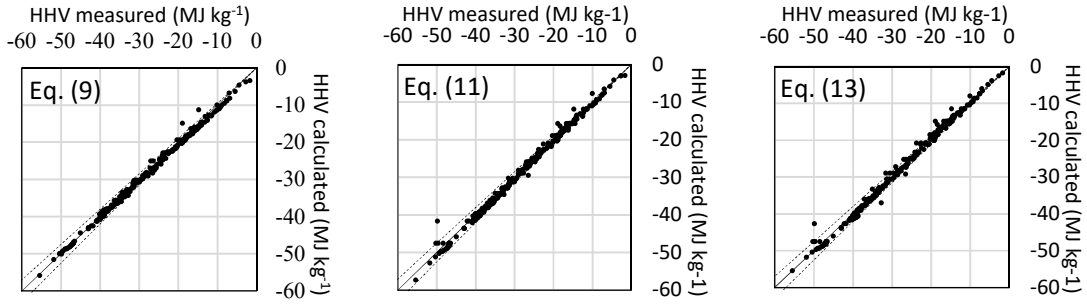

Figure 5: Comparison between calculated and measured $\Delta_c h^\circ\big|_{\mathrm{HHV}}$ using $1\,087$ data points, with dashed deviation boundaries of $\pm 5.0\ \%$

2.4. Implications of proposed correlations

It must be stressed that the significance of Equations 21 and 23 lies not simply in the statistical performance as demonstrated in Table 1, but also in the thermodynamic principles and implications that underlie their derivation. The chemical reduction of oxygen by a fuel as shown in Figure 3A results in heat being liberated, while the oxidation of carbon within the fuel conversely consumes some of this energy, resulting in a lowered heat of combustion. The role of oxygen in the combustion reaction is essential, in most cases contributing more than $100\ \%$ towards the heat of combustion (Figure 2), suggesting that the reduction half-reaction of oxygen is the principal reaction pathway responsible for the heat of combustion, rather than the oxidation half-reaction (pertaining to the fuel). Although hydrogen contributes to the heat of combustion only slightly compared with oxygen (Figure 2), because carbon is shown to reduce the heat of combustion, increasing the $\mathrm{H/C}$ ratio of fuel would result in enhanced energy quality. Coupled to this are the adverse effects of oxygenates on fuel properties, which cause increased acidity, hygroscopicity, polarity and instability in biofuels (Bridgwater, 2012; Dayton, 2017; Zhang, et al., 2007; Oasmaa, et al., 2010; Basu, 2010). Oxygenates hamper separation processes due to their inherent reactivity, making the separation of complex biofuel mixtures near to impossible.

The energy quality of fuel is also adversely affected by an increase in oxygenates and decrease in hydrogen content and can be demonstrated with the use of either Equation 21 or Equation 23. For example, using Equation 21 shows that increases in the $\mathrm{O/C}$ of the fuel from 0.0 to 2.0 decreases the HHV by $50.0\ \mathrm{MJ\ kg^{-1}}$ (demonstrated in Figure 6 by the carboxylic acid series),

which is synonymous with the increased oxidation of fuel. The same increase in the $\mathrm{H/C}$ ratio from 0.0 to 4.0 results in a comparatively modest increase in HHV of $22.7\ \mathrm{MJ\ kg^{-1}}$ (demonstrated by the n-alkane series, Figure 6). Increases in the oxygen content of carbon-rich fuel (with little to no hydrogen present), again by increasing the $\mathrm{O/C}$ from 0.0 to 2.0, results in a decrease in the HHV of $34.6\ \mathrm{MJ\ kg^{-1}}$(demonstrated by the carbon series, Figure 6). Considering all three examples in this figure, it is obvious that, in the case of fuels completely lacking in hydrogen, the energy quality would have an upper boundary at more or less the HHV of carbon, $\sim -33\ \mathrm{MJ\ kg^{-1}}$, and it is by increasing the hydrogen content that the highest energy quality may be achieved for a fuel. Although a second boundary pertaining to hydrogen is implied in Figure 6 by the dashed line of value $57.5\ \mathrm{MJ\ kg^{-1}}$, this boundary may be crossed by diatomic hydrogen and hydrogen-containing gaseous fuel mixtures. In the first example, the alteration to the HHV from $0.0\ \mathrm{MJ\ kg^{-1}}$ to $50.0\ \mathrm{MJ\ kg^{-1}}$ is due to decreased oxygen content by its dilution as a result of increased change length. Be aware that the sum of the changes in the HHV for examples 2 and 3 of $57.5\ \mathrm{MJ\ kg^{-1}}$ is more or less the same as for example 1 of $50.0\ \mathrm{MJ\ kg^{-1}}$. This implies that an HHV may be altered in a wider range by changing the oxygen content in the fuel, compared with changes in either carbon or hydrogen content alone.

Figure 6 shows that HHV is much more sensitive to oxygen-specific changes in the $\mathrm{O/C}$ for higher values of HHV, while sensitivity with respect to hydrogen- and carbon-specific changes in the $\mathrm{H/C}$ are less pronounced. Upgrading procedures for biofuels should therefore focus primarily on decreasing oxygen content via routes that are sacrificial towards carbon rather than hydrogen where possible. Catalysts used in upgrading of biofuels for example should be designed to reduce oxygen via decarboxylation and decarbonylation while supporting the hydrogenation of fuels for improved energy quality and stability. Upgrading routes that rely on hydrogenation of the fuel of biofuels similarly would support increases in energy quality although this may also invariably consume some of the valuable hydrogen via hydrodeoxygenation pathways.

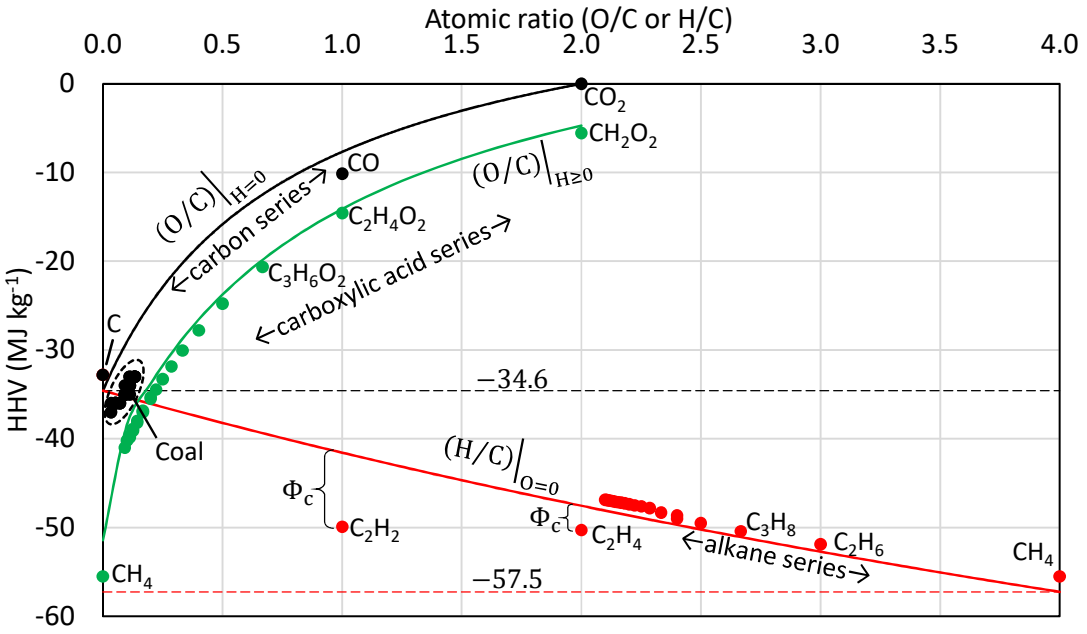

Figure 6: Changes in HHV with respect to changes in fuel atomic ratios O/C and H/C

In this chapter, only oxygen was considered as the oxidant in the combustion reactions analysed. If fluorine or other oxidants such as chlorine or bromine were to replace oxygen as the oxidant in these combustion reactions, it may be possible to determine whether the results of Figure 2 are only typical of oxygen or apply in general. A quick analysis of methane combusted with fluorine shows that fluorine (when using weighted averages in the calculations) contributes $110.6\ \%$ to the HHV, while carbon and hydrogen contribute negatively, at $-0.5\ \%$ and $-10.1\ \%$ respectively. Similarly, fluorine contributes $108.5\ \%$ for ethane, $107.6\ \%$ for propane, and $107.2\ \%$ for butane. If this trend continues for all fuels, and applies to all types of redox reactions, then it may very well be concluded that reduction half-reactions proceed exothermically while oxidation half-reactions proceed endothermically.

2.5. Summary

Up until now, the correlations available for approximating HHV of fuels have inadequately incorporated the thermodynamic fundamentals of the combustion process into their derivations. A correlation for estimating HHV accurately as a function of the mass fraction of oxygen consumed is presented. The correlation is a simplification of the equation derived using a theoretical and quantitative approach based on the reduction/oxidation half-

reactions of the combustion reaction. Although the theoretical equation is impractical to apply directly as is, the heat of combustion is found to be a strong function of changes in bond enthalpies with respect to the oxygen atom, while related changes with respect to the fuel elements have been shown to be comparatively insignificant. It is therefore possible to derive a modifier function $\mu_{D_H}(\omega_{O_2})$ that reduces complexity in the theoretical equation describing the heat of combustion. Since the modifier function is a function of the mass fraction of oxygen required for combustion only, it is possible to eliminate the prerequisite of specifying fuel-based parameters as coefficients in the resulting correlation. This implies that only the mass of fuel burnt, and the mass of oxygen consumed during the combustion reaction are necessary to estimate HHV. The coefficients used in the modifier function are determined from a set of 359 data points and may be adjusted for use with other types of data if need be. Variance in the modifier function between the limits of $\omega_{O_2} \rightarrow \{0; 1\}$ is shown to be small, and can be approximated by a constant, namely $\mu_{D_H} \approx -13.87\ \mathrm{MJ\ kg^{-1}}$. The strong correlation between the heat of combustion and mass of oxygen consumed implies that improvements in energy content of a fuel comes about by increasing the oxidation potential.

The correlation performs well statistically compared to similar correlations available in the literature. A set of 1 087 fuel data points with a wide range of chemical compositions based on the chemical formula of $C_{v_C}H_{v_H}O_{v_O}N_{v_N}S_{v_S}P_{v_P}$ is used for this comparison, and confirms the accuracy of most correlations including the one proposed here. Both equations using the modifier function and substitution of the modifier with a constant perform well statistically when compared to similar correlations from the literature. Since the proposed correlation is derived using a thermodynamic approach that describes the heat of combustion, it is possible to quantify the effects of fuel composition and oxygen consumption on the energy quality of biofuels. The HHV is found to be much more sensitive to changes in the oxygen content in the fuel compared to similar changes in the carbon and hydrogen content, but the hydrogen content enhances energy quality much more than the carbon content. Therefore, reduction of oxygen content in the fuel via deoxygenation pathways such as decarboxylation and decarbonylation is recommended over routes that sacrifice hydrogen (such as hydrodeoxygenation and dehydrogenation) where energy quality is a concern. As the correlation has been applied successfully to fuels containing other elements (i.e. sulphur, nitrogen, and phosphorus), and shows no deviation from trends pertaining to hydrogen and

carbon, these same results may hold for other elements too. Looking into other types of oxidants such as fluorine may provide further insight into the development of energy products. Most importantly, if the same results hold true for all oxidants, then it may be that reduction is responsible for the exothermicity observed in these types of chemical reactions and may affect the way in which electrochemistry is applied to energy systems in future.

Chapter 3: Fundamental principles of fuel enhancement

Determination and quantification of the objectives of upgrading processes

3.1. Introductory concepts of upgrading fuels

The phenomenon of pyrolysis occurs at elevated temperatures in oxygen-deplete environments, and can be induced for a wide range of temperatures and pressures. biomass typically undergoes a thermochemical conversion and typically occurs in a temperature range of between 300 °C and 600 °C (Panwar, et al., 2019). The carbonization of biomass, which constitutes slow pyrolysis, is achieved at temperatures of around 400 °C with heating rates of up to 50 °C s^{-1} and long residence times of hours to weeks. This conversion technology is typically used for the production of biochar, typically at a 35 % yield, and produces a similar amount of synthesis gas as well as some pyrolysis oil (at 30 %). Intermediate and fast pyrolysis processes aim to reduce conversion to biochar and synthesis gas in favour of pyrolysis oil. Fast pyrolysis is particularly is optimised for pyrolysis oil production, with liquid fraction yields as high as 75 %. This is achieved with fast heating rates of up to 500 °C s^{-1}, short residence times of around 0.5-2.0 s, and pyrolysis temperatures of between 400 °C and 600 °C (Schmitt, et al., 2019). Flash pyrolysis is similar to fast pyrolysis in terms of operating temperatures but uses extremely high heating rates greater than 1000 °C s^{-1} and even shorter residence times of less than 0.5 s. These conditions can achieve higher pyrolysis oil yields still, of around 75 % to 80 % (Puig-Arnavat, et al., 2019).

This flexibility of pyrolysis processes is however outweighed by other challenges due to the high diversity of biomass feedstock and the adverse physicals properties with regards to pyrolysis oils. Pyrolysis oils are highly reactive and unstable due to the polar, oxygenated nature of its constituents, and can even undergo aging when stored at room temperature (Sharifzadeh, et al., 2019). The low quality of pyrolysis oils has led to a concerted emphasis in developing feasible upgrading technologies, with the general consensus that the reduction of oxygenates in pyrolysis oils is essential in order for pyrolysis oils to be integrated effectively into the existing transportation fuel infrastructure (Czernik & Bridgwater, 2007; Wright, et al., 2010; Elliott, 2007). This defines the main objective of upgrading technologies applied to fast pyrolysis. The three dominating technologies used over the years to upgrade pyrolysis oils via

deoxygenation have been hydrotreating, zeolite-based catalytic conversion routes, and aqueous-phase processing (Serrano-Ruiz & Dumesic, 2012; Si, et al., 2017; Mortensen, et al., 2011). Coupled to this upgrading strategy of deoxygenation is the secondary objective of achieving favourable mass yields, which is based on the "yield metric" that governs performance targets of most chemical processes (Moran, et al., 2017). A third major objective cited in the literature is that of maximizing the energy yield and aims to conserve the energy balance of the process and its products (Wasiak & Orynycz, 2017; Liska & Cassman, 2008). These three objectives are used to measure the conversion efficiency of biomass to pyrolysis products. The objectives of upgrading technologies are thus threefold:

1. Reduce the presence of oxygenates in pyrolysis oils
2. Maximise mass yields, based on either:
    a. total oil yields, or
    b. carbon yields.
3. Maximize energy yields.

It is unclear when the objective of maximizing carbon yields was first adopted as a metric for evaluating the outcomes of pyrolysis upgrading technologies. A thorough literature search for either a direct validation and/or justification of its appropriateness as an objective is no more than a futile exercise. Any evidence of its validity is instead replaced by its frequent use as a means of evaluating the efficacy of converting biomass to biofuels. The appeal of using a carbon-based yield metric seems to be multifaceted:

- The objective of maximizing carbon yields is in support of the "green chemistry" perspective as a means of using renewable sources of carbon, sequestrating carbon, and limiting CO_2 emissions (Lapkin & Constable, 2008).
- Carbon forms the backbone of biomass-derived organic molecules and contributes the most to the mass yield compared to hydrogen.
- The concept of a carbon yield is used in other areas such as in the petroleum and pharmaceutical industries (Harrison, et al., 1980; Constable, et al., 2002).
- Utilization of all components of biomass may maximize profits, where carbon is the major contributor by mass (Chisti, 2007).

As the value of biofuels lies explicitly in their use as commodities of energy, the primary objective governing their manufacture and refining should also reflect this. Clearly, as was concluded in Chapter 2, the energy value and level of oxidation of a fuel, as well as the physical properties of the feedstock from which it is produced, go hand-in-hand to limit its calorific

potential and decreases the overall value of fuel as an energy product. For instance, if a feedstock with an HHV of $-18.0\ \mathrm{MJ\ kg^{-1}}$ produces a biochar consisting of pure carbon with an inherent HHV of $-32.8\ \mathrm{MJ\ kg^{-1}}$ (NIST, n.d.), any pyrolysis oil and syngas produced would collectively have a much lower heating value than both the feedstock and the biochar. The calorific value of either the pyrolysis oil or the gas may however be increased, where the calorific value of either is inversely proportional to how much oxygen *and* mass are apportioned to each. The following example illustrates this point further:

> If $100\ \mathrm{kg}$ of biomass (composed entirely of carbon, hydrogen and oxygen) with an HHV of $-18.0\ \mathrm{MJ\ kg^{-1}}$ produces $25\ \mathrm{kg}$ of char consisting of pure carbon, the total remaining mass of $75\ \mathrm{kg}$ would acquire an HHV of only $-13.1\ \mathrm{MJ\ kg^{-1}}$ if no additional energy is added. If pyrolysis oil with an HHV of $-18.0\ \mathrm{MJ\ kg^{-1}}$ is produced alongside this char, its mass must be no more than $54\ \mathrm{kg}$ with no energy reporting to the gas—in other words, the (dry) gaseous product would consist solely of CO_2, rather than CO, H_2, CH_4, etc. If the same gaseous product is produced, and less mass reports to the pyrolysis oil, the HHV of the pyrolysis oil would increase accordingly: for $30\ \mathrm{kg}$ of pyrolysis oil produced, an HHV of $-32.7\ \mathrm{MJ\ kg^{-1}}$ would be achieved, while $25\ \mathrm{kg}$ of pyrolysis oil would have an HHV of $-39.2\ \mathrm{MJ\ kg^{-1}}$. Conversely, a fully oxygenated liquid product would have no energy content (consisting solely of water) with all the energy from the feedstock reporting solely to the syngas (now containing less oxygenated compounds). The total amount of CO_2 and H_2O is of course limited to the amount of oxygen available, and further limits how much mass of energy-rich pyrolysis oil or gas could be produced.

The example above introduces some of the mechanisms by which energy entering the pyrolysis process via the feedstock may be apportioned to and concentrated within each of the products. The mechanism of fuel deoxygenation is based on removing oxygen from the fuel product as either H_2O, CO or CO_2. This concept may also be viewed in another way: the amount of oxygen with which the fuel will react during combustion is being increased. This may be achieved by either reducing the oxygen already present in the fuel, or diluting the oxygen by the addition of groups that would react with oxygen. A practical example of this is the addition of $–CH_2–$ to methanoic acid until decanoic acid is obtained. Each addition of

–CH_2– to methanoic acid dilutes the carboxyl group, and results in an increase in HHV, from $-5.5\ \mathrm{MJ\ kg^{-1}}$ for methanoic acid to $-35.5\ \mathrm{MJ\ kg^{-1}}$ for decanoic acid (Table 2). A similar increase in the HHV is achieved with additions of –CH_2– to methanal, where the HHV increases from $-18.9\ \mathrm{MJ\ kg^{-1}}$ for methanal to $-40.7\ \mathrm{MJ\ kg^{-1}}$ for decanal. The second mechanism for increasing energy quality is based on producing a fuel that can consume the highest possible amount of oxygen per mass of fuel combusted, not by removing oxygenates present in the fuel but by increasing the ratio of mass of oxygen consumed per mass of fuel. For instance, combustion of $1\ \mathrm{kg}$ of oxygen requires $0.25\ \mathrm{kg}$ methane with $13.9\ \mathrm{MJ}$ of energy released, whereas $0.29\ \mathrm{kg}$ of decane is required and releases $13.6\ \mathrm{MJ}$ of energy. The reason for this is that 3.0 times more carbon than hydrogen is required to consume one kilogram of oxygen, so fuels with higher hydrogen to carbon content consume more oxygen per mass of fuel. In other words, where $0.13\ \mathrm{kg}$ of hydrogen is required and releases a total of $17.8\ \mathrm{MJ}$ per kg oxygen consumed, $0.38\ \mathrm{kg}$ of carbon is required per kg of oxygen and releases $12.3\ \mathrm{MJ}$. Table 2 summarises the data for these three series of fuels and shows the effect that decreasing the oxygen content or increasing the hydrogen content of fuels has on their respective calorific values.

Table 2: Effect of oxygen and hydrogen content on the calorific value of fuels

Series	Data type	C-1	C-2	C-3	C-4	C-5	C-6	C-7	C-8	C-9	C-10
Alkanes:	HHV ($\mathrm{MJ\ kg^{-1}}$)	−55.5	−51.9	−50.4	−49.5	−49.0	−48.3	−47.8	−47.6	−47.5	−47.4
	O (mass %)	0.0	0.0	0.0	0.0	0.0	0.0	0.0	0.0	0.0	0.0
	H (mass %)	25.1	20.1	18.3	17.3	16.8	16.4	16.1	15.9	15.7	15.6
	C (mass %)	74.9	79.9	81.7	82.7	83.2	83.6	83.9	84.1	84.3	84.4
Aldehydes:	HHV ($\mathrm{MJ\ kg^{-1}}$)	−18.9	−26.9	−31.1	−34.2	−36.1	−37.6	−38.7	−39.5	−40.2	−40.7
	O (mass %)	53.3	36.3	27.5	22.2	18.6	16.0	14.0	12.5	11.2	10.2
	H (mass %)	6.7	9.2	10.4	11.2	11.7	12.1	12.4	12.6	12.8	12.9
	C (mass %)	40.0	54.5	62.0	66.6	69.7	72.0	73.6	74.9	76.0	76.9
Carboxylic acids:	HHV ($\mathrm{MJ\ kg^{-1}}$)	−5.5	−14.6	−20.6	−24.8	−27.8	−30.1	−31.8	−33.3	−34.5	−35.5
	O (mass %)	69.5	53.3	43.2	36.3	31.3	27.5	24.6	22.2	20.2	18.6
	H (mass %)	4.4	6.7	8.2	9.2	9.9	10.4	10.8	11.2	11.5	11.7
	C (mass %)	26.1	40.0	48.6	54.5	58.8	62.0	64.6	66.6	68.3	69.7

It should be realised that the carbon yield and its relation to the efficacy of converting biomass to biofuels has nowhere been implied by the preceding analysis. Although increases in the mass percentage of carbon do coincide with increases in calorific value for the aldehyde and carboxylic acid series in Table 2, the opposite trend is observed for the alkane series. The difference in trends is due to the presence of oxygen in the aldehyde and carboxylic series and its absence from the alkane series. The following example illustrates why the notion of a carbon yield metric is inadequate for evaluating the conversion efficacy of biomass-to-biofuel processes:

> Assume $100\ \mathrm{kg}$ of a biomass feedstock with a molecular proportionality of $\mathrm{C_{1.0}H_{2.0}O_{0.6}}$ and an HHV of $-21.1\ \mathrm{MJ\ kg^{-1}}$ produces a fully deoxygenated biofuel. The total energy in the biomass is therefore $2\ 110\ \mathrm{MJ}$. The maximum carbon yield of $88.0\ \%$ is achieved by depleting all the hydrogen so as to remove oxygen as water before carbon is used to remove the remaining oxygen as CO_2. The resulting HHV of the product is that of pure carbon, namely $-32.8\ \mathrm{MJ\ kg^{-1}}$. The total energy in this product is $1\ 443\ \mathrm{MJ}$, which relates to an energy yield of $68\ \%$. If only carbon is used to remove oxygen from the product as CO_2, a lower carbon yield is achieved of $68.8\ \%$. However, the HHV has increased to $-48.1\ \mathrm{MJ\ kg^{-1}}$. The total energy in this product is $2\ 057\ \mathrm{MJ}$ and relates to an energy yield of $97\ \%$.

Evidently in this example, a lower carbon yield gives rise to an increase in energy yield. As biofuel is an energy product, it would be more reasonable to apply an objective that maximizes the energy yield rather than the mass yield. This concept will be revisited in a later section.

3.2. Graphical analyses of upgrading principles

It is useful to visualize the various mechanisms used in upgrading fuels by plotting these as tie lines on a ternary diagram together with the elemental composition of the range of fuels and feedstocks being investigated. Figure 7 is one such plot representing data on a molar basis, and includes 327 data points of hydrocarbons (including oxygenated hydrocarbons, hydrogen and carbon monoxide), and nitrogenous compounds (Perry & Green, 2007), various grades of coal (British Coal Corporation, 1998; Demirbas, 2008; Directorate: Mineral Economics, 2005), a diverse range of biomass (Channiwala & Parikh, 2002; Demirbas, 1997; Jenkins, et al., 1998;

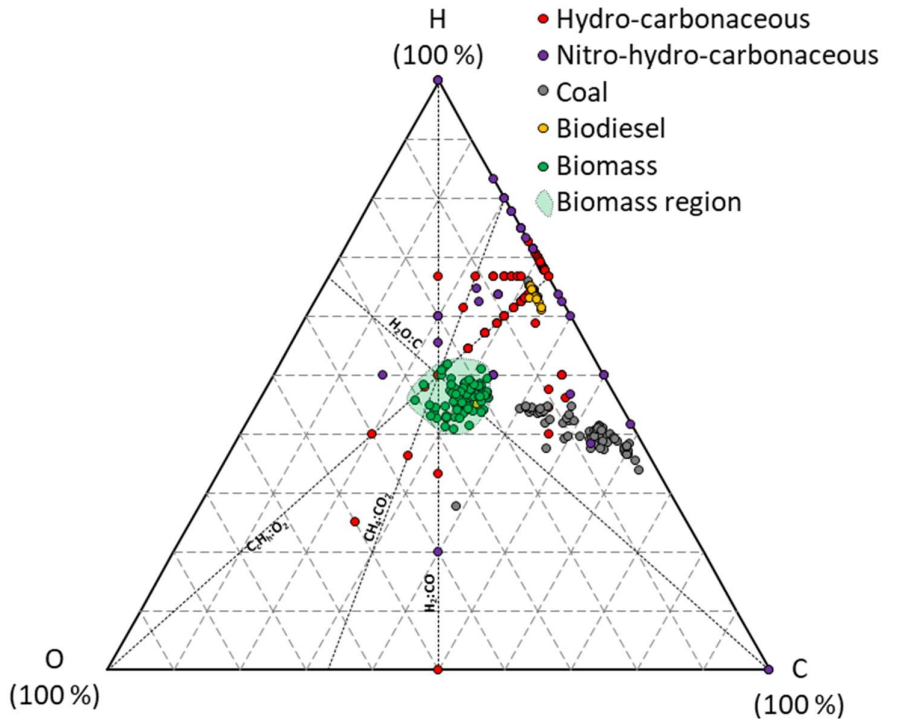

Figure 7: Ternary plot of various feedstock and fuels on a mole basis

Garcia, et al., 2014)and biodiesel (Grabolski, et al., 2003; Yuan, et al., 2004; Lin, et al., 2009). Four tie lines are included in Figure 7, namely:

- water-carbon tie line: $\mathrm{H_2O} \leftrightarrow \mathrm{C}$
- hydrocarbon-oxygen tie line: $\mathrm{C}_{v_\mathrm{C}}\mathrm{H}_{v_\mathrm{H}} \leftrightarrow \mathrm{O_2}$
- methane-carbon dioxide tie line: $\mathrm{CH_4} \leftrightarrow \mathrm{CO_2}$
- hydrogen-carbon monoxide tie line: $\mathrm{H_2} \leftrightarrow \mathrm{CO}$

The biomass data points in Figure 7 form a circular cluster through which all four tie lines cross and makes biomass particularly useful as a feedstock for generating the other compounds that radiate outwards from the intercept of the four tie lines. Of particular interest are the unoxygenated hydrocarbons that are liquids at ambient temperature, seen in Figure 7 as a red band lying on and located between where the $\mathrm{C}_{v_\mathrm{C}}\mathrm{H}_{v_\mathrm{H}} \leftrightarrow \mathrm{O_2}$ and the $\mathrm{CH_4} \leftrightarrow \mathrm{CO_2}$ tie lines meet the $\mathrm{H} - \mathrm{C}$ axis. Theoretically, by removing oxygen in the form of $\mathrm{CO_2}$ from a cellulosic feedstock, with a molecular formula of $(\mathrm{C_6H_{10}O_5})_n$, a hydro-carbonaceous product close to this group of hydrocarbons could supposedly be produced according to the reaction pathway:

$$n\mathrm{C_6H_{10}O_5} \rightarrow \frac{5n}{2}\mathrm{CO_2} + n\mathrm{C_{3.5}H_{10}}$$

where $n\mathrm{C_{3.5}H_{10}}$ $(\mathrm{H/C} = 2.9)$ represents the overall molecular formula of some mixture of gaseous hydrocarbons between ethane $(\mathrm{H/C} = 3.0)$ and propane $(\mathrm{H/C} = 2.7)$. If oxygen could be removed as pure $\mathrm{O_2}$ instead during pyrolysis, then cellulose, could be used to produce a hydrocarbon product of higher order that lies within this hydrocarbon group:

$$n\mathrm{C_6H_{10}O_5} \rightarrow \frac{5n}{2}\mathrm{O_2} + n\mathrm{C_6H_{10}}$$

where $n\mathrm{C_6H_{10}}$ could be an array of compounds, such as cyclohexene, 1,5-hexadiene, methylcyclopentene, or a complex mixture of more than 100 entities. It is highly improbable that only one or two of the reaction pathways described by the four tie lines would be utilized during the pyrolysis process, based on the complexity of pyrolysis oil, synthesis gas and biochar produced (Bridgwater, 2012; Dickerson & Soria, 2013; Zhang, et al., 2007; Patwardhan, et al., 2011). Nevertheless, each type of product is associated with a particular region on the ternary plot, which is bounded by pairs of tie lines in which many more tie lines can occur, depending on the types of compounds and reactions involved. Reaction pathways for the production of synthesis gas are located within a region bounded by the $\mathrm{H_2} \leftrightarrow \mathrm{CO}$ and $\mathrm{CH_4} \leftrightarrow \mathrm{CO_2}$ tie lines (Figure 8A) with the $\mathrm{CH_4} \leftrightarrow \mathrm{CO_2}$ and $\mathrm{C}_{v_\mathrm{C}}\mathrm{H}_{v_\mathrm{H}} \leftrightarrow \mathrm{O_2}$ tie lines forming the boundary for optimal fuel oil production (Figure 8B), and the $\mathrm{H_2O} \leftrightarrow \mathrm{C}$ and $\mathrm{C}_{v_\mathrm{C}}\mathrm{H}_{v_\mathrm{H}} \leftrightarrow \mathrm{O_2}$ tie lines forming the boundary for optimal biochar production (Figure 8C). The typical region associated with the production of pyrolysis oil is shown in the last plot of Figure 8D shaded in green.

At first, this graphical analysis of the primary reaction pathways of pyrolysis may seem like a considerable simplification of a very complex processes. The reaction pathways governing pyrolysis processes are in fact far too numerous and complex, making any detailed study by means of a graphical technique, such as applied to Figure 7, a tedious exercise. This apparent issue may be dealt with quite simply by considering only the initial and final mass and energy quantities of the pyrolysis process by treating these quantities as state variables. This choice of approach may be justified on account of the fact that we are interested only in how the final outcomes of the collection of reaction pathways differs from the initial conditions. Adopting this approach makes it possible to reach a satisfactory interpretation of the upgrading techniques of pyrolysis from the graphical analysis (Figure 9), without having to

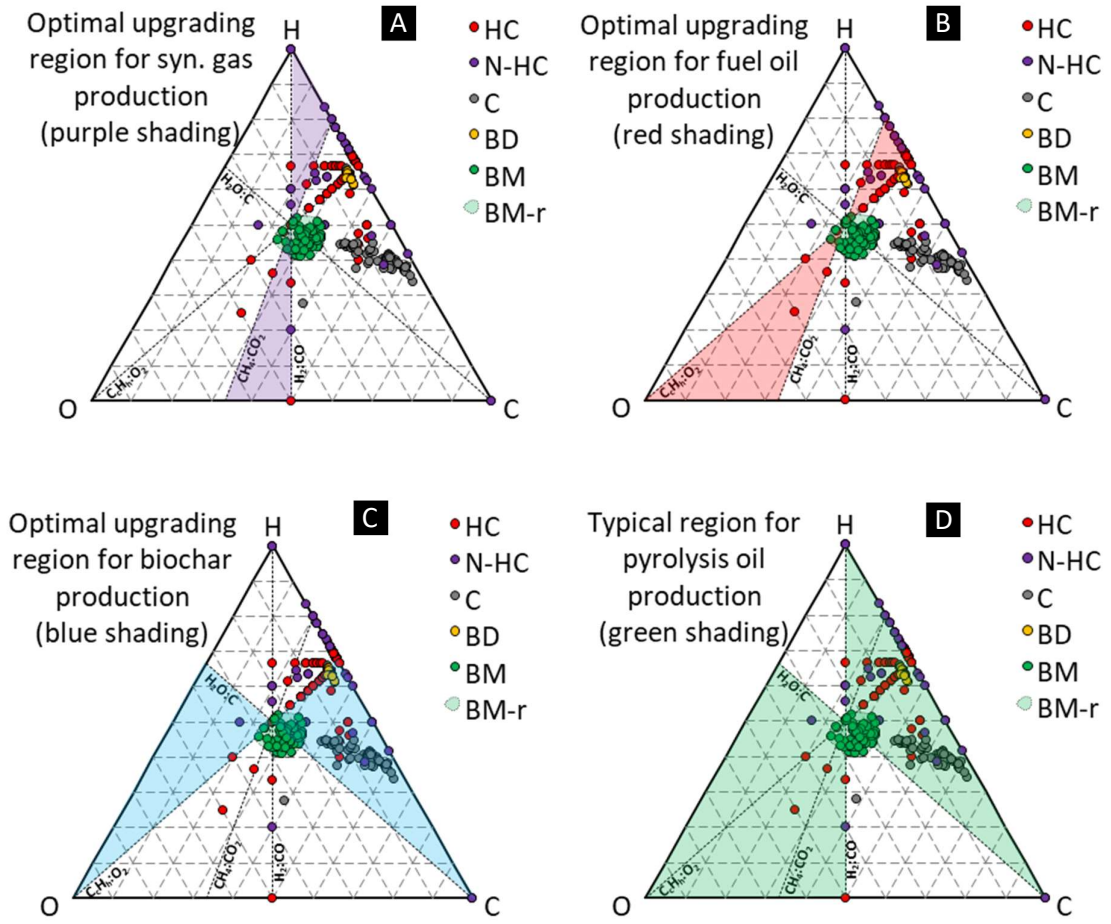

Figure 8: Ternary plot with bounded regions between various pairs of tie lines on a mole basis

delve into too much detail. This is not to say that the individual reaction pathways are unimportant, as they provide explanations for the limitations that exist for upgrading processes, such as why it is not possible to remove oxygenates as pure diatomic oxygen.

3.3. Energy-based metrics of biomass to biofuel efficacy: energy quality

It is not likely that oxygenates present in pyrolysis oils would be removed as pure O_2 or CO_2 with a selectivity of 100 % via the four primary reaction pathways. However, it is still sensible to steer upgrading processes and catalysts towards this ideal outcome by making use of these reaction pathways to achieve products close to those being targeted. Before going on to using ternary plots the analysis of these and other upgrading principles, the targeted products first need to be defined by some appropriate criteria. The general consensus from the literature

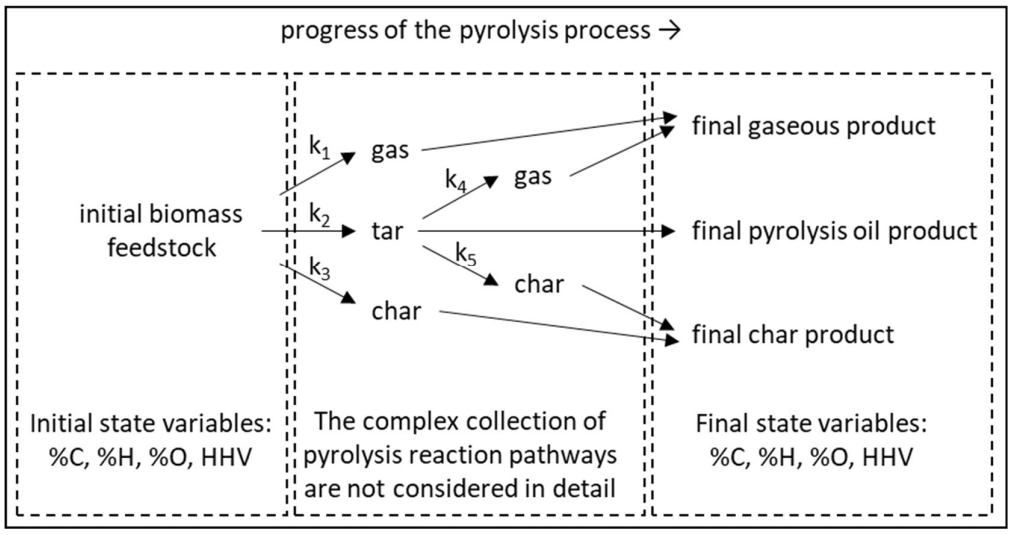

Figure 9: Representation of the initial and final conditions used to simplify the graphical analysis of upgrading techniques

makes it clear that pyrolysis oils should be deoxygenated (Bridgwater, 2012), and Chapter 2 discusses in further detail as to why this is the case, based primarily on the effect that deoxygenation has energy quality embodied in the higher heating value. Since pyrolysis oil is an energy product, it would be reasonable to conclude that upgrading procedures should be quantified as a function of the energy in the pyrolysis oil.

Çengel & Boles (1994) assert that energy has both quality (or more precisely, exergy—the maximum useful work possible) and quantity (the amount of energy available). In the case of fuel, energy is specifically in the form of *chemical energy*, which is the potential of fuel to undergo combustion, evolve energy and transform to the products of combustion in the process. The magnitude of this change is typically measured in an adiabatic bomb calorimeter at constant volume as the change in internal energy from fuel $\left(\Delta_{\mathrm{r}} U^{\circ}_{\mathrm{reactants}}\right)$ to products $\left(\Delta_{\mathrm{r}} U^{\circ}_{\mathrm{products}}\right)$, which is converted mathematically by the instrument to the enthalpy of combustion $\Delta_{\mathrm{c}} h^{\circ}\big|_{\mathrm{HHV}}$. The principle that a larger HHV characterizes a greater change in energy state from fuel to products will be used here to derive a definition of energy quality that can be applied to the graphical analysis discussed in this chapter. Assuming that all products of combustion are at the same energy quality of zero, the following assumptions are used to derive a suitable definition of energy quality:

- The magnitude of the HHV quantifies the liberation of energy by a fuel during complete combustion relative to its products at standard conditions.
- Products of complete combustion have zero energy quality.
- A fuel with a larger HHV has a higher energy quality relative to its combustion products
- The change in energy quality is reminiscent of a change in the HHV from one fuel to another.

The change in energy quality (ΔE_{Q}) that occurs during upgrading may be described as the difference between the product's HHV, $\Delta_{\mathrm{c}}h^{\circ}\big|_{\mathrm{HHV,product}}$, and the HHV of the feed that produced it, $\Delta_{\mathrm{c}}h^{\circ}\big|_{\mathrm{HHV,feed}}$ and divided by the HHV of the feed $\Delta_{\mathrm{c}}h^{\circ}\big|_{\mathrm{HHV,feed}}$, as follows (with the substitution of Equation 23):

$$\Delta E_{\mathrm{Q}} = \frac{\Delta_{\mathrm{c}}h^{\circ}\big|_{\mathrm{HHV,product}} - \Delta_{\mathrm{c}}h^{\circ}\big|_{\mathrm{HHV,feed}}}{\Delta_{\mathrm{c}}h^{\circ}\big|_{\mathrm{HHV,feed}}} = \frac{-13.87\left(m_{\mathrm{O_2}}\big|_{\mathrm{product}} - m_{\mathrm{O_2}}\big|_{\mathrm{feed}}\right)}{-13.87\, m_{\mathrm{O_2}}\big|_{\mathrm{feed}}} \tag{29}$$

which may be simplified to

$$\Delta E_{\mathrm{Q}} = \frac{m_{\mathrm{O_2}}\big|_{\mathrm{product}}}{m_{\mathrm{O_2}}\big|_{\mathrm{feed}}} - 1 \tag{30}$$

where the feed may be either biomass or an unrefined fuel that is yet to undergo upgrading. The variable $m_{\mathrm{O_2}}$ is specific to 1 kg of fuel, with units of $\mathrm{kg_{O_2}/kg_{fuel}}$, and may be rewritten as

$$m_{\mathrm{O_2}} = \frac{m_{\mathrm{O_2}}}{1\ \mathrm{kg_{fuel}}} = \frac{n_{\mathrm{O_2}}\big|_{\mathrm{fuel}} \times 2 \times \mathrm{M_{O_2}}}{1\ \mathrm{kg_{fuel}} \times \mathrm{M_{fuel}}} \tag{31}$$

Substituting Equation 31 into Equation 30 yields

$$\Delta E_{\mathrm{Q}} = \frac{n_{\mathrm{O_2}}\big|_{\mathrm{product}} \times 2 \times \mathrm{M_{O_2}}/1\ \mathrm{kg_{product}} \times \mathrm{M_{product}}}{n_{\mathrm{O_2}}\big|_{\mathrm{feed}} \times 2 \times \mathrm{M_{O_2}}/1\ \mathrm{kg_{feed}} \times \mathrm{M_{feed}}} - 1 \tag{32}$$

and with further simplification Equation 32 becomes

$$\Delta E_{\mathrm{Q}} = \frac{n_{\mathrm{O_2}}\big|_{\mathrm{product}}}{n_{\mathrm{O_2}}\big|_{\mathrm{feed}}} \frac{\mathrm{M_{feed}}}{\mathrm{M_{product}}} - 1 \tag{33}$$

where ΔE_{Q} may be reported on a percentage basis by multiplying Equation 33 by $100\ \%$.

3.4. Energy-based metrics of biomass to biofuel efficacy: energy yield

A second concept is the energy yield of the process, defined by how much of the energy that initially enters via the feedstock reports to the final product. The energy yield for a product of pyrolysis, $E_{\mathrm{Y}}|_{\mathrm{product}}$ may be described mathematically as the ratio of the HHV of the product $\Delta_{\mathrm{c}}h^{\circ}|_{\mathrm{HHV,product}}$ to the HHV of the feed $\Delta_{\mathrm{c}}h^{\circ}|_{\mathrm{HHV,feed}}$:

$$E_{\mathrm{Y}}|_{\mathrm{product}} = \frac{E_{\mathrm{product}}}{E_{\mathrm{feed}}} = \frac{\Delta_{\mathrm{c}}h^{\circ}|_{\mathrm{HHV,product}} \times m_{\mathrm{product}}}{\Delta_{\mathrm{c}}h^{\circ}|_{\mathrm{HHV,feed}} \times m_{\mathrm{feed}}} \tag{34}$$

Equation 34 may be simplified by the same substitutions of Equations 23 and 31 as were done for Equation 29, yielding the following:

$$E_{\mathrm{Y}}|_{\mathrm{product}} = \frac{\left(-13.869 n_{\mathrm{O_2}}\big|_{\mathrm{product}} \times 2 \times \mathrm{M}_{\mathrm{O_2}}/1\ \mathrm{kg}_{\mathrm{product}} \times \mathrm{M}_{\mathrm{product}}\right) \times m_{\mathrm{product}}}{\left(-13.869 n_{\mathrm{O_2}}\big|_{\mathrm{feed}} \times 2 \times \mathrm{M}_{\mathrm{O_2}}/1\ \mathrm{kg}_{\mathrm{feed}} \times \mathrm{M}_{\mathrm{feed}}\right) \times m_{\mathrm{feed}}}$$

$$E_{\mathrm{Y}}|_{\mathrm{product}} = \frac{n_{\mathrm{O_2}}\big|_{\mathrm{product}}}{n_{\mathrm{O_2}}\big|_{\mathrm{feed}}} \times \frac{\mathrm{M}_{\mathrm{feed}}}{\mathrm{M}_{\mathrm{product}}} \times \frac{m_{\mathrm{product}}}{m_{\mathrm{feed}}} = \frac{n_{\mathrm{O_2}}\big|_{\mathrm{product}}}{n_{\mathrm{O_2}}\big|_{\mathrm{feed}}} \times \frac{\mathrm{M}_{\mathrm{feed}}}{\mathrm{M}_{\mathrm{product}}} \times \omega_{\mathrm{product}} \tag{35}$$

Equation 35 may also be written entirely on a molar basis by simplifying it further to

$$E_{\mathrm{Y}}|_{\mathrm{product}} = \frac{\left(n_{\mathrm{O_2}} n_{\mathrm{product}}\right)\big|_{\mathrm{product}}}{\left(n_{\mathrm{O_2}} n_{\mathrm{feed}}\right)\big|_{\mathrm{feed}}} \tag{36}$$

For the production of pyrolysis oil from biomass, Equation 36 becomes

$$E_{\mathrm{Y}}|_{\mathrm{pyrolysis\ oil}} = \frac{\left(n_{\mathrm{O_2}} n_{\mathrm{pyrolysis\ oil}}\right)\big|_{\mathrm{pyrolysis\ oil}}}{\left(n_{\mathrm{O_2}} n_{\mathrm{biomass}}\right)\big|_{\mathrm{biomass}}} \tag{37}$$

which states that the energy yield is equal to the product of the moles of oxidant and reductant with respect to the pyrolysis oil divided by the product of the moles of oxidant and reductant with respect to the biomass feedstock. Of course, if hydrogen is removed from the feed as diatomic hydrogen $(\mathrm{H_2})$, or carbon is removed as carbon monoxide (CO), then some

of the energy that entered via the biomass would report to the resulting syngas, and the energy yield for the pyrolysis oil would decrease. Likewise, the production of biochar would also share some of the energy with the other products. The sum of the individual energy yields of each product would give the total energy yield of the products. Mathematically the total energy yield for the products, $E_{\mathrm{Y}}|_{\mathrm{total}}$, of a general pyrolysis process is expressed as

$$E_{\mathrm{Y}}|_{\mathrm{total}} = \frac{\left(n_{\mathrm{O_2}} n_{\mathrm{syngas}}\right)\big|_{\mathrm{syngas}} + \left(n_{\mathrm{O_2}} n_{\mathrm{pyrolysis\ oil}}\right)\big|_{\mathrm{pyrolysis\ oil}} + \left(n_{\mathrm{O_2}} n_{\mathrm{biochar}}\right)\big|_{\mathrm{biochar}}}{\left(n_{\mathrm{O_2}} n_{\mathrm{biomass}}\right)\big|_{\mathrm{biomass}}} \qquad 38$$

The derivations for the change in energy quality and the energy yield made use of the HHV, but it is also possible to obtain the exact same correlations using the LHV. If data for the HHV is plotted against the corresponding LHV data, a linear correlation between the HHV and LHV is obtained. This has been done for the same 357 data initially used in Chapter 2, and is shown in Figure 10. The correlation obtained is

$$\Delta_{\mathrm{c}} h^{\circ}\big|_{\mathrm{HHV}} = 1.06 \Delta_{\mathrm{c}} h^{\circ}\big|_{\mathrm{LHV}}$$

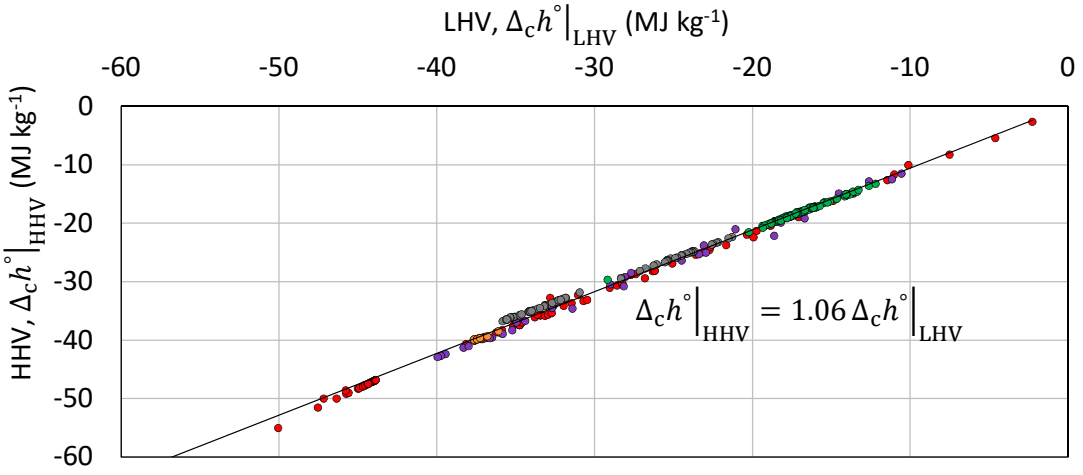

Figure 10: Plot of the higher heating value against the lower heating value. Note the linear correlation, for which there is not much deviation, despite data being presented for all types of gaseous, liquid and sold fuel.

3.5. Application of equations of energy yield and quality

A ternary plot on the mole basis, as in Figure 7 and Figure 8, lends itself well to illustrating visually how data sets correspond to one another. For mass balances, it is best to plot these data sets on the mass basis, as is done in Figure 11, since mass balances can be performed easily by applying the lever-arm rule. As most of the data lie near the bottom portion of Figure 11, only this half is shown for clarity. The biomass data cluster in Figure 11 spreads out parallel to the O–C axis, as changes to hydrogen on the mass basis are small due to the molar mass of hydrogen.

If the proportion of hydrogen in the molecular formula doubles from $\mathrm{C_1H_1O_1}$ to $\mathrm{C_1H_2O_1}$ for example, the mass percentage of hydrogen changes from $3.5\ \%$ to $6.7\ \%$, while carbon and oxygen decrease by only $1.4\ \%$ and $1.9\ \%$ respectively. If the proportion of carbon in the molecular formula were to double (i.e. from $\mathrm{C_1H_1O_1}$ to $\mathrm{C_2H_1O_1}$), the change in mass percentage for hydrogen would still be small (from $3.5\ \%$ to $2.5\ \%$), while the carbon mass percentage would double from $41.1\ \%$ to $82.8\ \%$. Comparable results are also obtained for similar changes to the proportion of oxygen.

The regions of most interest to the upgrading processes, those pertaining to deoxygenation, are shown in **Error! Reference source not found.** (mass basis) bounded by the $\mathrm{H_2O} \leftrightarrow \mathrm{C}$, $\mathrm{C}_{\nu_\mathrm{C}}\mathrm{H}_{\nu_\mathrm{H}} \leftrightarrow \mathrm{O_2}$, and $\mathrm{CH_4} \leftrightarrow \mathrm{CO_2}$ tie lines. For upgrading processes aiming to produce liquid

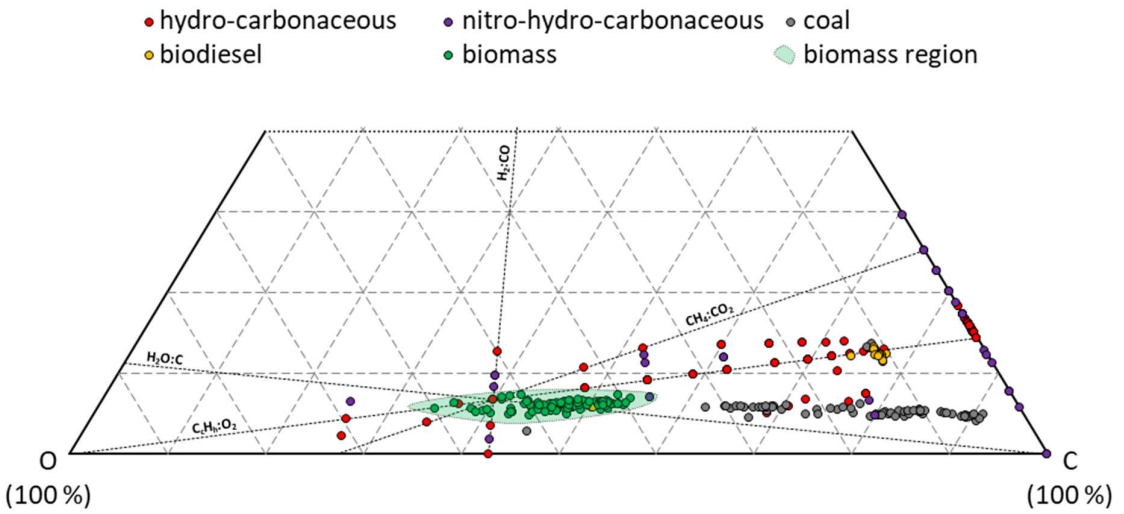

Figure 11: Ternary plot of various feedstock and fuels on a mass basis

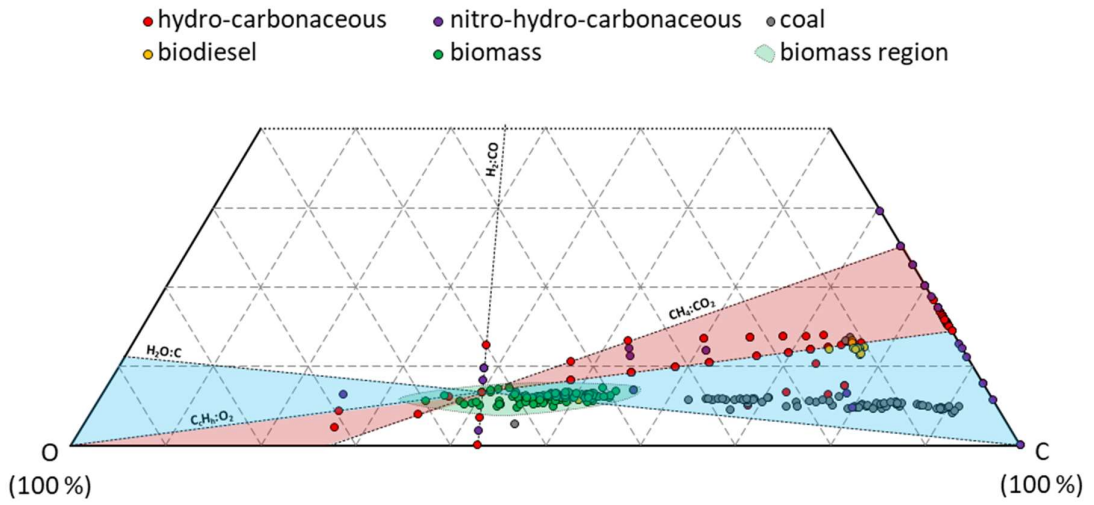

Figure 12: Ternary plot with bounded regions between $\mathrm{H_2O} \leftrightarrow \mathrm{C}$, $\mathrm{C}_{v_\mathrm{C}}\mathrm{H}_{v_\mathrm{H}} \leftrightarrow \mathrm{O_2}$, and $\mathrm{CH_4} \leftrightarrow \mathrm{CO_2}$ tie lines

transportation fuels, the "attainable" region is shown in Figure 13A (yellow). This region is bounded by the tie lines (red) ending at the model compounds of pentane ($\mathrm{C_5H_{12}}$) and heptadecane ($\mathrm{C_{17}H_{36}}$) (both liquids at ambient temperature) and represents the attainable upper and lower limits in the H/C ratio. Incorporating the regions of deoxygenation of Figure 12 into Figure 13A produces Figure 13B. The average biomass composition and calorific value is given in Table 3 and is also indicated in Figure 13 by the yellow dot, with the molecular formula of $\mathrm{C_{1.00}H_{1.52}O_{0.75}}$, and lies almost directly on the $\mathrm{H_2O} \leftrightarrow \mathrm{C}$ tie line. Complete deoxygenation for this model biomass compound by dehydration would result in a fuel product consisting mostly of pure carbon, according to the reaction pathway shown in Figure 14A. The resulting fuel product would contain only trace amounts of hydrogen (0.2 %, mass basis) and achieve, with $\Delta_\mathrm{c}h^\circ = -33.0\ \mathrm{MJ\ kg^{-1}}$, $E_\mathrm{Y} = 100\ \%$, and $\Delta E_\mathrm{Q} = 112\ \%$ (Table 3). Alternatively, complete deoxygenation may be achieved by generating $\mathrm{CO_2}$ (i.e. decarboxylation, Figure 14B) instead and would result in a fuel product with an average molecular formula of $\mathrm{C_{1.00}H_{2.43}}$. Such a product would have an HHV of $\Delta_\mathrm{c}h^\circ = -49.3\ \mathrm{MJ\ kg^{-1}}$ and $E_\mathrm{Y} = 100\ \%$, and $\Delta E_\mathrm{Q} = 181\ \%$.

For both routes of deoxygenation, energy yields of $100\ \%$ were achieved, even though the mass of some of the elements of which hydrocarbon-based fuels are comprised was removed to do so. The reason for this is that these two routes of deoxygenation remove carbon (decarboxylation) and hydrogen (dehydration) that have already undergone oxidation and

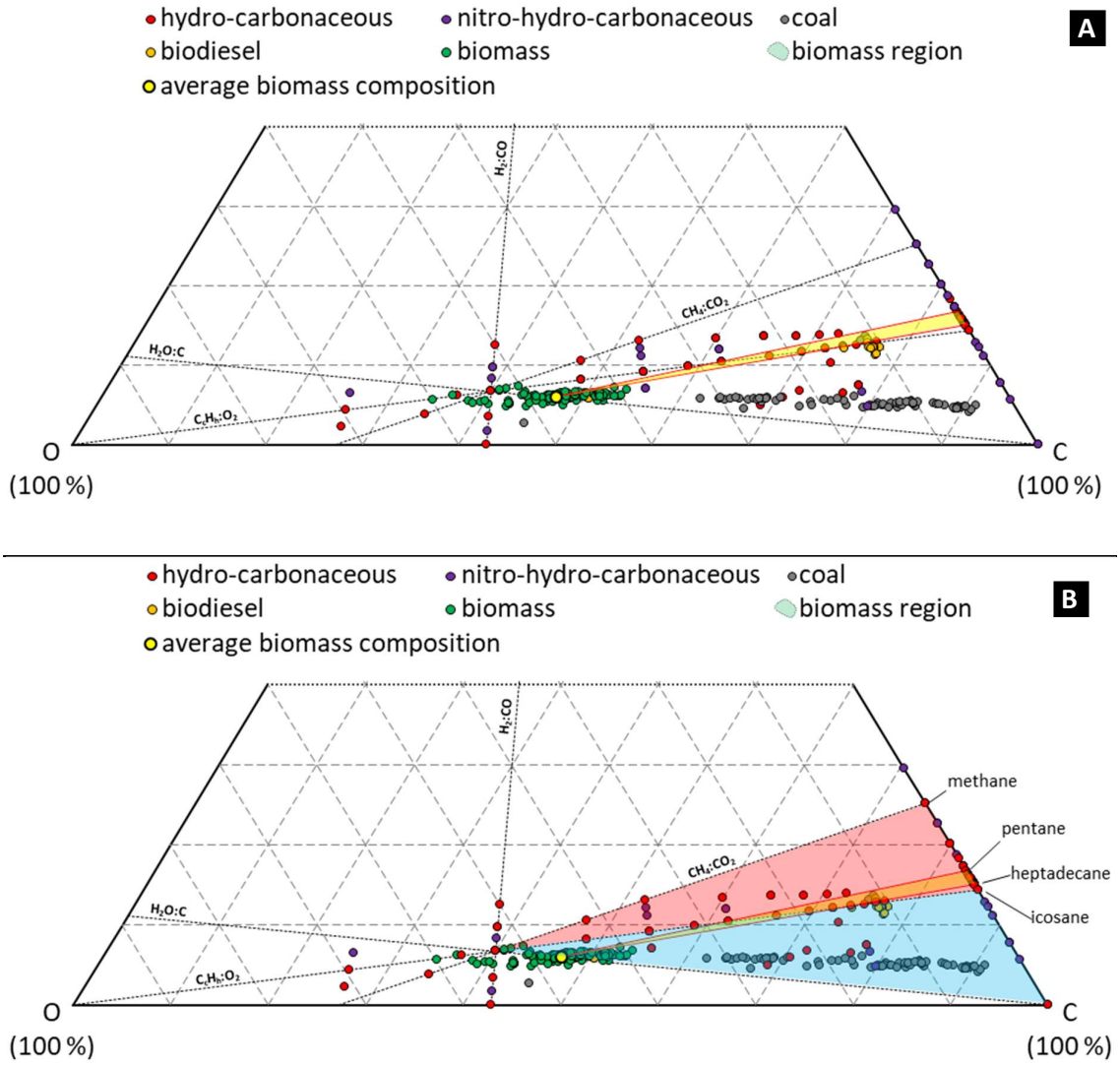

Figure 13: (A) Upgrading region (yellow) for biomass to the liquid alkanes bounded by pentane (C_5H_{12}) and heptadecane ($C_{17}H_{36}$); (B) overlapping upgrading regions dominated by dehydration (blue) and decarboxylation (red).

would not have participated in the combustion process. This may be demonstrated further by rearranging the molecular formula of biomass in the following reaction equations:

- *dehydration*: $C_{1.00}H_{1.52}O_{0.75} \leftrightarrow C_{1.00}H_{(1.52-0.75\times2)} \cdot 0.75(H_2O) \rightarrow C_{1.00}H_{0.03} + 0.75H_2O$
- *decarboxylation*: $C_{1.00}H_{1.52}O_{0.75} \leftrightarrow C_{(1.00-0.38)}H_{1.52} \cdot 0.38(CO_2) \rightarrow C_{1.00}H_{2.43} + 0.38CO_2$

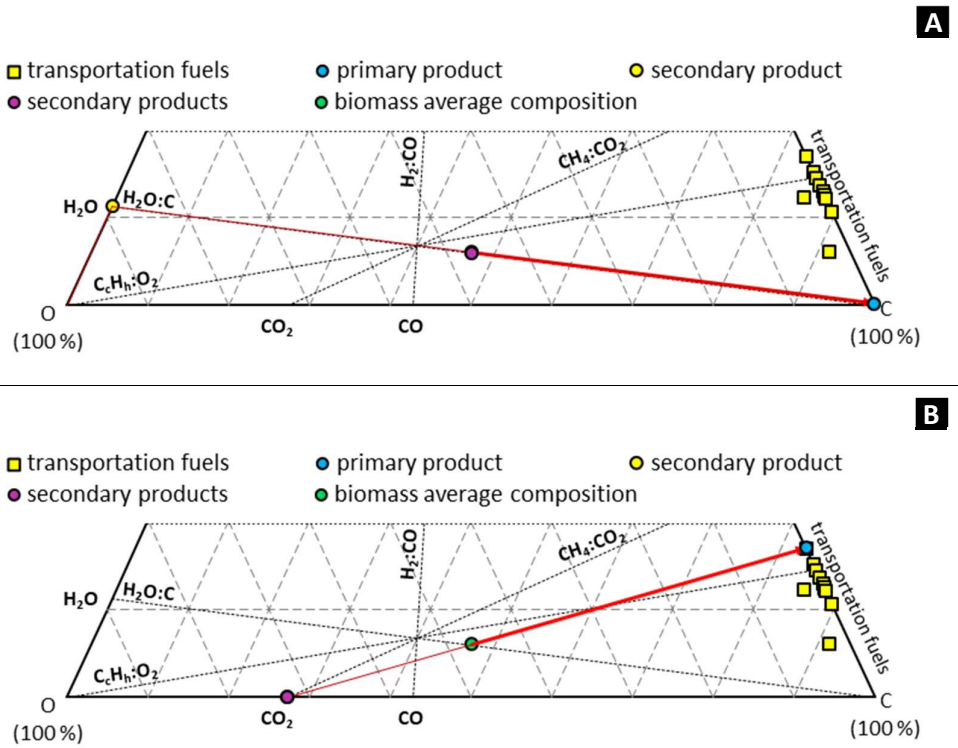

Figure 14: Deoxygenation tie lines for biomass via dehydration (A) and decarboxylation (B)

Table 3: Average biomass composition and calorific value

Mass Distribution			Calorific Value, $\Delta_c h^\circ$
C (%)	H (%)	O (%)	(MJ kg^{-1})
47.1	6.0	46.9	-17.5

If oxygen is removed from biomass using a compound that is not completed oxidized, such as with the liberation of CO via the decarbonylation reaction pathway, the energy yield in the main product would be reduced, even if the change in energy quality increases due to the decrease in oxygenates. Such is the case for the third example of Table 4 for deoxygenation via CO, which attains a lower energy yield of $63\ \%$, while increasing energy quality by $251\ \%$. The much higher change in energy quality is achieved since this reaction pathway utilized is closer in relation to that of the $\mathrm{H}_2 \leftrightarrow \mathrm{CO}$ tie line than for other reaction pathways, which leads to the production of energy-rich hydrogen. If dehydration, decarboxylation, and/or upgrading

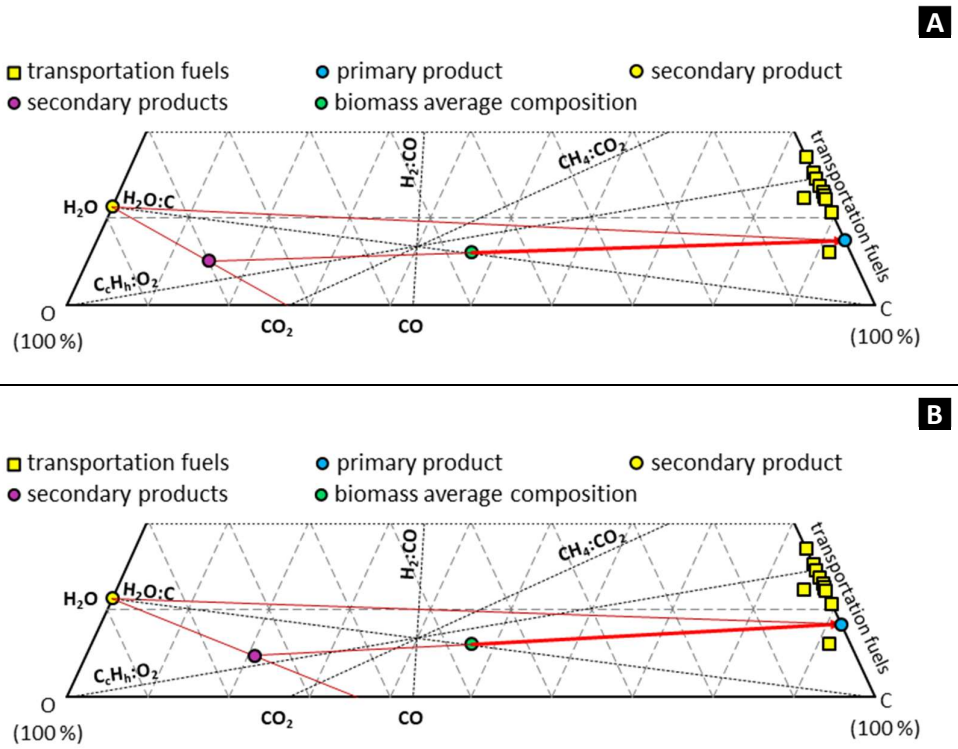

Figure 15: Different combinations of dehydration and decarboxylation routes for biomass

decarbonylation occur together, the by-product of deoxygenation, collectively as H_2O, CO_2, and/or CO, would lie on its own tie line. Figure 15 shows the H_2O, CO_2 with the by-product composition forms when deoxygenation occurs equally by dehydration and decarboxylation (see also example 4 in Table 4). Various liquid transportation fuels are also shown as yellow squares (Theodore, et al., 2009; Reed, 2014). An example of a process utilising all three deoxygenation mechanisms of dehydration, decarboxylation and decarbonylation is given in the 5th example in Table 4 and is also shown in Figure 15B. Here, $25\ \%$ of the oxygen present in the biomass is removed via dehydration, while the balance of $75\ \%$ is removed as CO_2 and CO at a ratio of 1/3. The resulting product lies between pentane and heptadecane.

If production of a transportation fuel from biomass is desired, this method of analysis suggests that the overall trend of upgrading pathways should ideally lie within a small region between pentane and heptadecane, according to Figure 13. The average molecular formula of the primary product located at the midpoint between these two bounds would be $C_{1.00}H_{2.26}$, or between heptane and octane. It is possible to achieve this composition with the conditions of the 5th example of Table 4, namely that $75\ \%$ of oxygen removed from biomass leaves as a

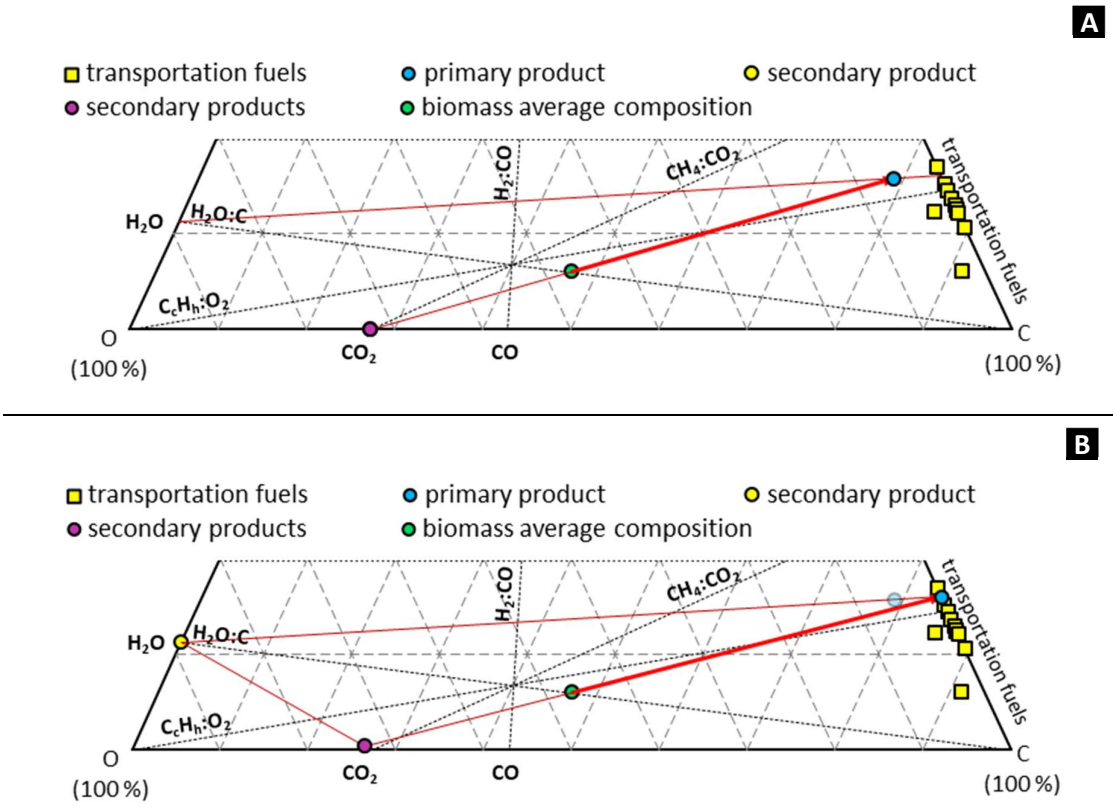

Figure 16: Optimal upgrading routes (A→B) for producing liquid transportation fuel from biomass

1-to-3 ratio of $\mathrm{CO_2}$ and CO with the remaining leaving as water. This results in an energy yield of $79\ \%$ due to the formation of CO, and a change in energy quality of $177\ \%$. It is however possible to produce the same transportation fuel composition via decarboxylation and dehydration while avoiding decarbonylation, as shown in Figure 16. This yields the desired product with an HHV of $\Delta_c h^\circ = -48.6\ \mathrm{MJ\ kg^{-1}}$ while retaining the full energy yield of $100\ \%$ and increasing the energy quality by $177\ \%$. It must be stressed that these examples represent the ideal outcomes for upgrading procedures using model feeds and products, and by no means prescribe what must be. What these examples do quantify the maximum attainable outcomes possible for upgrading procedures if ideality could be achieved in some way or another. It is highly unlikely that a hydroxyl group of cellulose would have a high selectivity towards liberation as carbon dioxide, since the best leaving group would be water, and this reflects the reality of most biomass constituents.

Table 4: Data for various scenarios of upgrading biomass to a primary fuel product via deoxygenation

Deoxygenation route	Mass distribution			$\Delta_c h^\circ$	E_Y	ΔE_Q	Carbon yield
	C (%)	H (%)	O (%)	(MJ kg^{-1})	(mass %)	(mass %)	(mass %)
via H_2O	99.8	0.2	0.0	-33.0^*	100	112	100.0
via CO_2	83.1	16.9	0.0	-49.3	100	181	62.7
via CO	66.5	33.5	0.0	-61.4	63	251	25.3
1/1: H_2O/CO_2	92.6	7.4	0.0	-42.4	100	142	81.3
1/3: H_2O/CO_x with 1/3: CO_2/CO	84.1	15.9	0.0	-48.6	79	177	51.0
95.5 % via CO_2	78.9	15.6	0.0	-45.6	100	160	64.3
95.5 % via CO_2 & balance to H_2O	84.1	15.9	0.0	-48.6	100	177	64.3

* calculated using individual $\Delta_c h^\circ$ values for carbon and hydrogen

3.6. Comparisons between energy and mass metrics: total mass yield

Maximizing oil yields for biomass pyrolysis is a major objective cited in the literature, as this satisfies the reasoning that the higher production rates of oil correspond to higher profit margins and higher conversion efficiency of the biomass (Akhtar & Amin, 2012; Czernik & Bridgwater, 2007; Mohan, et al., 2006). It is well-known that lower yields in pyrolysis oil are obtained in exchange for higher biochar yields when the pyrolysis temperature is below the optimum range of $450\ ^\circ C - 550\ ^\circ C$. The same is true when this optimum range is exceeded, and results in higher production of gaseous products due to cracking of the pyrolysis vapours. The yield in pyrolysis oil also depends on the operating conditions such as residence time, particle size distribution, heat transfer rate, and feedstock composition (Akhtar & Amin, 2012; Mohan, et al., 2006). Again, as with the carbon yield metric, the mass yield metric underlying the objective of maximizing pyrolysis oil production is often applied to pyrolysis processes yet is poorly substantiated. The following question arises: are these mass-based metrics correctly assumed by the proponents of fast pyrolysis research? Assume that pyrolysis oil is produced from cellulose via a pyrolysis process according to the following reaction:

$$nC_6H_{10}O_5 \rightarrow nv_1C + nv_2CO_x + nv_3H_2 + vn_4H_2O + nC_{(6-v_1-v_2)}H_{(10-2[v_3+v_4])}O_{(5-xv_2-v_4)}$$

where $n\mathrm{C}_{(6-v_1-v_2)}\mathrm{H}_{(10-2[v_3+v_4])}\mathrm{O}_{(5-xv_2-v_4)}$ is the average molecular formula of the pyrolysis oil constituents. The maximum oil yield is obtained when all of the mass of cellulose is converted into oil. This occurs when $v_1 = v_2 = v_3 = v_4 = 0$, and the chemical composition of pyrolysis oil becomes:

$$n\mathrm{C}_{(6-v_1-v_2)}\mathrm{H}_{(10-2[v_3+v_4])}\mathrm{O}_{(5-xv_2-v_4)}\big|_{v_1,v_2,v_3,v_4=0} = n\mathrm{C}_6\mathrm{H}_{10}\mathrm{O}_5$$

Staying with the previous assumption, this results in a pyrolysis oil made up of organic molecules that together exhibit the same average chemical formula as the feedstock that produced them. Obviously, the energy yield would remain the same while no change in energy quality would occur. What would have occurred is a change in morphology from cellulose to pyrolysis oil accompanying a change in phase from solid to liquid, and the generation of a plethora of value-adding chemical products. If the end use of this pyrolysis oil is as an intermediate for generating high-value chemical products, then maximizing the pyrolysis oil yield would be favourable. If, instead, production of a biofuel is the intention, then this process would result in the production of a biofuel with the same energy quality as its feedstock, and much lower compared to conventional transportation fuels. This inferior quality is well-known, and much effort has gone into improving the quality of biomass pyrolysis oils, with a focus on the reduction of oxygenates and physical properties brought on by their presence (Oasmaa & Czernik, 1999; Krutof & Hawboldt, 2016; Bridgwater, 2012). Clearly, directing the process outcomes towards a maximum pyrolysis oil does not result in a biofuel of adequate energy quality. To illustrate this point further, data are presented in Table 5 with the corresponding mass yields for comparison. The highest mass yield of $47.2\ \%$ is obtained for the dehydration of biomass to char, but this also achieves the lowest energy quality of $112\ \%$. In contrast, the lowest mass yield of $17.9\ \%$ is obtained via decarbonylation and also results in the highest change in energy quality of $251\ \%$ being achieved. In fact, plotting the change in energy quality against the total mass yield for biomass (Table 5) undergoing various degrees of dehydration, decarboxylation and decarbonylation produces a generally negatively correlated cluster of data (Figure 17, green points).

Table 5: Comparisons between mass and energy metrics for various pyrolysis scenarios

Deoxygenation route	$\Delta_c h^\circ$	E_Y	ΔE_Q	Primary product mass yields	
	(MJ kg^{-1})	(mass %)	(mass %)	(carbon yield %)	(total yield %)
via H_2O	-33.0^*	100	112	100.0	47.2
via CO_2	-49.3	100	181	62.7	35.5
via CO	-61.4	63	251	25.3	17.9
1/1: H_2O/CO_2	-42.4	100	142	81.3	41.4
1/3: H_2O/CO_x with 1/3: CO_2/CO	-48.6	79	177	51.0	28.6
95.5 % via CO_2	-45.6	100	160	64.3	38.4
95.5 % via CO_2 & balance to H_2O	-48.6	100	177	64.3	36.1

* calculated using individual $\Delta_c h^\circ$ values for carbon and hydrogen

The data are plotted in sets that are distinguishable as trends moving from left to right within the boundaries of the cluster. The top most data set coincides with the purple trendline indicating the maximum deoxygenation that can be achieved through decarboxylation and decarbonylation. The boundary that corresponds to the maximum energy yield ($E_Y|_{total} = 100\ \%$) lies along the red trendline (representing decarboxylation) and the black dotted trendline (representing dehydration), while the minimum energy yield lies along the boundary indicated by the blue trendline (representing decarbonylation). From a general perspective, any improvement in energy quality of the biomass feedstock is accompanied by an overall decrease in mass yield. More specifically for each data set, small increases in mass yield locally correspond to slight increases in energy quality for data located below $\Delta E_Q \cong 111\ \%$ ($\pm 1\ \%$), while the opposite is true for data sets above this location. The local change in mass yield corresponding to the largest change in ΔE_Q occurs along the green trendline of Figure 15, where ΔE_Q changes by $69\ \%$. It should be remembered that shifts in data from left to right are also accompanied by increases in energy yield due to deoxygenation shifting from decarbonylation to decarboxylation. Therefore, although it is possible to achieve maxima in energy yield and total mass yield locally, a decrease in mass yield is nevertheless required in order to increase the energy quality of the product produced via pyrolytic deoxygenation. This is obvious when considering that all data lie to the left of and diverge from the biomass datum.

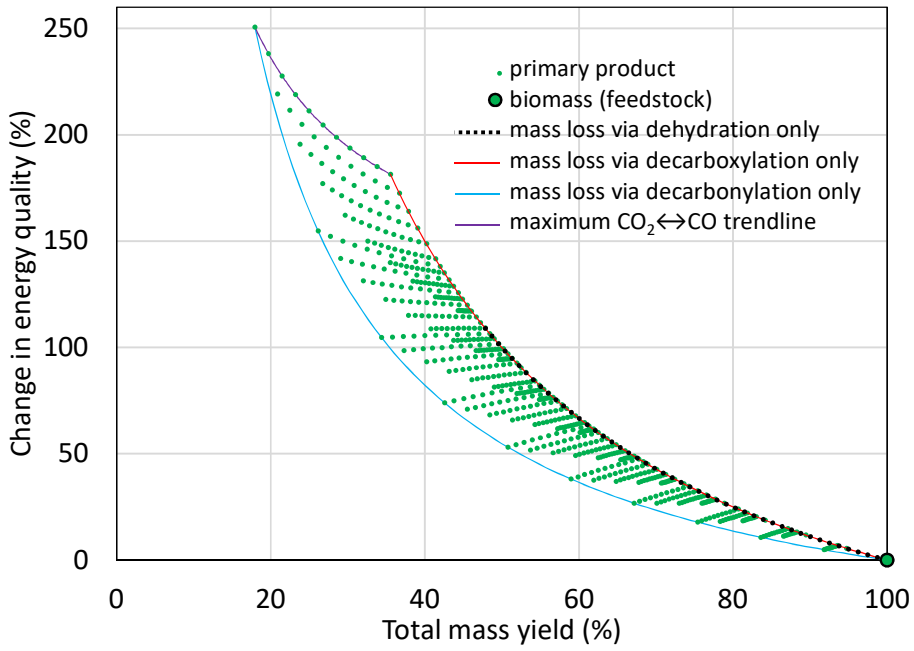

Figure 17: Plot of primary pyrolysis product mass yield against change in energy quality as a result of pyrolytic deoxygenation

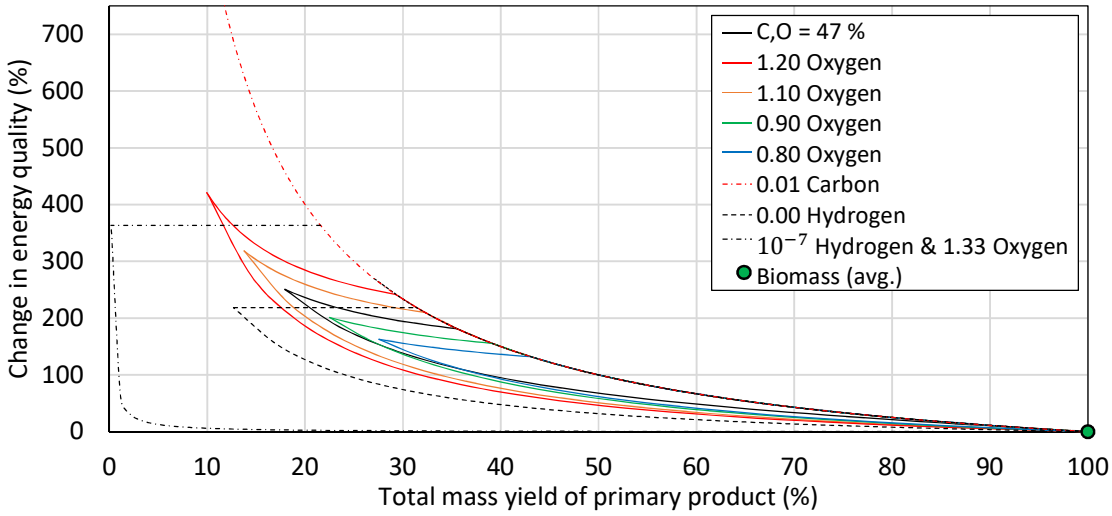

Figure 18: Upgrading boundaries for pyrolytic deoxygenation of biomass of varying composition

How do these results compare to variations in biomass composition? Figure 18 plots trendlines for changes in biomass oxygen content (solids lines of varying colour) together with a hydrogen-free (black dashed lines) and carbon-free (red dotted and dashed line)

composition with respect to the average biomass composition of Table 5. Firstly, irrespective of the biomass composition, the location of the decarboxylation-dehydration boundary remains unchanged, albeit increasing in scale as the percentage of oxygen present in the biomass is increased. Secondly, the location and degree of curvature in the decarbonylation boundary changes in various ways with changes in the biomass composition. An increase in biomass oxygen content shifts the decarbonylation boundary upwards and to the left while increasing the degree of curvature proportionally. Variations in carbon content bring about similar changes, but the proportion by which the degree of curvature changes is not the same as for the changes brought about by varying the oxygen content. The absence of hydrogen in the feedstock also flattens out the decarbonylation-decarboxylation trendline so that it is parallel with the x-axis (black dashed line, and black dashed and dotted line). In other words, for hydrogen-free feedstock, changes in mass yield do not affect the energy quality of the product. The energy yield however will change proportionally with the amount of partially oxidised carbon being removed from the primary product via decarbonylation. If oxygen is in excess, the decarbonylation boundary (black dotted and dashed curve) shifts closer to the y-axis while the decarboxylation-decarbonylation line shifts away from the x-axis. Thirdly, for feedstock containing little to no carbon, decarboxylation and decarbonylation are negligible/absent (unless carbon is introduced to the process by some other means) and only the dehydration is present, shown by the red dotted and dashed curve in Figure 18. Lastly, the boundary limit for deoxygenation via decarbonylation is obtained for a feedstock with a molar carbon-oxygen ratio (C:O) (i.e. the molecular formula for carbon monoxide), where the boundaries are the x-axis and y-axis. The boundary limit for deoxygenation via dehydration is obtained for a molar hydrogen-oxygen ratio (H:O) of 2:1 (i.e. the molecular formula for water) and is simply the dehydration curve. These boundary limits become much clearer when plotting a very large amount of data for the total mass yield of some primary product(s) produced from the upgradation of some arbitrary C:H:O-containing feedstock(s) (Figure 19). More than 16 million data points were used to produce the plot of Figure 19 by varying the mass percentages of carbon, hydrogen and oxygen between $0\ \%$ and $100\ \%$ (Figure 20, grey region) – those compositions that lie within an “unattainable” region are excluded (Figure 20, non-grey region). In other words, the data plotted in Figure 19 are applicable to the upgradation of more or less all practical compositions of material composed of carbon,

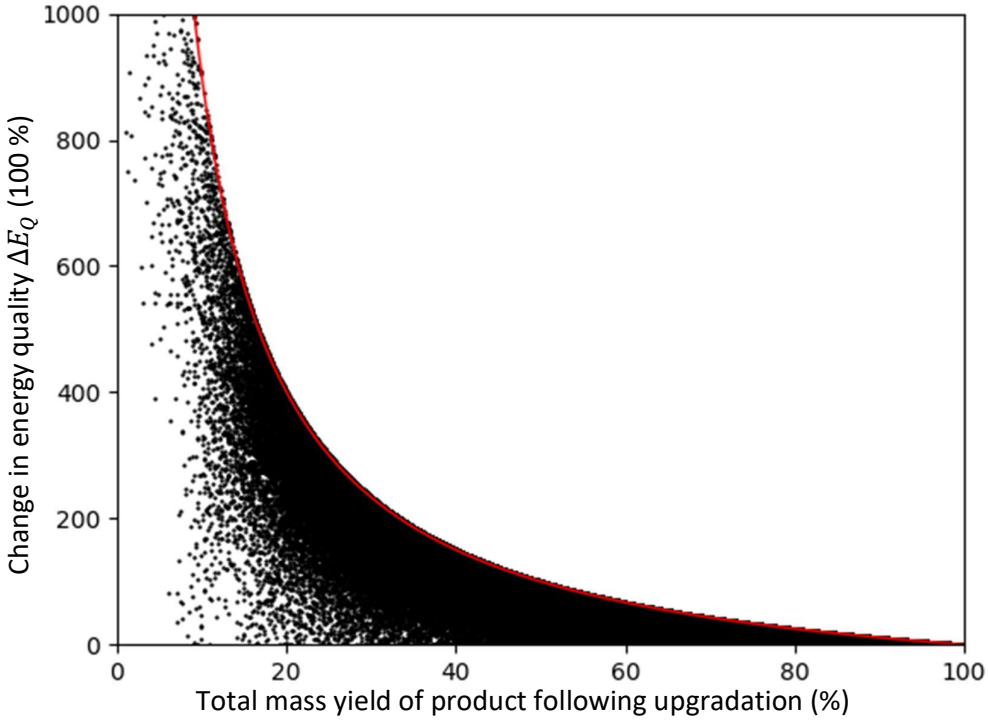

Figure 19: Total mass yield of primary product of upgradation for C:H:O-containing feedstocks

hydrogen and oxygen. Note that although this exercise is purely theoretical, it nonetheless has real-life implications associated with it.

Regardless of variations in biomass/feedstock composition, any increase in energy quality must be accompanied by a decrease in the mass yield. Since the oxygen content has a negative effect on energy quality and biomass invariably will contain oxygen, the mass yield must be decreased according to how much oxygen is removed. The ratio of hydrogen to carbon in the product too must be adjusted accordingly to bring about changes in energy quality and will also contribute to a reduction in mass yield. Since carbon exhibits a lower energy quality compared to hydrogen while having a higher mass than hydrogen, an increase in energy quality from an adjustment in H/C will result in a substantial reduction in mass yield of the product being upgraded. Inevitably, the reduction in mass yield will be required for pyrolytic upgrading via deoxygenation since the product datum must fall within the attainable region (shown in Figure 21 as red shading). Therefore, it is not possible to increase the mass yield beyond a certain limit without affecting the energy quality of the fuel being produced.

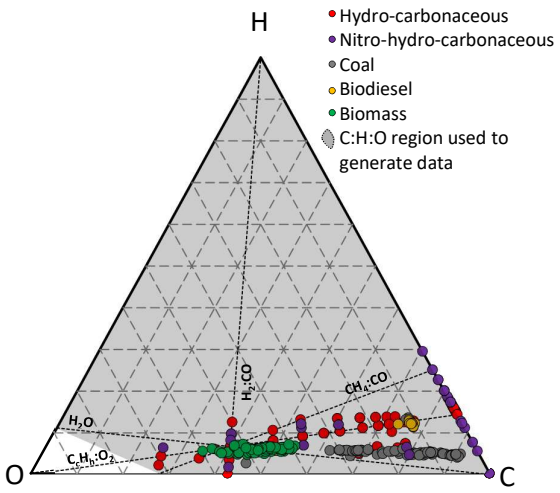

Figure 20: Extent of distribution of C:H:O data (grey shading) used to generate Figure 19

What equation describes the boundary limit presented in Figure 19 & Figure 21: (shown by the red curve)? First consider an oxygenated hydrocarbonaceous compound with the formula of $\mathrm{C}_{v_\mathrm{C}}\mathrm{H}_{v_\mathrm{H}}\mathrm{O}_{v_\mathrm{O}}$, and where $v_\mathrm{O} \leq 2v_\mathrm{C}$ and $2v_\mathrm{O} \leq v_\mathrm{H}$ so that all the oxygen may be removed as CO_2 and/or $\mathrm{H}_2\mathrm{O}$ using only endogenous carbon and/or hydrogen. The boundary limit is thus approached and may be represented by a rearrangement of the molecular formula as:

$$\underset{m_i}{n\mathrm{C}_{v_\mathrm{C}}\mathrm{H}_{v_\mathrm{H}}\mathrm{O}_{v_\mathrm{O}}} \leftrightarrow \underset{m_i = m_v + m_f}{n(0.5v_\mathrm{O}\mathrm{CO}_2)\mathrm{C}_{v_\mathrm{C}-0.5v_\mathrm{O}}\mathrm{H}_{v_\mathrm{H}}} \xrightarrow[\text{upgrad.}]{} \underset{m_f}{n\mathrm{C}_{v_\mathrm{C}-0.5v_\mathrm{O}}\mathrm{H}_{v_\mathrm{H}}} + \underset{m_v}{0.5nv_\mathrm{O}\mathrm{CO}_2} \qquad 39$$

The specific energy referred to here is simply the heat of combustion $\Delta_\mathrm{c}h^\circ$ (and may also be expressed as a higher or lower energy value with respect to the heat of vaporisation of water):

$$\Delta_\mathrm{c}h^\circ\big|_{\mathrm{HHV},i} = \frac{\Delta_\mathrm{c}H^\circ\big|_{\mathrm{HHV},i}}{m_i} \qquad 40$$

where the subscript i denotes the initial form of matter before upgradation has taken place, while the subscript f denotes the upgraded state of matter:

$$\Delta_\mathrm{c}h^\circ\big|_{\mathrm{HHV},f} = \frac{\Delta_\mathrm{c}H^\circ\big|_{\mathrm{HHV},f}}{m_f} \qquad 41$$

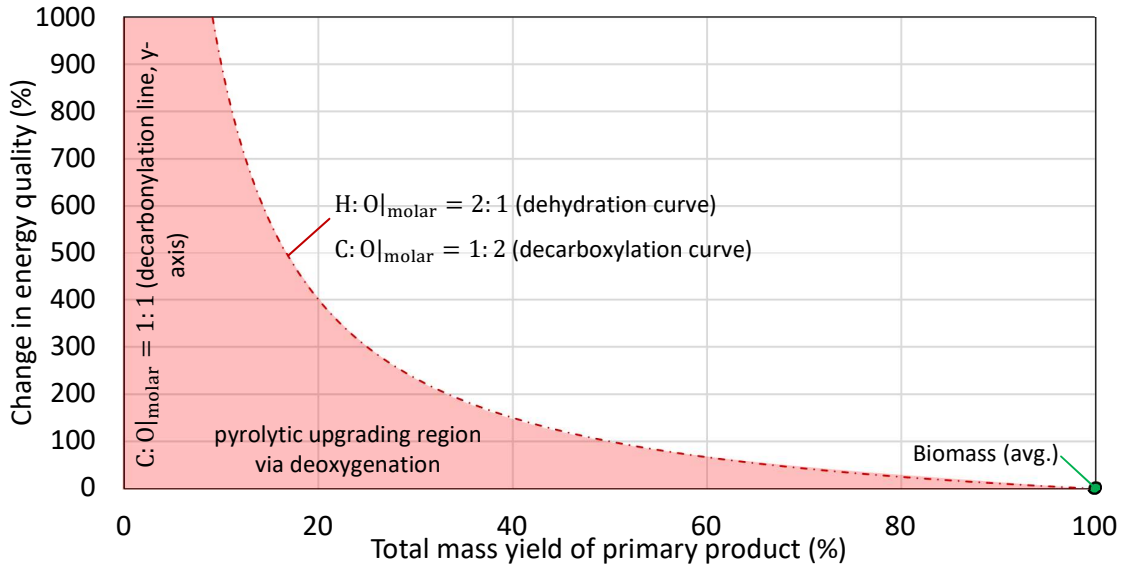

Figure 21: Boundary limit for pyrolytic upgrading via deoxygenation for biomass feedstock

Subtracting Equation 40 from Equation 41 and dividing by is $\Delta_c h^\circ|_{\mathrm{HHV},i}$ the procedure as what was performed with Equation 29:

$$\frac{\Delta_c h^\circ|_{\mathrm{HHV},f} - \Delta_c h^\circ|_{\mathrm{HHV},i}}{\Delta_c h^\circ|_{\mathrm{HHV},i}} = \frac{1}{\Delta_c h^\circ|_{\mathrm{HHV},i}}\left(\frac{\Delta_c H^\circ|_{\mathrm{HHV},f}}{m_f} - \frac{\Delta_c H^\circ|_{\mathrm{HHV},i}}{m_i}\right) \quad 42$$

since

$$\frac{\Delta_c h^\circ|_{\mathrm{HHV},f} - \Delta_c h^\circ|_{\mathrm{HHV},i}}{\Delta_c h^\circ|_{\mathrm{HHV},i}} = \Delta E_Q \quad 43$$

Equation 40 is used to simplify Equation 42 and on simplifying yields:

$$\Delta E_Q = \frac{m_i}{\Delta_c H^\circ|_{\mathrm{HHV},i}}\left(\frac{\Delta_c H^\circ|_{\mathrm{HHV},f}}{m_f} - \frac{\Delta_c H^\circ|_{\mathrm{HHV},i}}{m_i}\right) = \frac{m_i\,\Delta_c H^\circ|_{\mathrm{HHV},f}}{m_f\,\Delta_c H^\circ|_{\mathrm{HHV},i}} - 1 \quad 44$$

It is possible to simplify Equation 44 by showing by means of an energy balance that $\Delta_c H^\circ|_{\mathrm{HHV},f} = \Delta_c H^\circ|_{\mathrm{HHV},i}$ when the initial material m_i produces the upgraded product mass m_f when the mass removed via upgradation m_v is either CO_2 or H_2O:

$$m_i \Delta_c h^\circ\big|_{\mathrm{HHV},i} = \Delta_c H^\circ\big|_{\mathrm{HHV},i} = m_v \Delta_c h^\circ\big|_{\mathrm{HHV},v} + m_f \Delta_c h^\circ\big|_{\mathrm{HHV},f} \quad (45)$$

As $\Delta_c h^\circ\big|_{\mathrm{HHV},v} = 0$ for both $\mathrm{CO_2}$ or $\mathrm{H_2O}$, Equation 45 becomes

$$\Delta_c H^\circ\big|_{\mathrm{HHV},i} = m_f \Delta_c h^\circ\big|_{\mathrm{HHV},f}$$

$$\Delta_c H^\circ\big|_{\mathrm{HHV},i} = \Delta_c H^\circ\big|_{\mathrm{HHV},f} \quad (46)$$

Consequently, Equation 44 reduces to

$$\Delta E_Q = \frac{m_i}{m_f} - 1 \quad (47)$$

Despite it being an ostensibly unremarkable equation, the properties of Equation 47 provide the strongest criticism against the objectives of maximizing the mass yields of biofuels that have until now been applied *prima facie* to evaluate the outcomes of biofuel synthesis. The greatest increase in energy quality of a material intended for use as a fuel comes from the greatest decrease in redundant mass (i.e. energy-deficient mass removed through upgradation such as $\mathrm{CO_2}$ or $\mathrm{H_2O}$), where ΔE_Q approaches when the upgradation mass m_i approaches the mass of the material undergoing upgradation ($m_v \to m_i$), or rather $m_f \to 0$:

$$\lim_{m_f \to 0} \Delta E_Q = \lim_{m_f \to 0} \frac{m_i}{m_f} - 1 \to \infty \quad (48)$$

If no upgradation takes place (in other words, $m_v = 0$ and $m_f = m_i$), then there will be no change in energy quality:

$$\Delta E_Q\big|_{m_f = m_i} = \left.\frac{m_i}{m_f}\right|_{m_f = m_i} - 1 = 0 \quad (49)$$

The consistency of Equation 47 is apparent from the limits presented in Equation 48 and Equation 49. If an energy yield of $100\ \%$ is achieved in all, then a $100\ \%$ mass yield would simply mean that no change in energy quality was achieved – biomass remained as biomass. On the other hand, a $0\ \%$ mass yield would result in no mass being associated with the $100\ \%$

energy yield – although energy evolution via the combustion reaction requires there to be some mass association and attaining this limit would be nonsensical and probably impossible.

3.7. Comparisons between energy and mass metrics: carbon mass yield

Analysis of the relationship between the change in energy quality and the carbon yield is not as straight forward as for the total mass yield, and the understanding that biofuels are energy-based products, not mass based is used to aid this analysis. Consider the following example:

> Say a fuel with an HHV of $10\ \mathrm{MJ\ kg^{-1}}$ is used for a heating application. In order to liberate $1\ 000\ \mathrm{MJ}$ of energy every second, $100\ \mathrm{kg}$ of fuel would need to be combusted every second: $100\ \mathrm{kg\ s^{-1}} \rightarrow 1\ 000\ \mathrm{MJ\ s^{-1}}$. If a fuel with an HHV of $50\ \mathrm{MJ\ kg^{-1}}$ is used instead, only a fifth of the amount of this fuel would be required to deliver the same amount of energy per second: $20\ \mathrm{kg\ s^{-1}} \rightarrow 1\ 000\ \mathrm{MJ\ s^{-1}}$. Again, this is a hypothetical example for the simple purpose of illustrating this point.

This example describes how the energy quality may be indirectly proportional to the mass of the fuel in general, which is the main conclusion of the previous section. What is not apparent in this example is what the particular contributions of carbon, hydrogen and oxygen are towards the change in energy quality specifically with respect to a product of some upgradation process. If the same data used to generate the plot of Figure 19 are used to plot the change in energy quality with respect to the carbon yield following upgradation, the plot in Figure 22 is generated.

Unlike the boundary limits evident in Figure 19, Figure 22 presents no such boundary limits other than where $\Delta E_Q = 0$ for all values of m_{p_C}, where m_{p_C} is the carbon yielded to the product produced from upgradation. It cannot for instance be concluded that maximizing carbon yield results in the highest change in energy quality. Recall that the data used to plot Figure 22 represents just about all feed compositions possible based on a composition comprising carbon, hydrogen and oxygen. Of these data, $99.9\ \%$ of points correspond to a maximum change in energy quality of $116\ \%$ (Figure 23):

$$\Delta E_Q\big|_{\text{cumulative mass = 99.9 \%}} = 116\ \% \qquad 50$$

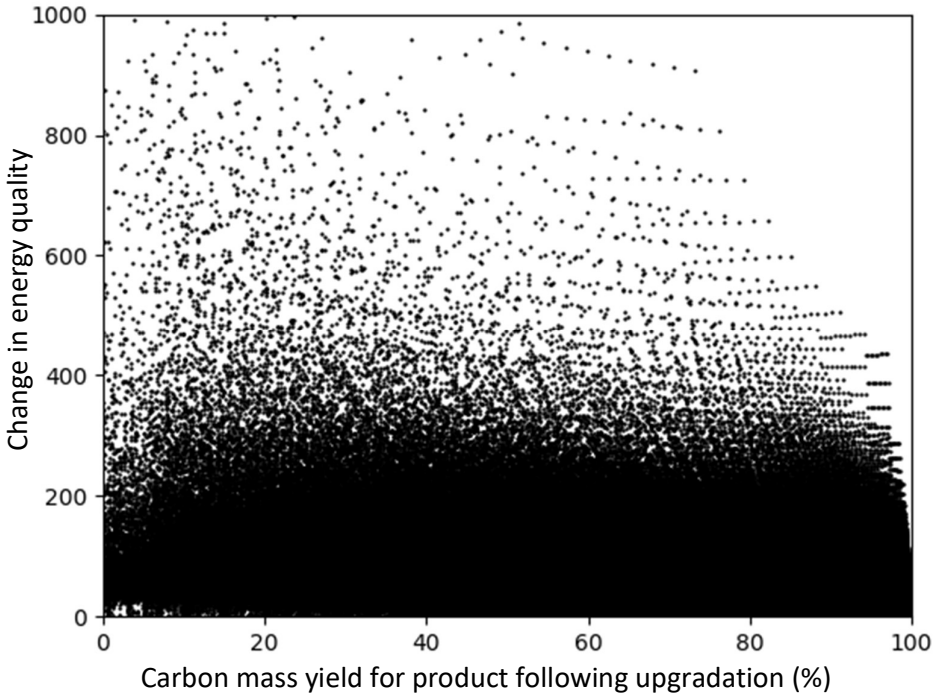

Figure 22: Total mass yield of primary product of upgradation for C:H:O-containing feedstocks

This implies that by achieving a favourable carbon yield in the product following an upgradation process, a change in energy quality of no more than $116\ \%$ can be expected with any higher change being unlikely for most feedstock. If the average biomass feedstock (with the elemental composition given in Table 3) is considered for upgradation to a fuel, the maximum possible change in energy quality obtained for a $100\ \%$ carbon yield is $\Delta E_Q = 108\ \%$. The respective ΔE_Q versus mass yield plots are given in Figure 24, and include the maximum carbon yield possible as a green line, with the boundary limit of $\Delta E_Q = \frac{m_i}{m_f} - 1$ shown in Figure 24A (red line).

The elemental mass yield that correlates the best with the data for total mass yield of Figure 24is with respect to oxygen, which is shown in Figure 24D. Point 1 represents the upper limit of upgradation via the decarboxylation pathway and achieves the second highest ΔE_Q value for pure decarboxylation. This point corresponds to a maximum yield of hydrogen ($100\ \%$, Figure 24C-1), a total reduction in oxygen (with a yield of $0\ \%$, Figure 24D-1), and a carbon yield of $62.6\ \%$ (Figure 24B-1).

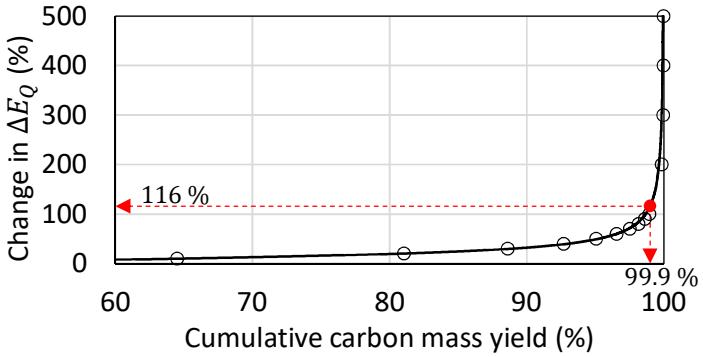

Figure 23: Relationship between cumulative carbon mass yield and the change in energy quality

The decarbonylation upgradation pathway, labelled as point 2 in Figure 24, results in the highest attainable ΔE_Q and produces similar outcomes for the hydrogen and oxygen yields while achieving the lowest carbon yield possible. The highest ΔE_Q of 108 % is achieved for a carbon yield of 100 % (Figure 24, point 3) and leads to a reduction in oxygen of almost 100 % via dehydration. This results in a substantial loss in hydrogen with a yield 3.2 % (Figure 24C-3). At this ΔE_Q the transition through points 3, 4 & 5 corresponds to changes in deoxygenation from dehydration (point 3), to decarboxylation (point 4), to decarbonylation (point 5).

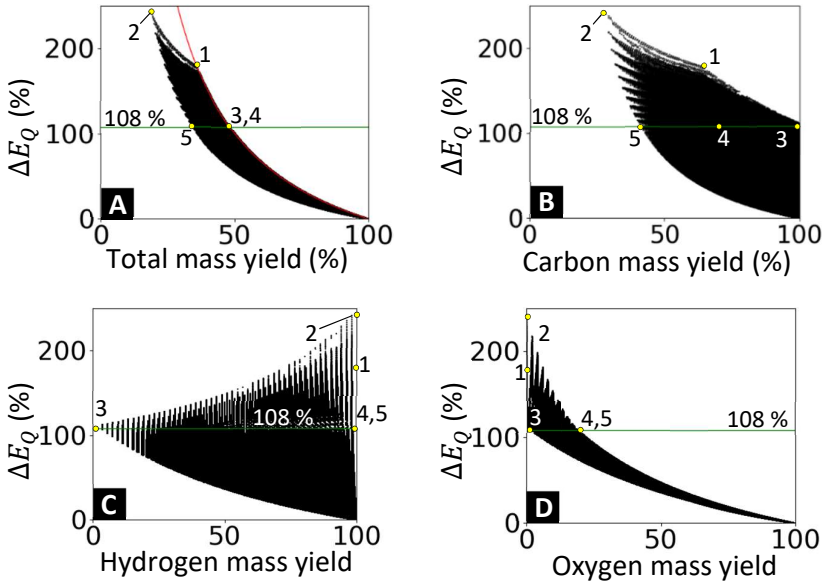

Figure 24: Comparisons of total mass yield and mass yields on a carbon, hydrogen and oxygen basis with respect to the change in energy quality using the average biomass composition of Figure 19

These results make the choice in the approach to upgradation difficult when considering maximizing a yield of one or more of the elements. If, for instance, the carbon yield is maximized, the maximum ΔE_Q cannot be achieved as hydrogen is removed almost entirely from the product. If instead the highest ΔE_Q is targeted, a reduction in the carbon yield is the necessitated result to spare the loss in hydrogen. Yet in both these instances oxygen is removed, whether by decarboxylation or dehydration, and is required if ΔE_Q is to be increased. Of the points 1,2 & 3, all of which maximize oxygen removal during upgradation, point 1 seems to be the compromise between achieving an optimal ΔE_Q and carbon yield (Figure 24D-1). This compromise supports the last approach to upgradation of the average biomass feedstock mentioned in Table 5 – where $95.5\,\%$ of oxygen is removed by decarboxylation with the remainder being removed by dehydration – limiting the loss of hydrogen from the fuel product. Hence, energy quality may be enhanced by ensuring that the hydrogen yield is optimized while decreasing oxygen as much as possible.

3.8. Summary

The shift in thinking that was introduced in Chapter 2, namely that oxygen is responsible for the exothermicity of combustion reactions, has led to further considerations concerning the objectives currently applied to biofuel synthesis and upgradation. By making use of Equation 23, it is shown that the change in energy quality, ΔE_{Q}, is dependent on the mass of oxygen consumed. The equation for ΔE_{Q}, derived with the use of Equation 23 is simply the ratio of the mass of oxygen required for combustion with respect to the product and the feed, minus 1:

$$\Delta E_{\mathrm{Q}} = \frac{m_{\mathrm{O_2}}\big|_{\mathrm{product}}}{m_{\mathrm{O_2}}\big|_{\mathrm{feed}}} - 1$$

This equation implies that improvements in ΔE_{Q}must be accompanied by increases in oxygen consumed during combustion. By using this equation in the analysis of more than 16 million data points, it is further demonstrated that a boundary limits exists for ΔE_{Q}, described as:

$$\Delta E_Q = \frac{m_i}{m_f} - 1$$

This implies that a decrease in the fuel (i.e. redundant) mass must occur in order to improve the energy quality for that fuel. These results challenge the *prima facie* objectives of maximizing mass yields of biofuels. It is also shown that maximizing carbon yields is a poor metric to use when evaluating the outcomes of biofuel synthesis.

Chapter 4: Predicting catalytic activity with pyrolysis-GC/MS data

Estimating pyrolysis oil energy quality, composition and catalytic activity by cumulative atomic ratios applied to py-GC/MS data

4.1. Introduction

It is not surprising that the physical dissociation brought about by pyrolysis processes creates products that are reminiscent of their parent feedstock – both on a mass and energy basis – in accordance with the conservation of mass and energy. Through the primary pathways of char formation, depolymerization and fragmentation, biomass is fragmented into the three products of biochar, pyrolysis oil and synthesis gas, respectively (Collard & Blin, 2014; Jahirul, et al., 2012; Mohan, et al., 2006). The similarities in physical properties pertaining to elemental composition and calorific value are very much apparent when comparing the biomass feedstock and its resulting pyrolysis oil. According to the law of mass conservation, the differences in mass distribution for pyrolysis oil when compared to biomass (i.e. percentage differences in m_{C}, m_{H}, & m_{O}) will be balanced by the simultaneous formation of synthesis gas and biochar (not shown in Table 6). Likewise, pyrolysis oils tend to have calorific values similar to those of the feedstock that produced them. However, as a biofuel, pyrolysis oil requires upgradation to increase its energy quality relative to its parent feedstock – as discussed in detail in Chapter 3 – as well as its physical properties (Bridgwater, 2012). The main issues surrounding pyrolysis oil are its inherent instability and incompatibility for use as fuel for existing transportation fuel technologies and infrastructure. Several attempts have been made to improve the quality of pyrolysis oil. Filtration is used to reduce solid particulate matter, especially biochar, while homogenization may be achieved through blending pyrolysis oil with solvents; it also decreases both instability and viscosity (Diebold & Czernik, 1997; Oasmaa, et al., 2004). An alternative blending technique aims to emulsify pyrolysis oils with conventional fuels such as diesel with the addition of surfactants (Ikura, 2003; Chiaramonti, et al., 2003).

While these methods sought to improve the physical properties of pyrolysis oils, the constituents and inherent calorific potential of pyrolysis oils remained unaltered. Catalytic upgradation differs in that it aims to modify the constituents of pyrolysis oils through catalytic

vapour cracking (Park, et al., 2011), hydrotreating (Wildschut, et al., 2010), esterification (Li, et al., 2011), and gasification for the production of Fischer-Tropsch liquids (Wright, et al., 2008). Nolte & Shanks are of the opinion that high oxygen contents in pyrolysis oils are the cause for the major challenges in utilizing pyrolysis oils, in agreement with my own conclusions made in the previous chapters of this thesis. This is partially in contrast to the theory developed by Venderbosch who suggests that oxygen is not necessarily a direct measure of pyrolysis oil quality since increases in viscosity are observed following dehydration (Venderbosch, 2015). Regardless, catalyst development for upgrading pyrolysis oils remains the focal point for research in fast pyrolysis. An analysis of the bibliometrics for the field of fast pyrolysis may be completed with the aid of the software tools VOSViewer (van Eck & Waltman, 2019), CitNetExplorer (van Eck & Waltman, 2019), and publication databases such as ScienceDirect, Web of Science and Scopus. A summary of the ten most used keywords in publications on the topic of fast pyrolysis is provided in Table 7, and shows both the number of hits and the percentage that subordinate keywords are coupled to the main keywords of "fast pyrolysis." These are ranked against the ScienceDirect dataset, as the size of the dataset dwarfs that of Web of Science and Scopus. The first three major terms relate to that of the process of fast pyrolysis, namely the temperature utilized (95 % relevance), the type of technology employed (64 %), and the type of conversion achieved (54 %).

Table 6: Most popular keywords associated with fast pyrolysis publications

Keywords		Total score					
Rank	Description	ScienceDirect		Web of Science		Scopus	
		Count	%	Count	%	Count	%
#	*Fast pyrolysis*	55 449	100	7 077	100	6 596	100
1	fast pyrolysis temperature	52 944	95	3 502	49	3 284	50
2	fast pyrolysis technology	35 396	64	805	11	711	11
3	fast pyrolysis conversion	29 726	54	2 065	29	1 150	17
4	fast pyrolysis kinetics	21 687	39	975	14	950	14
5	Catalytic fast pyrolysis	20 719	37	1 837	26	1 433	22
6	fast pyrolysis biomass	17 496	32	4 299	61	2 725	41
7	Fast pyrolysis catalysis	10 221	18	217	3	407	6
8	fast pyrolysis fluidized bed	10 217	18	1 152	16	710	11
9	Fast pyrolysis dehydration	9 101	16	182	3	143	2
10	fast pyrolysis GC/MS	9 033	16	811	11	722	11

Table 7: Data for pyrolysis oils produced from various biomass feedstock

Reference	Feedstock	Biomass properties						Pyrolysis oil properties					
		Elemental mass (%)					HHV ($\mathrm{MJ\ kg^{-1}}$)	Elemental mass (%)					HHV ($\mathrm{MJ\ kg^{-1}}$)
		C	H	O	N	S		C	H	O	N	S	
(Zheng, 2008)	maize stalk	49.1	6.1	43.7	0.7	0.1	−17.6	44.3	6.3	47.5	0.6	0.3	−26.6
(Zheng, et al., 2007)	cotton stalk	42.3	7.9	49.4	0.3	0.2	−19.4	42.3	7.9	49.4	0.3	0.2	−17.8
(Mullen & Boateng, 2008)	switchgrass	47.5	6.8	42.5	0.5	0.0	−19.8[a]	47.5	7.0	45.2	0.4	0.0	−19.0[a]
	alfalfa-early bud	44.3	5.4	38.2	2.5	0.2	−19.4[a]	53.9	8.5	32.7	4.6	0.1	−26.0[a]
	alfalfa-full flower	46.0	5.5	40.6	1.6	0.1	−18.9[a]	56.8	7.9	31.3	3.7	0.1	−26.4[a]
(Beis, et al., 2002)	safflower seed	60.5	9.1	27.4	3.1	0.0	−23.9	72.7	11.4	14.5	1.4	0.0	−38.5
								75.5	12.1	10.7	1.7	0.0	−41.1
(Oasmaa, et al., 2003)	forestry residue - green	51.4	6.0	40.0	0.5	0.0	−20.8	43.9	7.5	48.0	0.1	0.0	−22.5
								38.2	7.8	53.0	0.4	0.0	−23.2
								41.2	7.0	52.0	0.3	0.0	−22.4
								38.7	7.4	53.0	0.3	0.0	−22.1
	forestry residue - brown	51.1	5.9	38.7	0.5	0.0	−20.5	43.0	7.4	49.0	0.1	0.0	−22.9
	Pinus sylvestris	50.3	6.0	43.5	0.1	0.0	−20.6	45.7	7.0	47.0	0.1	0.0	−22.5
								43.5	7.1	49.0	0.1	0.0	−22.6
								46.7	6.7	46.0	0.1	0.0	−22.7
(Uzun & Pütün, 2006)	olive oil residue	49.1	5.6	44.2	1.1	0.0	−16.4	70.4	8.4	28.3	1.6	0.0	−30.9
								64.7	8.5	25.0	1.8	0.0	−29.7
								69.5	8.6	21.2	0.6	0.0	−32.1
								70.2	8.4	19.7	1.6	0.0	−32.4
(Acıkgoz, et al., 2004)	linseed	61.0	8.5	28.2	2.3	0.0	−28.1	75.4	10.3	13.8	1.5	0.0	−38.5
(Mullen, et al., 2010)	corn cobs	47.4	5.9	38.1	0.7	0.2	−21.2	55.1	7.6	36.9	0.6	0.0	−19.5
	corn stover	46.6	5.0	40.1	0.8	0.2	−20.9	54.0	6.9	37.9	1.2	0.0	−22.1

[a] Determined using Equation 23

The next two major terms relate to the reaction kinetics (39 %) and associated enhancements brought on by catalysis (37 %). This simple analysis of the literature affirms the critical link between the development of catalysts, upgradation via catalytic fast pyrolysis processes, and the intention of producing high-quality liquid transportation fuels. This goal is further brought to light by Liu et al. in their analysis of catalytic fast pyrolysis of lignocellulosic biomass (Liu, et al., 2014), based on a review of the major publications in the field of fast pyrolysis (Figure 25). Figure 25 was generated using the CitNetExplorer software and represents 40 of the 1 174 core publications identified from 13 887 publications with 5 or more citations for the period of 1898 to 2019 – although the first significant publications on fast pyrolysis appear in 1997.

An additional analysis can be completed by identifying what are the main textual terms appearing in the title and abstracts published in this area with the aid of the software tool VOSviewer (van Eck & Waltman, 2019). A threshold of 1 % of the top terms appearing in titles and abstracts was selected, in which 1 023 out of 10 291 terms qualified. Of these, 60 % of the most relevant terms was then selected to generate the bibliometric chart presented in Figure 26. In this Figure, lines represent a relation between two terms, where the strength of the link is weighted as being indicative of the number of publications in which two terms appear simultaneously. The terms and their respective links form a network and are grouped into and may belong to only one cluster, based on these networks. The prominence of each term is based on its weight and score, and is represented as a variance in size of each sphere. The term “catalyst”, for instance, appears to be the most prominent term of relevance to the area of fast pyrolysis according to Figure 26. The relationship between catalyst, its structure, the feedstock undergoing catalytic upgradation and the resulting fuel is an important aspect of catalyst development, as shown in Figure 27. The morphology of the catalyst for instance affects its activity toward a certain pathway of upgradation and also the selectivity of target molecules. An example is in the catalytic pyrolysis of woody biomass using zeolite-type catalysts, where zeolites selectively isomerize aromatics, aromatize low molecular weight oxygenates such as acids, alcohols, aldehydes, and deoxygenate aromatic compounds derived from the pyrolytic depolymerization of lignin (Naqvi, et al., 2015; Zheng, et al., 2014; Li, et al., 2012; Rahman, et al., 2018).

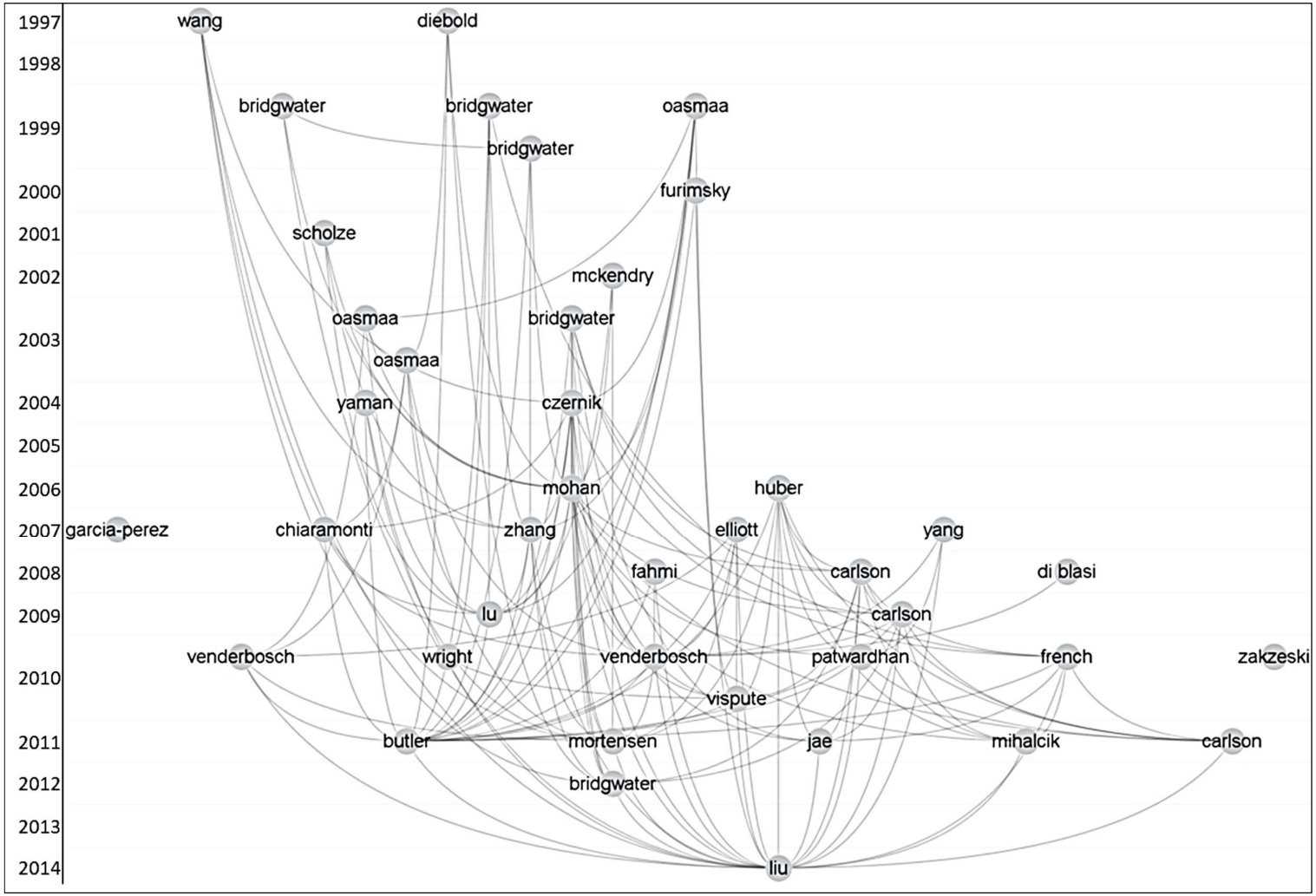

Figure 25: Graphical representation of the major publications in the field of fast pyrolysis

The conversion of glucose, the monomer that constitutes cellulose, to platform chemicals has also been demonstrated via zeolite catalysis (Puértolas, et al., 2016). Zeolites have for some time now been the go-to catalyst for upgrading pyrolysis oils, and research in this area has focused strongly on their modification, such as the incorporation of transition metals, surface modifications by chemical deposition, or altering the acidity of the catalyst by varying the Si:Al ratio. But while the development of zeolites has improved their performance in the area, more is needed to overcome the limitations that are inherent in zeolites. The search for a single-step route for upgrading complex pyrolysis oils is yet another dilemma that may require not only bifunctional and/or multiple types of catalyst, but also better process design and catalyst handling (Yildiz, et al., 2016; Dickerson & Soria, 2013). What is needed is for catalyst design to be more focused on improved catalyst performance towards cracking, with deoxygenation via decarboxylation being targeted by limited hydrogen and carbon reduction, and by resistance against deactivation via coking, etc. (Yildiz, et al., 2017).

py-GC/MS is a useful and convenient tool for research in catalytic fast pyrolysis, as quantitative investigations of product distributions following catalytic fast pyrolysis are easily completed over a wide range of temperatures, residence times, and for screening various types of catalysts (Lu, et al., 2011; Zhang, et al., 2015; Mullen & Boateng, 2010; Ohra-Aho & Linnekoski, 2015; Lu, et al., 2010). This technique achieves the quantification of pyrolysis volatiles using only small sample sizes in the milligram range, and is especially valuable where the manufacture of potential catalysts is expensive and their performance is still uncertain, and where materials & equipment available to perform pyrolysis experiments are limited. The ability to separate volatile pyrolysis products in the gas phase and identify them via GC/MS makes the analytical technique of py-GC/MS a powerful method for analysing product distributions and the approximating of syringol-guaiacol ratios associated with lignin pyrolysis, as well as catalytic activity and selectivity (Meier & Pereira, 1999; Lu, et al., 2010; Mullen & Boateng, 2010), and for identifying or optimizing selectivity for desired compounds (Lu, et al., 2013). However, the technique is not without its limitations. If additional information is required with respect to the physical properties of the pyrolysis oil as a whole, additional analytical techniques will need to be employed using larger sample/product volumes. GC/MS analysis is also limited by the availability of and access to standard reference spectra, the successful comparison of these spectra with and identification of the generated

spectra, and the sophistication of the software being used to accomplish this (Sparkman, et al., 2011).

A group of indirect methods of analysis of py-GC/MS data is proposed for estimating the calorific value, extent of deoxygenation, elemental composition and the extent of catalytic upgradation of pyrolysis oils. The development of such a method is based on the following assumptions and approaches:

- The products of pyrolysis are reminiscent of the parent feedstock.
- Gaseous compounds that remain in the gas phase at ambient conditions are not considered as part of the liquid fraction.
- Isomeric variations of molecules have a negligible effect on the overall calorific value and elemental composition of the pyrolysis oil.
- For simplicity of the validation and application of the methods, all compounds' calorific values are estimated using Equation 23 – noting that the measured calorific values could also be found in the literature if available.
- The order of the products of pyrolysis does not affect the other assumptions made, i.e. they are commutative and associative with respect to each other and do not affect the physical properties of the pyrolysis products as a whole.

Two indirect methods for determination of the elemental compositions and one graphical approach to estimating calorific values of the pyrolytic products comprising the pyrolysis oil are proposed based on these assumptions. The proposed methods are derived theoretically, demonstrated using modelled data, validated with data from the literature, and then applied to the catalytic upgrading of pyrolysis oils as follows:

- The mathematical descriptions for the two methods are derived using the abovementioned assumptions and the procedure for their application is described.
- GC chromatograms are generated for use as "pseudo-GC/MS" datasets from 357 data using a randomized approach in the determination of the mass percentages of each compound and the efficacy of the two methods are demonstrated.
- The two methods are applied to 19 sets of data from the literature that described the elemental compositions and calorific values of pyrolysis oils.
- Lastly, the two methods are lastly used in the analysis of catalysts evaluated for their effectiveness in upgrading pyrolysis oil produced from *Eucalyptus grandis* wood.

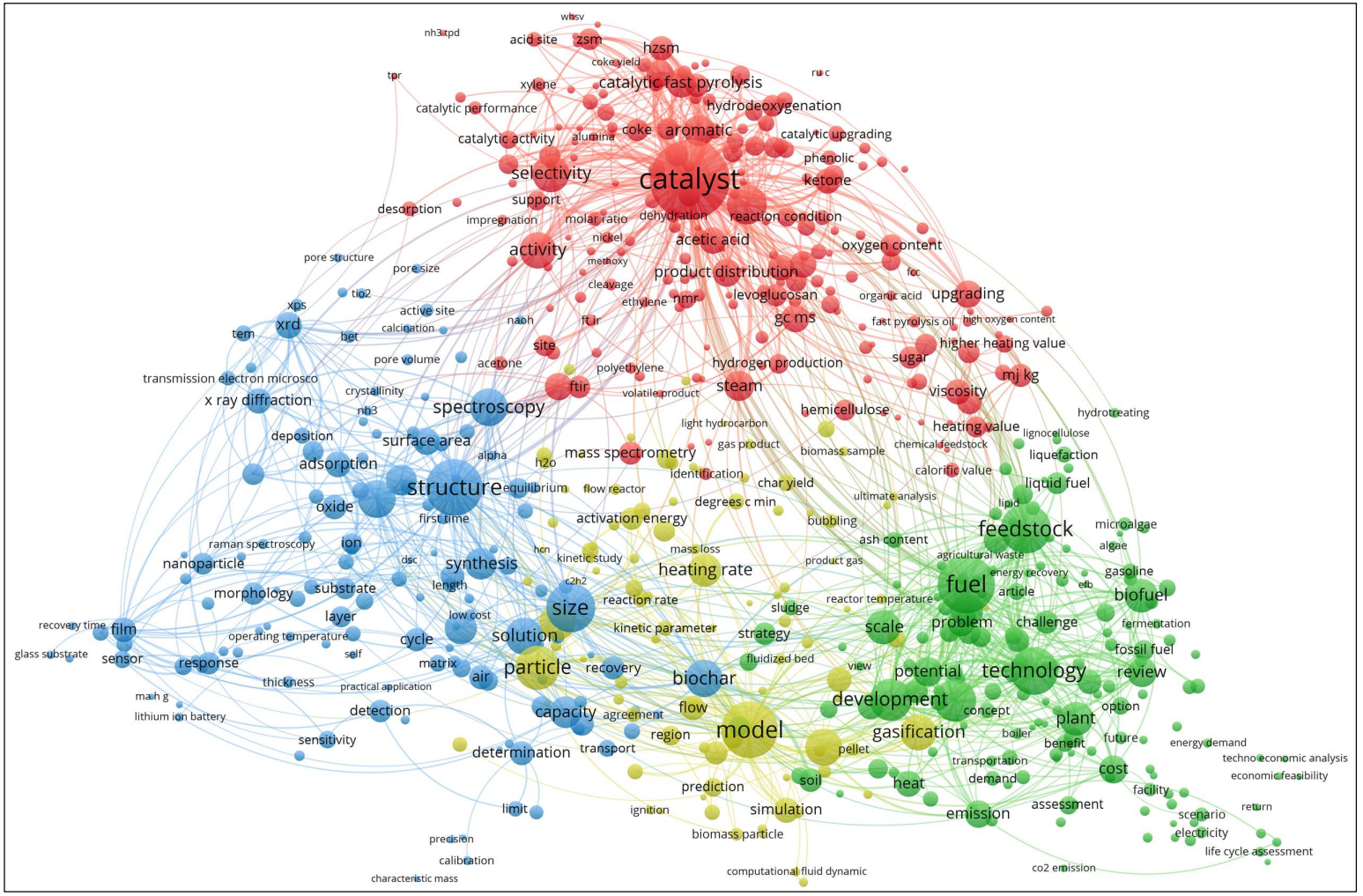

Figure 26: Graphical bibliometric analysis of major text data appearing in titles and abstracts of fast pyrolysis publications

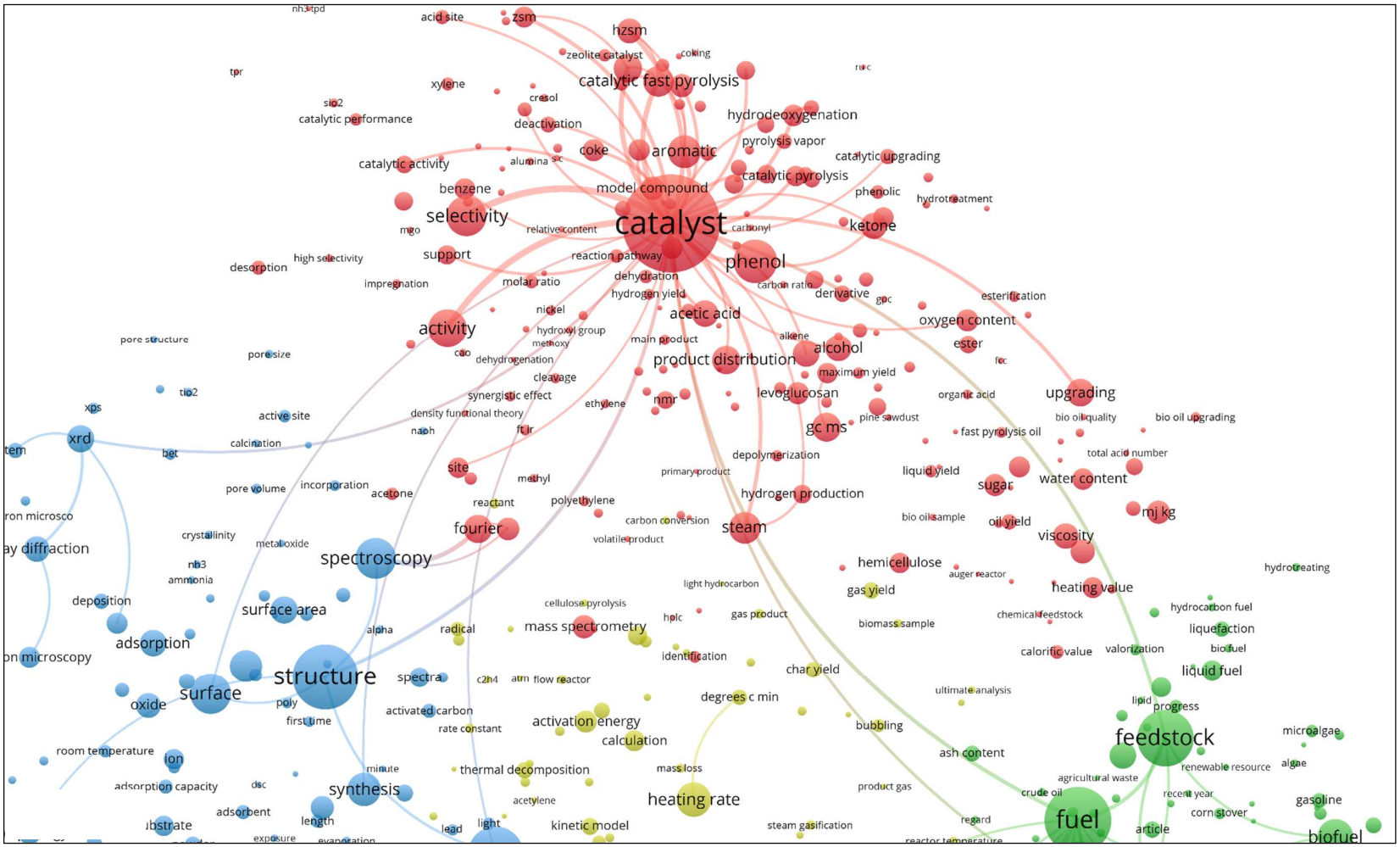

Figure 27: Graphical bibliometric analysis of fast pyrolysis showing main linkages with respect to the catalyst-related cluster

Indirect methods for the determination of mass distribution and HHV

4.1.1. Method 1: Graphical analysis using atomic ratios

If all compounds comprising pyrolysis oil are identifiable, then the atomic ratios with respect to hydrogen and oxygen, denoted as $v_{\mathrm{H}}/v_{\mathrm{C}}|_{\mathrm{pyro.oil}}$ and $v_{\mathrm{O}}/v_{\mathrm{C}}|_{\mathrm{pyro.oil}}$, are assumed to be approximated by the average atomic ratios of the individual components (i.e. on a mole basis) multiplied by the respective mass fraction of their parent molecule, respectively as:

$$\frac{v_{\mathrm{H}}}{v_{\mathrm{C}}}\Big|_{\mathrm{pyro.oil}} \sum_{i=1}^{n} \omega_i \approx \sum_{i=1}^{n} \frac{v_{\mathrm{H}_i}}{v_{\mathrm{C}_i}} \omega_i \qquad 51$$

and

$$\frac{v_{\mathrm{O}}}{v_{\mathrm{C}}}\Big|_{\mathrm{pyro.oil}} \sum_{i=1}^{n} \omega_i \approx \sum_{i=1}^{n} \frac{v_{\mathrm{O}_i}}{v_{\mathrm{C}_i}} \omega_i \qquad 52$$

where ω_i is the mass fraction of each compound in the pyrolysis oil and $\sum_{i=1}^{n} \omega_i = 1$, and the first terms on the right-hand side of approximations 51 & 52 represent the average atomic ratios (note that these equations are self-derived). If the left-hand side of approximations 51 & 52 represent true atomic ratios for pyrolysis oil, then the right-hand side is the approximation based on an average of all the atomic ratios of the components of the pyrolysis oil. In the unlikely event that every component has exactly the same atomic ratio as in the parent feedstock, then the approximations may instead be described by equations. The error ϵ is defined as the difference between the left- and right-hand sides of approximations 51 and 52:

$$\epsilon = \sum_{i=1}^{n} \frac{v_{\mathrm{H}_i}}{v_{\mathrm{C}_i}} \omega_i - \frac{v_{\mathrm{H}}}{v_{\mathrm{C}}}\Big|_{\mathrm{pyro.oil}} \sum_{i=1}^{n} \omega_i \qquad 53$$

and

$$\epsilon = \sum_{i=1}^{n} \frac{v_{\mathrm{O}_i}}{v_{\mathrm{C}_i}} \omega_i - \frac{v_{\mathrm{O}}}{v_{\mathrm{C}}}\Big|_{\mathrm{pyro.oil}} \sum_{i=1}^{n} \omega_i \qquad 54$$

Applying Equations 53 and 54 to Approximations 52 & 53 and rearranging yields the following

$$\sum_{i=1}^{n} \frac{v_{\mathrm{H}_i}}{v_{\mathrm{C}_i}} \omega_i = \left.\frac{v_{\mathrm{H}}}{v_{\mathrm{C}}}\right|_{\text{pyro.oil}} \sum_{i=1}^{n} \omega_i + \epsilon \qquad 55$$

and

$$\sum_{i=1}^{n} \frac{v_{\mathrm{O}_i}}{v_{\mathrm{C}_i}} \omega_i = \left.\frac{v_{\mathrm{O}}}{v_{\mathrm{C}}}\right|_{\text{pyro.oil}} \sum_{i=1}^{n} \omega_i + \epsilon \qquad 56$$

with $\sum_{i=1}^{n} \frac{v_{\mathrm{H}_i}}{v_{\mathrm{C}_i}} \omega_i = f(\sum_{i=1}^{n} \omega_i)$ and $\sum_{i=1}^{n} \frac{v_{\mathrm{O}_i}}{v_{\mathrm{C}_i}} \omega_i = f(\sum_{i=1}^{n} \omega_i)$, with $v_{\mathrm{H}}/v_{\mathrm{C}}|_{\text{pyro.oil}}$ and $v_{\mathrm{O}}/v_{\mathrm{C}}|_{\text{pyro.oil}}$ being the gradients of Equation 55 and Equation 56 respectively. As not all compounds would be known, Equation 55 and Equation 56 can only be applied to j number of compounds with the rest remaining unknown according to the expressions

$$\sum_{i=1}^{j} \frac{v_{\mathrm{H}_i}}{v_{\mathrm{C}_i}} \omega_i + \sum_{i=j}^{n} \frac{v_{\mathrm{H}_i}}{v_{\mathrm{C}_i}} \omega_i = \left.\frac{v_{\mathrm{H}}}{v_{\mathrm{C}}}\right|_{\text{pyro.oil}} \sum_{i=1}^{j} \omega_i + \left.\frac{v_{\mathrm{H}}}{v_{\mathrm{C}}}\right|_{\text{pyro.oil}} \sum_{i=j}^{n} \omega_i + \epsilon$$

$$\sum_{i=1}^{j} \frac{v_{\mathrm{H}_i}}{v_{\mathrm{C}_i}} \omega_i = \left.\frac{v_{\mathrm{H}}}{v_{\mathrm{C}}}\right|_{\text{pyro.oil}} \sum_{i=1}^{j} \omega_i + \left.\frac{v_{\mathrm{H}}}{v_{\mathrm{C}}}\right|_{\text{pyro.oil}} \sum_{i=j}^{n} \omega_i - \sum_{i=j}^{n} \frac{v_{\mathrm{H}_i}}{v_{\mathrm{C}_i}} \omega_i + \epsilon$$

and if

$$\left.\frac{v_{\mathrm{H}}}{v_{\mathrm{C}}}\right|_{\text{pyro.oil}} \sum_{i=j}^{n} \omega_i \cong \sum_{i=j}^{n} \frac{v_{\mathrm{H}_i}}{v_{\mathrm{C}_i}} \omega_i$$

then

$$\sum_{i=1}^{j} \frac{v_{\mathrm{H}_i}}{v_{\mathrm{C}_i}} \omega_i = \left.\frac{v_{\mathrm{H}}}{v_{\mathrm{C}}}\right|_{\text{pyro.oil}} \sum_{i=1}^{j} \omega_i + \epsilon \qquad 57$$

and similarly

$$\sum_{i=1}^{j} \frac{v_{\mathrm{O}_i}}{v_{\mathrm{C}_i}} \omega_i = \frac{v_{\mathrm{O}}}{v_{\mathrm{C}}}\Big|_{\mathrm{pyro.oil}} \sum_{i=1}^{j} \omega_i + \epsilon \qquad 58$$

Equation 57 and Equation 58 may be used to estimate the atomic ratios $v_{\mathrm{H}}/v_{\mathrm{C}}|_{\mathrm{pyro.oil}}$ and $v_{\mathrm{O}}/v_{\mathrm{C}}|_{\mathrm{pyro.oil}}$, which are the respective gradients of Equation 57 and Equation 58, by plotting data for $\sum_{i=1}^{j} \frac{v_{\mathrm{H}_i}}{v_{\mathrm{C}_i}} \omega_i$ and $\sum_{i=1}^{j} \frac{v_{\mathrm{O}_i}}{v_{\mathrm{C}_i}} \omega_i$ against their respective mass fractions $\sum_{i=1}^{j} \omega_i$.

4.1.2. Method 2: Graphical analysis using elemental mass fractions

The total mass fraction for entity A is given by

$$\frac{m_A}{m} = \omega_A \qquad 59$$

and the mass fraction of entity A for molecule i is similarly defined as

$$\frac{m_{A_i}}{m_i} = \omega_{A_i} \qquad 60$$

Equation 59 and Equation 60 relate to each other by the following equation:

$$\frac{m_A}{m} = \frac{m_{A_1} + m_{A_2} + \cdots + m_{A_{n-1}} + m_{A_n}}{m_1 + m_2 + \cdots + m_{n-1} + m_n} = \frac{\sum_{i=1}^{n} m_{A_i}}{\sum_{i=1}^{n} m_i} = \sum_{i=1}^{n} \frac{m_{A_i}}{m_i} \qquad 61$$

Equation 61 may be rewritten into sum notation and rearranged as

$$\sum_{i=1}^{n} m_{A_i} = \frac{m_A}{m} \sum_{i=1}^{n} m_i \qquad 62$$

where m_A/m is constant and represents the gradient, while $\sum_{i=1}^{n} m_{A_i} = f(\sum_{i=1}^{n} m_i)$. This describes an ideal case where all n number of compounds are known, whereas in reality only j number of compounds are actually known, according to the expression

$$\sum_{i=1}^{n} m_{A_i} = \frac{m_A}{m} \sum_{i=1}^{j} m_i + \frac{m_A}{m} \sum_{i=j}^{n} m_i \qquad 63$$

with the last term $\frac{m_A}{m}\sum_{i=j}^{n} m_i$ representing the sum of the masses for all unknown compounds. Equation 63 may be rewritten using Equation 60 as

$$\sum_{i=1}^{n}\left(\omega_{A_i} m_i\right) = \frac{m_A}{m}\sum_{i=1}^{j} m_i + \frac{m_A}{m}\sum_{i=j}^{n} m_i \qquad 64$$

Since $\frac{m_A}{m}$ is constant and can be written as $\frac{m_A}{m} = \frac{\sum_{i=1}^{n} m_{A_i}}{\sum_{i=1}^{n} m_i} = \frac{\sum_{i=j}^{n} m_{A_i}}{\sum_{i=j}^{n} m_i}$, Equation 64 may also be rewritten and rearranged as follows:

$$\sum_{i=1}^{n}\left(\omega_{A_i} m_i\right) = \frac{m_A}{m}\sum_{i=1}^{j} m_i + \frac{\sum_{i=1}^{n} m_{A_i}}{\sum_{i=1}^{n} m_i}\sum_{i=j}^{n} m_i = \frac{m_A}{m}\sum_{i=1}^{j} m_i + \sum_{i=j}^{n} m_i \frac{m_{A_i}}{m_i}$$

$$\sum_{i=1}^{n}\left(\omega_{A_i} \cdot m_i\right) = \frac{m_A}{m}\sum_{i=1}^{j} m_i + \sum_{i=j}^{n} m_i \omega_{A_i}$$

$$\sum_{i=1}^{n}\left(\omega_{A_i} \cdot m_i\right) - \sum_{i=j}^{n} m_i \omega_{A_i} = \frac{m_A}{m}\sum_{i=1}^{j} m_i$$

$$\sum_{i=1}^{j}\left(\omega_{A_i} m_i\right) = \omega_A \sum_{i=1}^{j} m_i \qquad 65$$

The first assumption applied in the derivation of Equation 65 is that the pyrolytic products are reminiscent of their parent feedstock. This is only an approximation and some deviation with respect to $\sum_{i=1}^{j} \omega_{A_i}$ and ω_A is expected from the ideal such that

$$\sum_{i=1}^{j}\left(\omega_{A_i} m_i\right) \approx \omega_A \sum_{i=1}^{j} m_i \qquad 66$$

An expression describing this deviation, ϵ, may be derived as follows:

$$\epsilon = \omega_A \sum_{i=1}^{j} m_i - \sum_{i=1}^{j}\left(\omega_{A_i} m_i\right)$$

$$\epsilon = \sum_{i=1}^{n} \omega_{A_i} \sum_{i=1}^{j} m_i - \sum_{i=1}^{j} (\omega_{A_i} m_i)$$

$$\epsilon = \left(\sum_{i=1}^{j} \omega_{A_i} + \sum_{i=j}^{n} \omega_{A_i} \right) \sum_{i=1}^{j} m_i - \sum_{i=1}^{j} (\omega_{A_i} m_i)$$

$$\epsilon = \sum_{i=1}^{j} \omega_{A_i} \sum_{i=1}^{j} m_i + \sum_{i=j}^{n} \omega_{A_i} \sum_{i=1}^{j} m_i - \sum_{i=1}^{j} (\omega_{A_i} m_i)$$

$$\epsilon = \sum_{i=j}^{n} \omega_{A_i} \sum_{i=1}^{j} m_i \qquad 67$$

Adding Equation 67 to Equation 66 yields the following:

$$\sum_{i=1}^{j} (\omega_{A_i} m_i) = \omega_A \sum_{i=1}^{j} m_i + \sum_{i=j}^{n} \omega_{A_i} \sum_{i=1}^{j} m_i$$

$$\sum_{i=1}^{j} (\omega_{A_i} m_i) = \sum_{i=1}^{j} m_i \left(\omega_A + \sum_{i=j}^{n} \omega_{A_i} \right) \qquad 68$$

Similar to the Equation 57 and Equation 58 of the first method, Equation 68 may be used to estimate the mass fraction for component A in the whole pyrolytic product, ω_A, by plotting the sum of the known elemental mass fractions of A, $\sum_{i=1}^{j} (\omega_{A_i} m_i)$, against the sum of the respective mass fractions, $\sum_{i=1}^{j} m_i$.

4.2. Generation of pseudo-GC/MS data

Three randomized sets of data are generated to model three GC chromatograms with peak areas all known quantitatively, the data of which are collectively referred to here as pseudo-GC/MS data. To generate these three sets of data, the same 327 data points that produced Figure 7 are used, but with compounds containing non-typical atoms being excluded (such as Cl, Br, P, etc.). Firstly, the 357 data are sorted relative to their oxygen content on a molar

basis, where compounds with $v_{\mathrm{O}}/v_{\mathrm{C}} < 0.21$ are classified as being low in oxygen content, compounds with $0.21 \leq v_{\mathrm{O}}/v_{\mathrm{C}} < 0.67$ are moderately oxygenated, and compounds with $0.67 \leq v_{\mathrm{O}}/v_{\mathrm{C}}$ are classified as being high in oxygen content. Secondly, each compound is allocated a randomly generated peak area. The compounds are thirdly sorted into three groups based on their oxygen content classification of low oxygen, moderate oxygen and high oxygen. Fourthly, for every group, each compound area is plotted consecutively at randomized time intervals, as shown in Figure 28. As the mass percentages and calorific values are easily determined for the 357 data used to generate the three pseudo-GC/MS data sets, it is easy to test the two indirect methods proposed here against that of the pseudo-GC/MS. The implementation of the first indirect method estimates all the atomic ratios for each set of compounds with the use of Equation 57 and Equation 58. These are presented as six plots in Figure 29. The data for each set of low, moderate, and high oxygen content shows adequate linearity for both atomic ratios. The estimation of the O/C ratios are similar, with average absolute errors of 0.01 for both the low and high oxygen datasets, and 0.03 with respect to the high oxygen dataset. It is an easy task to convert these H/C & O/C ratios to mass percentages for the elements by selecting a basis of 1 mole of carbon, using the following calculation:

$$m_A = \frac{v_A \times M_A}{\left(1 + \frac{v_{\mathrm{H}}}{v_{\mathrm{C}}} + \frac{v_{\mathrm{O}}}{v_{\mathrm{C}}}\right)} \times 100\ \%$$

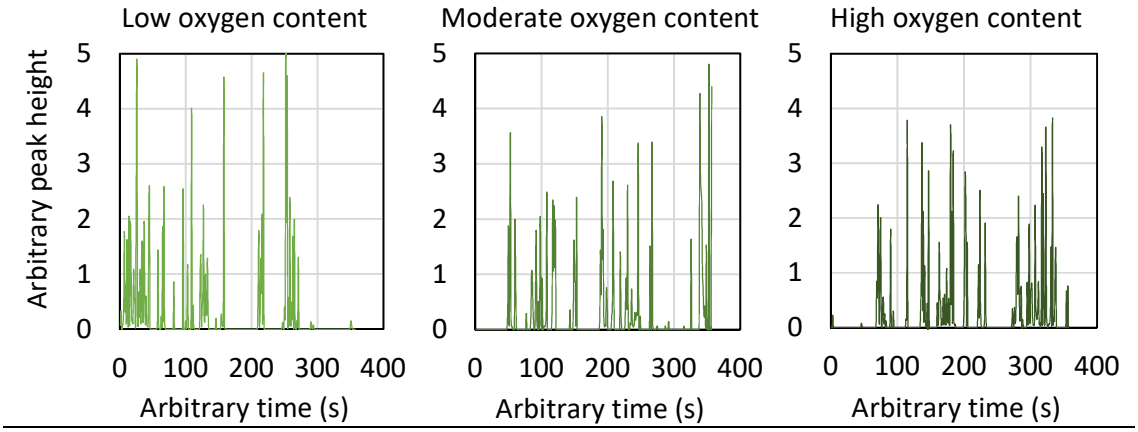

Figure 28: Plot of randomly generated pseudo-GC/MS chromatograms

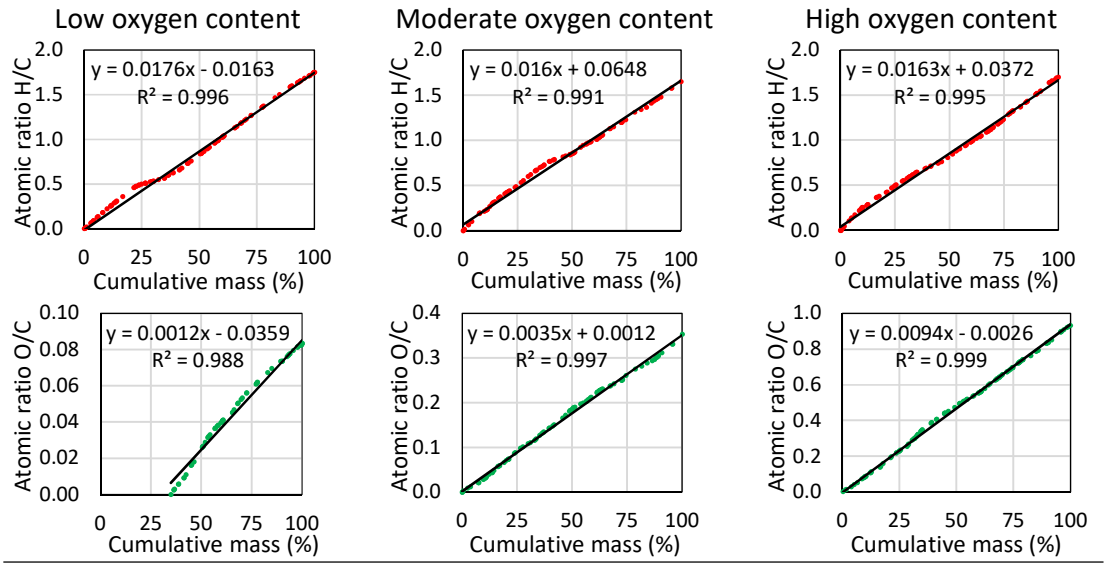

Figure 29: Plot of cumulative H/C and O/C ratio fractions against the respective cumulative mass fractions for three sets of model data for low, moderate, and high oxygen-containing compounds

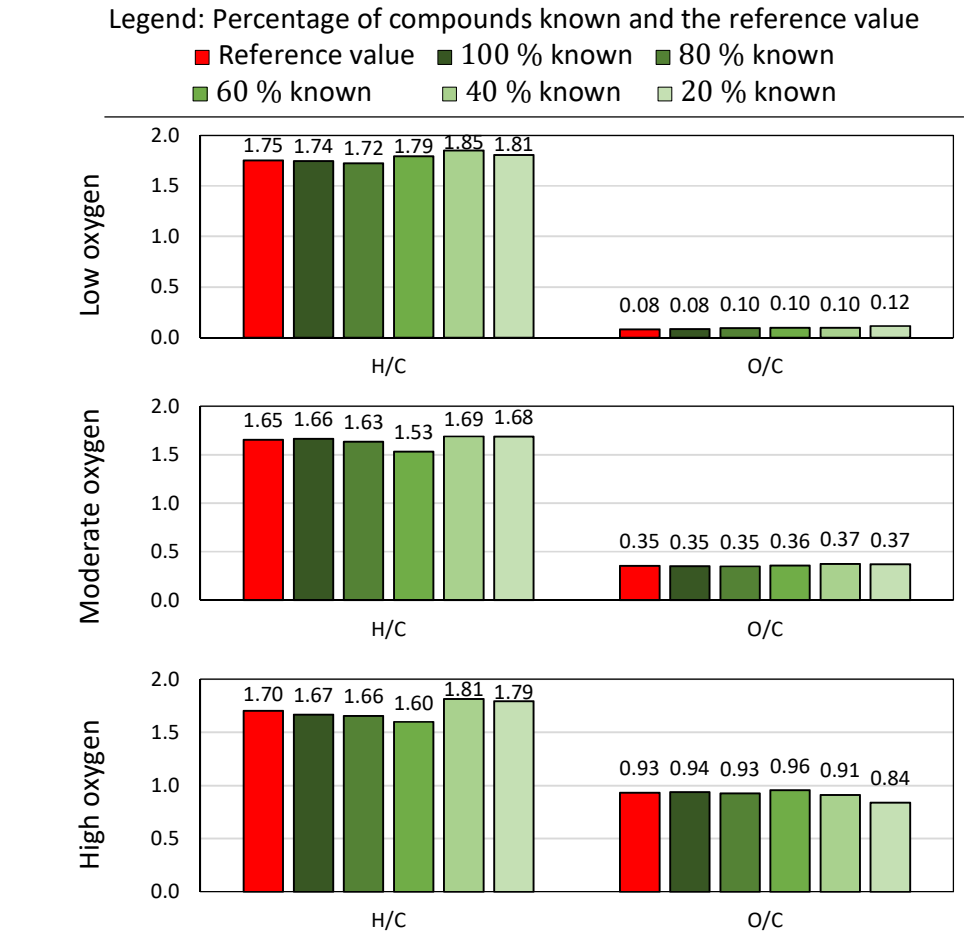

Figure 30: Sensitivity analysis of estimating atomic ratios using Equations 57 and 58

These data of elemental mass percentages, calculated at the various oxygen contents and for different portions of the pseudo-GC/MS datasets specified, are summarized (Estimation-1) with the known compositions (Model data) in Table 8. The absolute error more or less increases with a decrease in the percentage of data used or available. For example, with the low oxygen-based dataset, if between $60\,\%$ and $80\,\%$ of data is used to estimate the elemental mass composition in this estimation, an error of roughly $5.5\,\%$ is obtained. If, however, only $20\,\%$ of data is used or available instead, the error almost doubles to $12.6\,\%$. This is expected, as the total elemental masses always have to be extrapolated regardless of the linearity presented in the data plotted in Figure 29. The maximum absolute error is, however, lower in the case of the high oxygen-based data ($7.2\,\%$) and more so for the dataset with moderate oxygen ($2.9\,\%$).

The second method of estimating the elemental masses is more direct and concise compared to the first, since the latter first requires the determination of the atomic ratios graphically and then a conversion of these ratios to the respective masses. The second indirect method plots the mass percentages immediately with the aid of Equation 68 and extrapolates the elemental masses using the trendline equation obtained from the data trend. The plots for the application of this second method applied to the pseudo-GC/MS data, where $100\,\%$ of each data set is used, are given in Figure 31. The same linearity is observed using this method as was observed with the first. Likewise, the magnitude of absolute errors for the second indirect method, shown in Table 8 as Estimation-2, is similar to the first for all three of the pseudo-GC/MS datasets. In this theoretical demonstration, it appears that both indirect methods provide reasonably good approximations of the elemental compositions of the pseudo-GC/MS datasets. Where less than $100\,\%$ of data is used for evaluating the accuracy of the second indirect method, the respective plots are provided in Figure A5 to Figure A13 in the Appendix. Subsequently, if a close approximation of the elemental composition is possible, this may be used in the determination of the calorific value. For this we may either make use of the accurate one parameter Equation 23 to determine the higher heating value, or source measured calorific values from the literature. The cumulative calorific values for each component may be used in a similar fashion as the cumulative atomic ratios are used in Equation 57 and Equation 58, where the cumulative higher heating values are directly substituted, being described as a function of the cumulative mass fraction as follows:

Table 8: Summary of elemental mass percentages determined directly (model) and indirectly (estimated) for three pseudo-GC/MS datasets using two indirect methods

Oxygen content	Known compounds	Model data			Estimation-1 data				Estimation-2 data			
		Elemental mass			Elemental mass			AE	Elemental mass			AE
		% C	% H	% O	% C	% H	% O	%	% C	% H	% O	%
Low	100	79.5	11.7	8.8	79.5	11.6	8.9	0.42	80.3	11.2	7.9	5.34
	80				78.7	11.4	10.0	5.45	79.4	11.2	8.8	1.59
	60				78.1	11.8	10.1	5.46	79.2	11.9	7.8	4.46
	40				77.9	12.1	10.0	6.17	79.0	12.2	8.4	3.32
	20				76.6	11.6	11.8	12.63	76.8	11.3	11.5	12.35
Moderate	100	62.1	8.6	29.2	62.2	8.7	29.1	0.40	62.6	8.7	28.7	1.19
	80				62.5	8.6	28.9	0.74	62.9	8.6	28.5	1.35
	60				62.4	8.0	29.6	2.94	62.8	8.1	28.9	2.86
	40				61.0	8.6	30.3	1.90	61.4	8.6	30.0	1.34
	20				61.1	8.6	30.2	1.75	61.6	8.6	29.8	0.98
High	100	41.9	6.0	52.1	41.9	5.9	52.3	0.97	42.6	5.9	51.4	1.47
	80				42.1	5.9	52.0	0.98	43.0	6.0	51.1	1.69
	60				41.6	5.6	52.9	3.15	42.4	5.7	51.8	2.32
	40				42.3	6.4	51.3	3.23	43.0	6.5	50.5	4.63
	20				44.1	6.6	49.2	7.22	44.7	6.6	48.7	7.90

$$\sum_{i=1}^{j} \Delta_c h^{\circ}\big|_{\mathrm{HHV},i}\,\omega_i = \Delta_c h^{\circ}\big|_{\mathrm{HHV}} \sum_{i=1}^{j} \omega_i + \epsilon \qquad 69$$

where Equation 69 adopts the same form as Equation 57 and Equation 58. Also, as with Equation 57 and Equation 58, the gradient of Equation 69 represents the total calorific value for the pyrolytic product being assessed, and is taken as an estimate if less than 100 % of compounds are used to determine this value.

The application of Equation 69 to the three pseudo-GC/MS datasets yields the plots shown in Figure 32. The coefficients of determination for the three sets of data are very close to 1.00, which suggests almost no deviation from the linear correlation proposed by Equation 69—since low residual variances accompany high coefficients of determination. The effects of using a smaller portion of the pseudo-GC/MS datasets for calorific predictions on the absolute error and variances in these estimations are only slight (Table 9, Estimation-1), with no clear or obvious increases or decreases in the estimated HHVs.

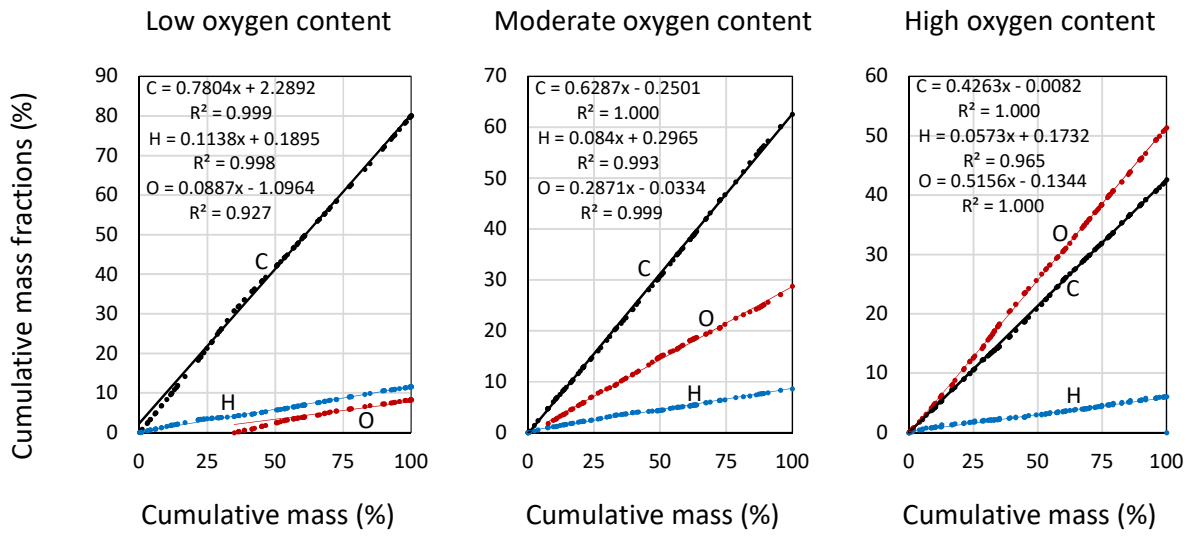

Figure 31: Plot of cumulative elemental mass fractions against the respective cumulative mass fractions for three sets of model data for low, moderate, and high oxygen-containing compounds

Comparable results are produced when the estimations of elemental mass composition obtained by the second indirect method are used to predict the HHV's for the three pseudo-GC/MS datasets. The average absolute errors and variances of the three datasets are very similar, and it is therefore not easy to decide whether the first or second indirect method is more suitable in predicting calorific values for pyrolysis products from GC/MS data. The small deviation in estimating calorific values, even when only 20 % of data is used to do so, was not expected. Unlike real data for pyrolytic products produced from a more homogeneous feedstock such as woody biomass, the data used to produce the three sets of pseudo-GC/MS data vary considerably, from various forms hydrocarbons (some containing nitrogen and/or oxygen too), to coals, to biodiesel and biomass.

Together, these results support the notion that a linearity exists between the cumulative fractions of atomic ratios and their respective cumulative mass fractions, and is a validation of the assumption that products of pyrolysis are reminiscent to their parent feedstock on a mass and energy basis. At least on this theoretical basis, the cumulative fractions of atomic ratios as well as calorific values as functions of the cumulative mass fractions are good predictors of the overall elemental compositions and calorific values, respectively. Such methods are characterized by low residual variances and acceptable accuracies, regardless of how well datasets are characterized.

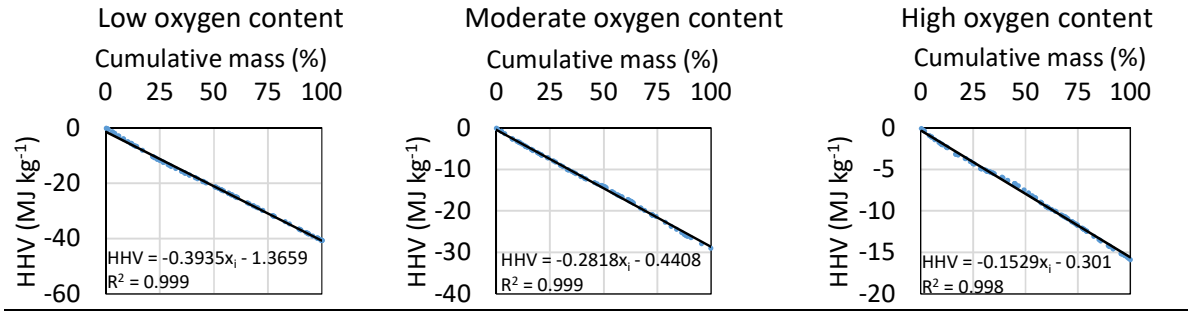

Figure 32: Cumulative calorific value of each component plotted against the mass fraction of the respective component

Table 9: Accuracy of estimations of heating values for modelled pyrolysis oil of various oxygen contents

Oxygen content	Known compounds	Model data	Estimation-1 data				Estimation-2 data			
		HHV	HHV	AE			HHV	AE		
		$MJ\ kg^{-1}$	$MJ\ kg^{-1}$	%	Avg. (%)	Var. (%)	$MJ\ kg^{-1}$	%	Avg. (%)	Var. (%)
Low	100	−40.7	−41.0	0.3	0.5	0.3	-41.5	0.8	0.8	0.8
	80		−40.2	0.5			−40.7	0.1		
	60		−40.5	0.2			−41.7	1.0		
	40		−40.8	0.1			−41.6	1.0		
	20		−39.5	1.1			−39.4	1.3		
Moderate	100	−29.0	−28.4	0.6	0.6	0.1	−28.7	0.2	0.6	0.1
	80		−28.8	0.2			−28.8	0.2		
	60		−28.0	1.0			−28.1	0.8		
	40		−28.2	0.7			−28.0	1.0		
	20		−28.3	0.7			−28.1	0.8		
High	100	−15.9	−15.6	0.3	0.8	0.9	−15.1	0.7	0.7	0.7
	80		−15.5	0.4			−15.4	0.5		
	60		−14.8	1.1			−14.8	1.1		
	40		−16.3	0.5			−16.0	0.2		
	20		−17.5	1.7			−17.1	1.2		

4.3. Model validation: elemental composition estimation

In the previous section, only pseudo GC/MS data were used to develop and validate the two indirect methods proposed for use in estimating the elemental mass compositions and calorific values from limited availability of data. Although this was on the theoretical basis, a greater variance of data used to generate these pseudo-GC/MS datasets was introduced by including materials that were unsimilar in composition and unrelated to one another in morphology and/or calorific value. This exercise in the development and validation of the two indirect methods is concluded with some favourable results and warrants further validation using data from the literature.

In order to validate both methods of indirect determination of elemental mass composition and calorific value, literature sources are sourced based on meeting the following criteria:

- The elemental compositions for pyrolysis oils are reported.
- GC/MS data are provided for pyrolysis oils.
- Calorific values of the pyrolysis oils are reported.

A total of 10 sources were identified that comply with all these criteria, providing data for 19 different types of pyrolysis oil, produced from various feedstocks and by various pyrolysis processes. Ingram et al. (2008) report four sets of data for wood and bark of pine and oak pyrolyzed using an auger reactor. Zheng (2008) reports data for pyrolysis oil produced from maize stalk using an electrically heated fluidized bed pyrolyzer with sand as the bed material. In a similar setup, Zheng et al. (2007) produce pyrolysis oil from cotton stalk. Zhang et al. (2005) carry out pyrolytic upgradation of sawdust in a fluidized bed. A comparison of the corrosive properties of pyrolysis oil produced from rice husk, and emulsions of the same with diesel, is reported by Lu et al. (2008). In an investigation of improving the properties of pyrolysis oils, Scholze (2002) provides an extensive analysis of four different pyrolysis oils produced from beech wood, mixed hardwood, *Eucalyptus* wood, and pine wood. Mullen et al. (2009) give an analysis and comparison of three pyrolysis oils produced from barley-based substrates, and additional data are reported for two pyrolysis oils produced from corn cobs and stover (Mullen, et al., 2010). Ateş & Işikdağ (2008) evaluate the relationship between pyrolytic temperature for pyrolysis oils produced from wheat and oat straws. These data collectively are summarized in Table 10 with respect to the elemental analyses of pyrolysis

oils and in Table 11 with respect to the calorific values. The reported data pertaining to elemental analyses are compared in Table 10 to estimations using either the indirect method of cumulative HHVs (Estimation 1.1), the determination of atomic ratios using Equation 57 and Equation 58 (Estimation-1.2), or the second indirect method which estimates the elemental compositions directly (Estimation-2). Estimations for nitrogen and sulphur are also possible using these two indirect methods of estimation, but are not included as these two elements are assumed to contribute negligibly to the overall purpose of validation. Absolute errors, given in units of per cent, are shown for each estimation as an average for each of the elements, using the formula

$$\mathrm{AE} = \frac{1}{n}\sum_{i=1}^{n}\left|m|_{A_i,\mathrm{est.}} - m|_{A_i,\mathrm{meas.}}\right| \times 100\ \% \qquad 70$$

With regard to the elemental analyses, most of the estimations fare well according to the absolute errors reported in Table 10. Out of 19, only two estimations have absolute errors of greater than $10\ \%$ for estimation-1, while three estimations are above this threshold for Estimation-2. One of these estimations with an absolute error of $22\ \%$ (based on Estimation-1, and $21\ \%$ according to Estimation-2) also presents conflicting data for the HHV reported (Table 10; Mullen, et al., 2009). If the elemental analysis is used to calculate the HHV using Equation 23, a value of $-37.4\ \mathrm{MJ\ kg^{-1}}$ is obtained, which is much higher than the reported $-18.7\ \mathrm{MJ.\ kg^{-1}}$ (Table 11; Mullen, et al., 2009). However, when the same estimations of the elemental analyses are used to determine the HHV using Equation 23, HHVs are obtained that are very similar to the reported value of $-18.7\ \mathrm{MJ\ kg^{-1}}$, namely between $-19.2\ \mathrm{MJ\ kg^{-1}}$ and $-18.7\ \mathrm{MJ\ kg^{-1}}$ for Estimation-1, and $-19.2\ \mathrm{MJ\ kg^{-1}}$ for Estimation-2 (Table 11, Mullen, et al., 2009). It should also be noted that only $9\ \%$ of the total mass is characterized, which may also have contributed to some of this error. The only other set of elemental mass data that produces an absolute error of greater than $10\ \%$ is that of Zheng, et al. (2007), which has an absolute error of $12\ \%$ for Estimation-1 and $16\ \%$ for Estimation-2. In the analysis of HHV estimations that make use of the two indirect methods previously developed (Table 11), two options of estimation are provided for the first method and one for the second indirect method. Estimation-1.1 uses the graphical approach for estimating the HHV, which employs 69 data points and the resulting data are plotted to fit a linear trendline.

Table 10: Comparison of estimations of elemental compositions with measured values reported in the literature

GC/MS characterization data from literature		Elemental composition												
References	Mass characterized (% of total)	Reported values (mass %)					Estimation-1 (mass %)			AE (%)	Estimation-2 (mass %)			AE (%)
		C	H	O	N	S	C	H	O		C	H	O	
(Ingram, et al., 2008)	28	53	8	40	0.1	0.0	57	6	37	3	59	6	34	4
	35	47	5	50	0.1	0.0	54	6	40	6	56	6	37	8
	31	54	7	38	0.4	0.0	56	7	37	1	52	6	42	2
	18	45	6	48	0.3	0.3	58	6	36	8	61	6	33	10
(Zheng, 2008)	23	44	6	48	0.6	0.3	56	7	37	7	58	8	35	9
(Zheng, et al., 2007)	22	42	8	49	0.3	0.2	60	7	33	12	66	8	26	16
(Zhang, et al., 2005)	34	60	7	42	0.9	0.0	49	8	43	4	51	8	41	3
(Lu, et al., 2008)	7	38	8	54	0.6	0.0	40	7	53	2	46	8	46	6
(Scholze, 2002)	23	52	8	40	0.37	0.0	47	7	47	4	48	7	45	3
	19	57	6	36	0.32	0.0	45	7	48	8	47	7	46	7
	18	54	6	39	0.39	0.0	44	7	49	7	45	7	48	6
	19	55	6	39	0.47	0.0	46	7	47	6	47	7	46	5
(Mullen, et al., 2010)	29	55	8	37	0.56	0.0	48	7	45	5	50	7	43	4
	33	54	7	38	1.18	0.0	45	7	48	6	47	7	46	5
(Mullen, et al., 2009)	19	51	3	44	1.37	0.0	48	7	44	3	49	8	43	3
	18	55	5	38	1.79	0.0	48	7	45	5	49	7	44	5
	4	74	9	12	5.05	0.4	47	6	46	22	49	6	44	21
(Ateş & Işikdağ, 2008)	96	71	9	20	0.5	0.0	71	8	22	1	72	9	19	0
	93	65	7	27	1.3	0.0	73	7	19	5	74	8	18	6
									Average AE:	6			Average AE:	6

Table 11: Comparison of estimations of elemental compositions with measured values reported in the literature

Data sourced from the literature			Estimation of higher heating values								
Reference	Reported HHV		HHV estimations (MJ kg^{-1})			Difference (%)			Absolute error (MJ kg^{-1})		
	Method	Value (MJ kg^{-1})^{daf}	Est.-1.1*	Est.-1.2*	Est.-2	Est.-1.1*	Est.-1.2*	Est.-2	Est.-1.1*	Est.-1.2*	Est.-2
(Ingram, et al., 2008)	Measured	−26.1	−24.2	−23.7	−24.8	−7	−9	−5	1.9	2.4	1.3
	Measured	−24.1	−22.5	−21.9	−22.5	−7	−9	−7	1.6	2.2	1.6
	Measured	−22.8	−20.3	−24.7	−20.3	−11	8	−11	2.5	1.9	2.5
	Measured	−24.4	−24.9	−24.5	−24.9	2	0	2	0.5	0.1	0.5
(Zheng, 2008)	Measured	−26.6	−24.8	−24.6	−24.8	−7	−8	−7	1.8	2.0	1.8
(Zheng, et al., 2007)	Measured	−25.7	−29.6	−26.7	−29.6	15	4	15	3.9	1.0	3.9
(Zhang, et al., 2007)	Not specified	−21.3	−21.7	−21.9	−21.7	2	3	2	0.4	0.6	0.4
(Lu, et al., 2008)	Measured	−22.7	−18.9	−15.3	−18.9	−17	−33	−17	3.8	7.4	3.8
(Scholze, 2002)	Measured	−19.1	−19.0	−19.1	−19.0	−1	0	0	0.1	0.0	0.1
	Measured	−18.5	−18.4	−18.5	−18.4	−1	0	0	0.1	0.0	0.1
	Measured	−17.3	−17.2	−17.3	−17.2	−1	0	−1	0.1	0.0	0.1
	Measured	−18.6	−18.6	−18.6	−18.6	0	0	0	0.0	0.0	0.0
(Mullen, et al., 2010)	Measured	−19.5	−20.5	−20.5	−20.5	5	5	5	1.0	1.0	1.0
	Measured	−24.3	−26.9	−18.8	−18.6	11	−23	−23	2.6	5.5	5.7
(Mullen, et al., 2009)	Measured	−20.9	−20.6	−20.9	−20.6	−1	0	−1	0.3	0.0	0.3
	Measured	−20.4	−19.9	−20.4	−19.9	−2	0	−2	0.5	0.0	0.5
	Measured	−18.7	−19.2	−18.7	−19.2	3	0	3	0.5	0.0	0.5
(Ateş & Işikdağ, 2008)	Calculated	−34.0	−33.6	−34.0	−33.6	−1	0	−1	0.4	0.0	0.4
	Calculated	−34.6	−33.0	−34.6	−34.0	−5	0	−2	1.6	0.0	0.6
					Averages:	−1.2	−3.2	−2.7	1.2	1.3	1.3

* Both estimations-1.1 and -1.2 make use of the indirect method to determine HHV. Estimation-1.1 uses the cumulative HHV approach to determine the HHV graphically, while estimation-1.2 makes use of the elemental analysis calculated from the atomic ratios estimated using the first indirect method

Estimation-1.2 instead uses the elemental masses that are determined by Equation 57 and Equation 58 and calculates the HHV using Equation 23. The overall average absolute error obtained when using the graphical approach of Estimation-1.1 ($1.2\ \mathrm{MJ\ kg^{-1}}$) is only slightly better than for Estimation-1.2 ($1.3\ \mathrm{MJ\ kg^{-1}}$) and Estimation-2 ($1.3\ \mathrm{MJ\ kg^{-1}}$). The average error for each estimation is similarly low, where the error is defined as

$$\text{average error} = \frac{1}{n}\sum_{i=1}^{n}\frac{\Delta_c h^\circ\big|_{\text{HHV,est.},i} - \Delta_c h^\circ\big|_{\text{HHV,meas.}i}}{\Delta_c h^\circ\big|_{\text{HHV,meas.},i}} \times 100\ \% \qquad 71$$

All average errors are also negative, which suggest that on average all methods of estimation under predict the HHV, and the estimations are therefore lower than the actual value and are conservative. Some estimations deviate significantly from data reported in the literature, and a closer analysis offers some insight as to why this is so and also offers possible adjustments for using this technique of indirectly predicting these properties. Lu et al. (2008) report an HHV of $-22.7\ \mathrm{MJ\ kg^{-1}}$, but an HHV of $-15.7\ \mathrm{MJ\ kg^{-1}}$ is calculated when using their own reported elemental analysis – a value that is closer to the values obtained by Estimation-1.1 ($-18.9\ \mathrm{MJ\ kg^{-1}}$), Estimation-1.2 ($-15.3\ \mathrm{MJ\ kg^{-1}}$) and Estimation-2 ($-18.9\ \mathrm{MJ\ kg^{-1}}$). However, on closer inspection of the trends for cumulative atomic ratios, the cumulative HHVs and the cumulative elemental masses of Figure A13 in the Appendix reveal that the initial data points tend to have a larger gradient than the final data points. Since the overall gradient is what is being used as the estimation values, the estimations overpredict the actual measured value in this case. If these data are split into two trends and their trendlines determined, then a weighted average HHV may be calculated using two gradients instead across their respective cumulative mass ranges (see Figure A13 in the Appendix, cumulative HHV plot for rice husk). An HHV of $-24.6\ \mathrm{MJ\ kg^{-1}}$ is obtained instead using this approach, which reduces the absolute error from $3.8\ \mathrm{MJ\ kg^{-1}}$ to $1.9\ \mathrm{MJ\ kg^{-1}}$. The estimation for the second HHV reported by Mullen et al. (2010) of $-24.3\ \mathrm{MJ\ kg^{-1}}$ can likewise be explained by considering again the plots of cumulative data (Figure A16 in the Appendix), where the gradients of the last part of the data decrease compared to the initial data, and therefore the trendlines obtained lead to overpredictions of the HHV. Splitting up the cumulative HHV data plot into two once again and using the resulting two trendlines (Figure A16 in the Appendix,

cumulative HHV plot) gives a weighted average HHV of $-24.1\ \mathrm{MJ\ kg^{-1}}$ and reduces the absolute errors from $2.6\ \mathrm{MJ\ kg^{-1}}$ to $0.2\ \mathrm{MJ\ kg^{-1}}$. In the case of errors observed with respect to the data presented by Zheng et al. (2007), it is not possible to determine from an analysis of the indirect methods used why these errors in estimation exist. Zheng et al. report a lower heating value of $-17.77\ \mathrm{MJ\ kg^{-1}}$ which is close to the higher heating value of $-17.5\ \mathrm{MJ\ kg^{-1}}$ that is calculated using their elemental analysis. It is also not clear from the experimental methods described by Zheng et al. whether the reported value is on a dry and ash free basis. These last inconsistencies unfortunately do not allow clarity on the deviations in estimated HHVs from the measured values, although they are still acceptably small, with absolute errors of $3.9\ \mathrm{MJ\ kg^{-1}}$ (Estimation-1.1), $1.0\ \mathrm{MJ\ kg^{-1}}$ (Estimation-1.2), and $3.9\ \mathrm{MJ\ kg^{-1}}$ (Estimation-2).

4.4. Application of indirect methods of estimation to py-GC/MS catalyst screening

The use of biofuels such as pyrolysis oils and the stability that they could bring to energy security has, moreover, been challenged by food security concerns, since biomass feedstocks may compete for agricultural lands and thus for food security. This deliberation has sparked much debate as to whether biomass-sourced fuels would improve energy security at the expense of food security (Field, et al., 2007; Shortall & Millar, 2012; Doornbosch & Steenblik, 2007; Yue, et al., 2014). However, present advances in silviculture may help to ease these concerns, where demands for lignocellulosic materials have expedited the establishment of plantations globally (Evans & Turnbull, 2004). These plantations can be established on marginal or degraded land and on land that is not suitable for agricultural use (Behrenfeld, et al., 2001). The most important and abundant tree species grown for tropical and subtropical silviculture are from the *Eucalyptus* and *Pinus* genera, with their respective species contributing $26\ \%$ and $42\ \%$ of the total tree species internationally (Brown, 2000; Portin & Lehtonen, 2012). The *Eucalyptus* genus in particular is considered to comprise some of the fastest-growing species of trees compared to all other wood-type genera, based on rotation periods and mean annual increments (Ugalde & Pérez, 2001; Kaipainen, et al., 2004). Furthermore, the commercial importance of eucalypts has grown substantially over the past 60 years as a consequence of the superior fibre and pulping properties that they exhibit. It is

their fast growth rates, shorter rotation periods and productivity that make eucalypts an attractive renewable source of biomass for energy production (Myburg, et al., 2014). Not surprisingly, the thermal decomposition of *E. grandis* has been well researched. *E. grandis* has been used to evaluate property variations of torrefaction in an oxidative environment (Klass, 1998). The energy yield verses mass yield for *E. grandis* has also been reported (Basu, 2010).

Residues from *E. grandis* were therefore selected for investigating their suitability for producing pyrolysis oils, as well as for evaluating upgrading possibilities, using the py-GC/MS analytical methods already developed in this chapter. Four catalysts were considered for upgrading pyrolysis oils, namely ZSM-5 zeolite and bentonite as candidates for acid-based catalysis, and the oxide C2013 and the oxide M1213 for alkali-based catalysis.

4.5. Materials and methods

4.5.1. Feedstock preparation

E. grandis was sourced from Sappi Southern Africa as sawdust rejects with a maximum particle size of 6.0 mm and was received dry. This size was further reduced using a Retsch cutting mill, model SM 100, to obtain a particle size distribution between $150\ \mu\mathrm{m}$ and $250\ \mu\mathrm{m}$. Moisture was hereafter measured at $8.88\ \%$ using a Mettler Toledo Moisture Analyser LJ16.

4.5.2. Catalysts

ZSM-5 zeolite (sourced from Acros Organics) with a minimum surface area of $300\ \mathrm{m^2\ g^{-1}}$ (BET) and a SiO_2:Al_2O_3 molar ratio between 400 and 570 was used. Bentonite clay was supplied in the form of a slurry ($19.2\ \%$ solids content, $\mathrm{pH} = 7.4$) by G&W Base and Industrial Minerals that was sourced from the Boane region in Mozambique. The cation exchange capacity was determined by the supplier to be $0.70\ \mathrm{meq\ g^{-1}}$ using the methylene blue method (Hang & Brindley, 1970). The bentonite slurry was centrifuged and washed using deionized water before being dried at $65\ ^{\circ}\mathrm{C}$. All catalysts were placed onto alumina supports to assist with catalysis.

4.5.3. Methods and equipment

Pyrolysis oils were produced and characterized by pyrolysis-GC/MS (Py-GC/MS) using a Shimadzu multi-functional pyrolyser EGA/PY-3030D from Frontier Laboratories, Japan. Evolved gas analysis (EGA-MS) was used to define the thermal desorption zone using a thermal programme of $100\ ^{\circ}\mathrm{C}$ to $600\ ^{\circ}\mathrm{C}$ at $20\ ^{\circ}\mathrm{C\ min^{-1}}$. Sample sizes were in the range of $1.1\ \mathrm{mg} \pm 0.1\ \mathrm{mg}$. Samples are placed into small cups after which they free fall into the pyrolyser furnace and are heated to pyrolytic temperatures in less than $20\ \mathrm{ms}$.

GC:

Injection method:	1:50 split
Column:	polydimethylsioxane, UA1: $30\ \mathrm{m} \times 0.25\ \mathrm{mm\ ID} \times 2\ \mu\mathrm{m}$ film thickness (2.0F) for pyrolysis at $500\ ^{\circ}\mathrm{C}$, $30\ \mathrm{m} \times 0.25\ \mathrm{mm\ ID} \times 1\ \mu\mathrm{m}$ film thickness (1.0F) for pyrolysis at $300\ ^{\circ}\mathrm{C}$
Flow rate:	Helium, $50\ \mathrm{mL\ min^{-1}}$, $98\ \mathrm{kPa}$
Temperature programming:	$30\ ^{\circ}\mathrm{C}$ for $3\ \mathrm{min}$, $20\ ^{\circ}\mathrm{C\ min^{-1}}$ to $350\ ^{\circ}\mathrm{C}$, hold for $10\ \mathrm{min}$

MS:

Interface temperature:	$300\ ^{\circ}\mathrm{C}$
Ion trap temperature:	$250\ ^{\circ}\mathrm{C}$
Electron ionisation (EI)	
Scan range:	m/z $50 - 650$

4.5.4. Indirect estimation of elemental analysis of pyrolysis oils

The two indirect methods for estimation of the elemental composition were used to determine the composition of pyrolysis oils produced via py-GC/MS under non-catalysed and catalysed fast pyrolysis. The fraction of products analysed using these methods was limited to those products whose normal boiling points equal or exceed $25\ ^{\circ}\mathrm{C}$ to exclude gases from skewing the data. The first method pertains to the prediction of the atomic ratios H/C and O/C as described by Equation 57 and Equation 58, while the second uses the cumulative

elemental masses with respect to carbon, hydrogen and oxygen according to Equation 68. Nitrogen and sulphur are taken as negligible in these analyses. Since some deviations from linearity were observed during the validation of these two methods, a more carefully chosen approach to estimation is applied. In the case of estimating atomic ratios and where a bigradient trend is obvious, the plotted data are split into two parts, and two trendlines are used instead to determine a weighted average gradient.

Alternatively, where this bigradient trend is less evident but a deviation from linearity is still observed, an estimate may still be made by using the last part of the data trend to determine a trendline. This is based on the assumption that the error obtained when using data that lie closer to the line of $x = 100$ is smaller than the error obtained when using data closer to the origin. This is illustrated in Figure 33, where a larger error is observed when using the first part of the data (yellow points, A) taken as the distance from A^* → C^*, compared to the error observed (B^* → C^*) when using intermittent data (orange points, B). The smallest error is obtained (position C^*) when the last part of the data is used instead (red points, C). Here, the linearity for the first two sets of data together is not strong, and therefore the best approach would be to use only the last set of data instead to estimate the quantity in question.

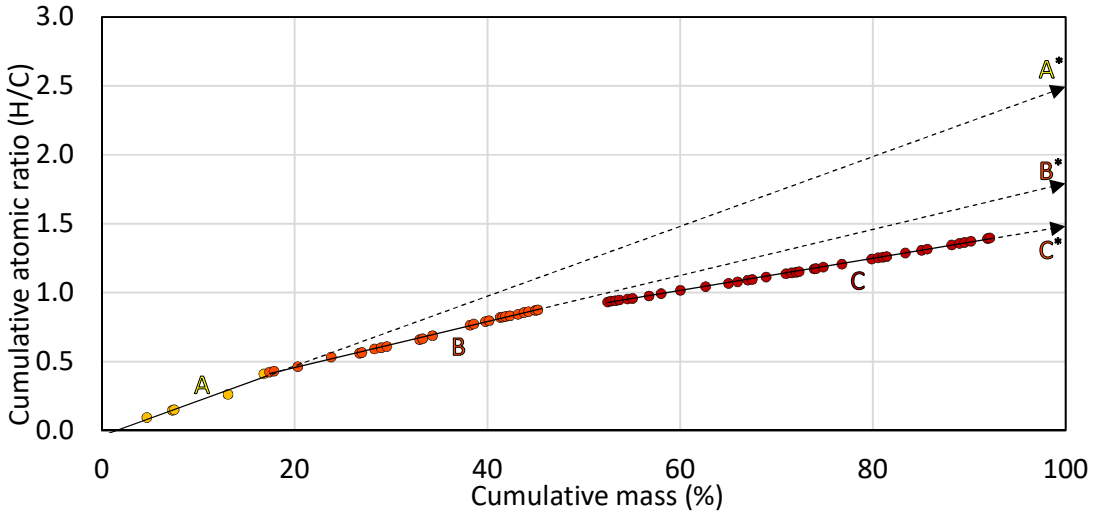

Figure 33: Deviations brought on by selection of compositional data

Three values for the HHVs of pyrolysis oils produced via py-GC/MS are reported, determined indirectly using the estimation of atomic ratios, elemental masses, or graphically by plotting the HHVs cumulatively, as in Figure 32.

4.6. Results

4.6.1. py-GM/CS results: neat pyrolysis oil

E. grandis wood typically has $6.0\ \%$ hydrogen on average, with the remaining balance distributed almost equally between carbon, which accounts for $48.4\ \%$ of the mass, and oxygen, which accounts for $44.8\ \%$ of the mass (Table 12:). This wood species only contains residual amounts of nitrogen and sulphur (both $\sim 2.0\ \%$ on average), and an average ash content of $0.8\ \%$. The average HHV of $-18.7\ \mathrm{MJ\ kg^{-1}}$is close to most individually reported values and close to the average calculated value of $-18.4\ \mathrm{MJ\ kg^{-1}}$. The average moisture content of $8.4\ \%$ reported in the literature is close to the measured value reported for this study.

A total of $74.8\ \%$ of the peaks by mass were characterized for neat pyrolysis oil produced from *E. grandis* pyrolyzed at $500\ ^{\circ}\mathrm{C}$. The pyrolysis oil contains the typical products of lignin and carbohydrate thermal degradation. The most abundant compounds produced from the lignin content of the biomass consist of 2,6-dimethoxy-phenol ($5.5\ \%$), 1-(3,4-dimethoxyphenyl)-ethanone ($3.9\ \%$), 2-methoxy-4-vinylphenol ($3.4\ \%$), 3-methoxy-1,2-benzenediol ($3.4\ \%$), 1,2,4-trimethoxybenzene ($3.3\ \%$) and eugenol ($2.6\ \%$). Of the products concerning the degradation of the carbohydrate fraction of the biomass, the most abundant are 2-hydroxy-2-cyclopentene-one ($3.8\ \%$), furfural ($3.8\ \%$), formaldehyde ($3.0\ \%$), and acetic acid ($2.5\ \%$).

The plot of the cumulative atomic ratios against the cumulative masses for neat pyrolysis oil shows some deviation form linearity, comprising two distinct linear trends in the data, meeting more or less at a mass percentage of $28.7\ \%$ Figure 34-A. The initial set of data predicts an H/C of 1.81 and an O/C of 0.51, while the rest predicts an H/C of 1.34 and an O/C of 0.38. The difference between these two data sets is quite large, and since the second data set carries on cumulatively from the first, it would be better to use the second trend for the

estimate of atomic ratios. The estimated atomic ratios of the second data set translates into elemental mass percentages of $61.6\ \%$ for carbon, $6.9\ \%$ for hydrogen, and $31.4\ \%$ for oxygen. These values are similar to what is estimated using the method of cumulative elemental masses (Figure 34-D), at $63.6\ \%$ for carbon, $7.1\ \%$ for hydrogen, and $29.3\ \%$ for oxygen. The HHV is estimated to be $-27.4\ \mathrm{MJ\ kg^{-1}}$ using the atomic ratios, $-28.1\ \mathrm{MJ\ kg^{-1}}$ using the elemental mass percentages, and $-27.2\ \mathrm{MJ\ kg^{-1}}$ using the graphical method (Figure 34), translating to an average HHV of $-27.6\ \mathrm{MJ\ kg^{-1}}$ for neat pyrolysis oil.

The weighted average of the two points results in the final estimated datum point for neat pyrolysis oil, which lies almost on the deoxygenation tie line (drawn with reference to the feed point, Figure 35B). What is also obvious from the plot of Figure 35B is that the decarboxylation tie line for the feed composition connects the feed point with the region representing liquid transportation fuels. Simply put, the conversion of *E. grandis* to transportation fuel would result from the overall decarboxylation of the feed with little to no change in the H/C ratio. This is not to say that the production of water, biochar or syngas is suppressed or absent, but rather that the ratio of hydrogen to carbon in the pyrolysis oil would reach some value comparable to that of some liquid transportation fuel such as diesel.

It would also be possible to convert the already manufactured neat pyrolysis oil if, say, *ex situ* carbonylation was achieved followed by dehydration (Figure 35B). This would however produce a fuel with a high H/C of ≈ 2.16, above what is typical for petrol ($\mathrm{H/C} \approx 2.00$) and kerosene (paraffin) ($\mathrm{H/C} \approx 1.88$). A better option, although overly simplified and not practically possible, would be to remove oxygen as mostly CO_2 with some oxygen removed as CO. This would reduce the H/C atomic ratio to around 1.87 for the oil product, closer to that of kerosene and other distillate fuels that have an H/C of between 1.68 and 2.00 (Reed, 2014). The possible reaction pathways that would result in the conversion of *E. grandis* to a liquid transportation fuel together form an upgradation region (e.g. catalytic upgradation, Figure 35B). An example of such upgradation attempts is the pyrolysis of *E. grandis* in the presence of bentonite (Figure 36). The plots of the initial data for cumulative atomic ratios and elemental masses for bentonite-catalysed pyrolysis oil deviate from linearity, while the last portion of the data is close to linear.

Table 12: Typical proximate and ultimate analyses for *E. grandis*

Ref.	Elemental analysis (mass %)					HHV[a]	HHV[b]	Ash	Water
	C	H	O	N	S	(MJ $\mathbf{kg^{-1}}$)	(MJ $\mathbf{kg^{-1}}$)	(%)	(%)
(Musinguzi, et al., 2012)	48.5	7.5	43.9	0.1	0.1	−19.2	−20.1	0.1	10.9
(Carrier, et al., 2014)	48.3	5.9	44.6	0.4	0.1	−18.4	−18.4	0.5	7.9
	53.9	5.6	40.0	0.5	1.0	−20.6	−20.6	0.5	9.8
(Montoya, et al., 2015)	46.6	5.9	43.4	0.1	0.1	−18.6	−18.5	3.9	5.3
(Heidari, et al., 2014)	49.8	6.0	43.7	0.1	0.0	−19.4	−19.0	0.6	7.9
(Louw, et al., 2016)	47.2	5.8	46.6	0.2	0.2	−18.1	−17.4	0.1	n.r.
(Amaya, et al., 2007)	47.1	5.9	46.6	0.1	0.0	−17.5	−17.5	0.3	n.r.
(Pereira, et al., 2013)	45.7	5.7	49.4	0.1	0.0	−17.9	−16.2	0.1	n.r.
Averages:	48.4	6.0	44.8	0.2	0.2	−18.7	−18.4	0.8	8.4

[a]Measured value

[b]Calculated value, using $\Delta_c h^\circ\big|_{\mathrm{HHV}} = -13.87\ m_{\mathrm{O_2}}$

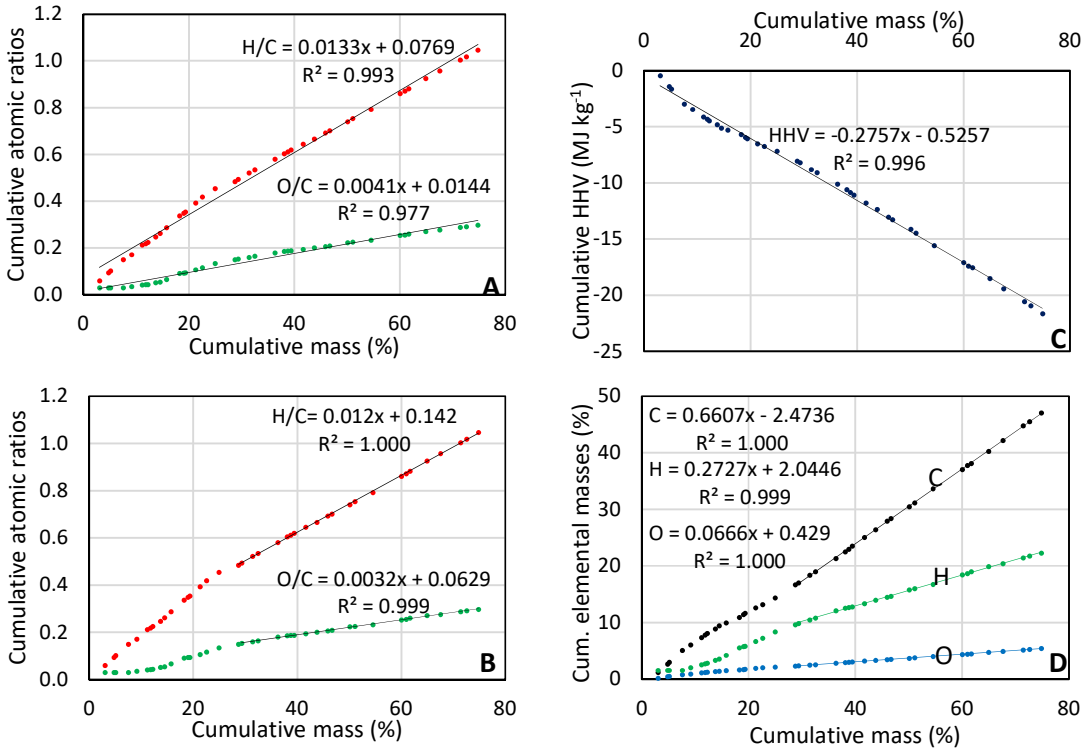

Figure 34: Plot of cumulative atomic ratios (A & B), cumulative higher heating values (C), and cumulative mass percentages (D) against the cumulative mass percentage for neat pyrolysis oil produced via py-GC/MS at 500 °C

Based on these linear trends, the elemental masses are estimated to be between 62.6 % and 65.8 % for carbon, 7.8 % for hydrogen, and between 26.5 % and 29.6 % for oxygen, with $H/C \approx 1.48$ and $O/C \approx 0.36$. The estimated higher heating value using the atomic ratios method is $-29.3\ \mathrm{MJ\ kg^{-1}}$, $-31.7\ \mathrm{MJ\ kg^{-1}}$ for the graphical method (Figure 36C), and $-29.2\ \mathrm{MJ\ kg^{-1}}$ using the elemental mass data. The average HHV is determined to be $-30.1\ \mathrm{MJ\ kg^{-1}}$, which is $-2.5\ \mathrm{MJ\ kg^{-1}}$ more than that of neat pyrolysis oil. The by-products leading to the formation of the bentonite-catalysed pyrolysis oil are shown graphically in Figure 37A as an equivalent ratio of water and carbon dioxide. This ratio could represent more complex mixtures formally referred to as syngas and biochar, in addition to the water and CO_2 that was indeed formed. However, this equivalent representation of these by-products allows an easier interpretation of the main routes of deoxygenation of pyrolysis oils, particularly when screening catalysts using the py-GC/MS method developed here.

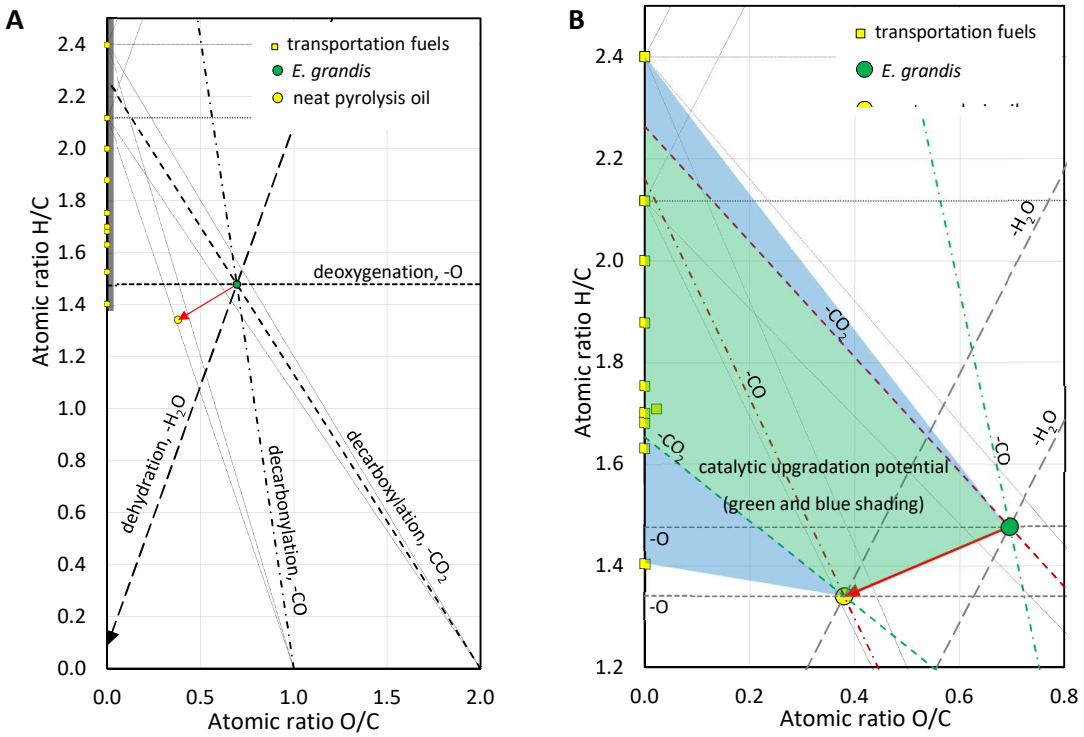

Figure 35: van Krevelen diagrams showing the pyrolysis of *E. grandis* in relation to its pyrolysis oil and various (liquid) transportation fuels and crude oils

The ratio for neat pyrolysis oil achieved an CO_2/H_2O of 1.9, and suggests that almost a third of deoxygenation was achieved for neat pyrolysis oil via a loss in carbon from the original biomass, whether this led to the production of biochar, CO or CO_2. Additionally, just over a third of the deoxygenation that was achieved led to the formation of water, or (when considered concurrently with the loss in carbon) light oxygenated hydrocarbons.

Even if the amount of biochar and syngas would not be known using this method, the mass balance that concerns the feed and its pyrolysis oil, as represented in Figure 37, may still be treated in the same way that state variables are handled, namely that only the changes between the initial and final state are of relevance. In comparison, bentonite-catalysed pyrolysis oil achieved a reduction in oxygen in relation to its parent feedstock of *E. grandis* by the formation of by-products equivalent to a ratio of CO_2/H_2O is $74.6/25.4 = 2.9$. Since mass balances are possible with ternary diagrams using the lever-arm rule, an equivalent mass of H_2O & CO_2 may also be determined, and for the formation of bentonite-catalysed

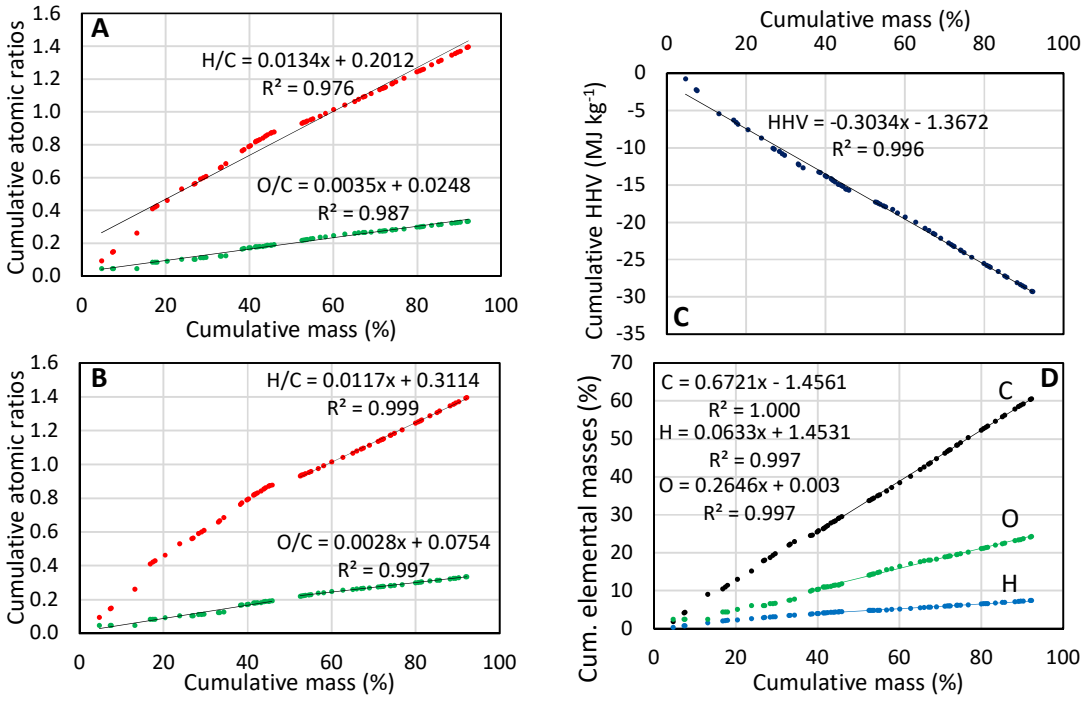

Figure 36: Plot of cumulative atomic ratios (A & B), cumulative higher heating values (C), and cumulative mass percentages (D) against the cumulative mass percentage for bentonite-catalysed pyrolysis oil produced via py-GC/MS at 500 °C.

pyrolysis oil this equates to $8.9\ \mathrm{kg_{H_2O}}/100\ \mathrm{kg_{E.\ grandis}}$ and $26.2\ \mathrm{kg_{CO_2}}/100\ \mathrm{kg_{E.\ grandis}}$, or a total of $35.1\ \mathrm{kg_{by-products}}/100\ \mathrm{kg_{E.\ grand}}$. Conversely, the mass yield of pyrolysis oil may be estimated to be $64.9\ \mathrm{kg_{pyrolysis\ oil}}/100\ \mathrm{kg_{E.\ grandis}}$. Since additional side reactions that reduce the mass yield of pyrolysis oil would invariably be present, this ratio of pyrolysis oil to feedstock represents the maximum production of pyrolysis oil possible, as shown in Figure 37B.

How do these results compare to zsm-5-catalyzed pyrolysis oil? The zsm-5 runs were compared at two temperatures, as the typical fast pyrolysis temperature of 500 °C produced poor results for upgradation, and a lower temperature of 300 °C was found to be optimum. Based on the mass data presented in Figure 38, pyrolysis at 500 °C of zsm-5 produces a pyrolysis oil comprising between 63.6 % and 65.7 % carbon, 7.2 % hydrogen, and between 27.1 % and 29.3 % oxygen on a mass basis, with the HHV estimated to be $-29.1\ \mathrm{MJ\ kg^{-1}}$. Pyrolysis at 300 °C (selected using EGA) in the presence of zsm-5 zeolite produces a pyrolysis oil with a slightly higher carbon content of between 65.2 % and 71.5 %, and 8.1 % hydrogen,

A

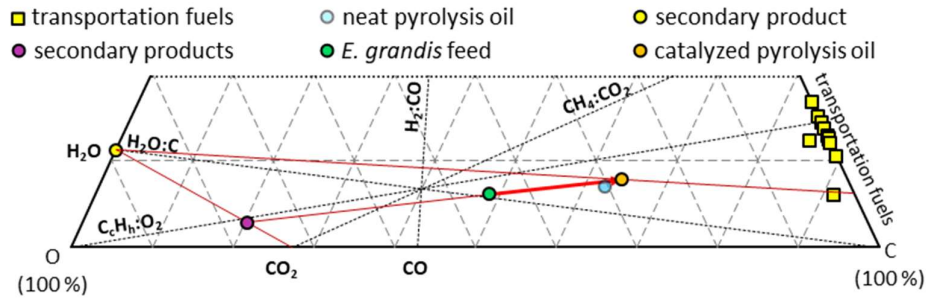

B

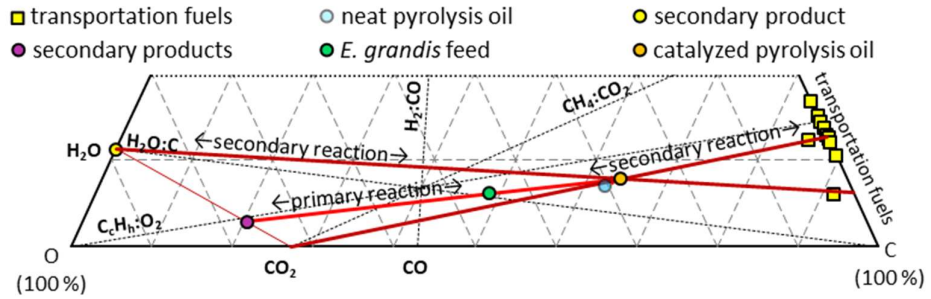

Figure 37: Ternary plot of bentonite-catalysed pyrolysis oil in association with neat pyrolysis oil and the feed of *E. grandis*

with a reduced oxygen content of between $20.4\ \%$ and $26.6\ \%$ (Figure 40). The HHV is also improved, and is estimated to be around $-32.5\ \mathrm{MJ\ kg^{-1}}$. There is a marked difference in the form the data trends when comparing zsm-5 catalysis at $500\ ^{\circ}\mathrm{C}$ (Figure 38) and $300\ ^{\circ}\mathrm{C}$ (Figure 40). Whereas zsm-5 catalysis at $500\ ^{\circ}\mathrm{C}$ takes on more or less a linear trend for all data sets with only slight deviation from linearity for the initial data, zsm-5 catalysis at $300\ ^{\circ}\mathrm{C}$ clearly has two distinct regions. In the initial portion of data with respect to the cumulative atomic ratios and elemental masses, oxygen increases sharply and thereafter drops off in the last portion of the data. This suggests that zsm-5 catalysis (at $300\ ^{\circ}\mathrm{C}$) is selective in its activity, where the first portion of data assumes an elemental mass distribution closer to that of the feedstock (Figure 39), with about $51.4\ \%$ carbon, $8.5\ \%$ hydrogen and $40.2\ \%$ oxygen. The second portion of data then reduces the oxygen substantially to $23.5\ \%$.

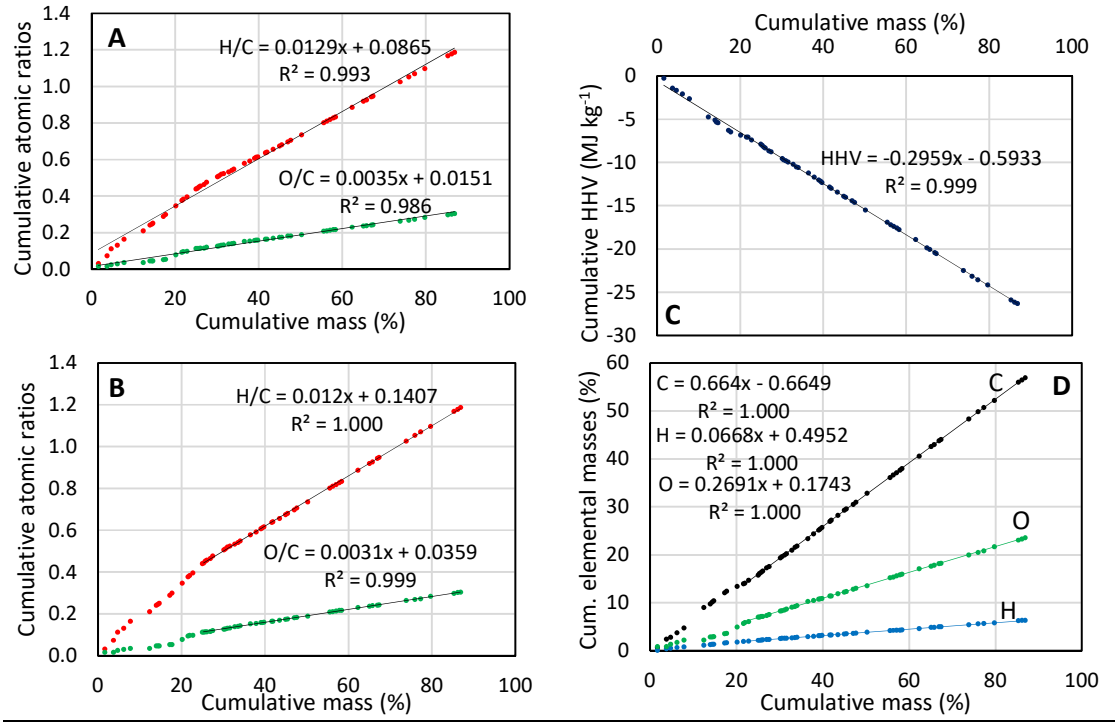

Figure 38: Plot of cumulative atomic ratios (A & B), cumulative higher heating values (C), and cumulative mass percentages (D) against the cumulative mass percentage for zsm-5 zeolite-catalysed pyrolysis oil produced via py-GC/MS at 500 °C.

A

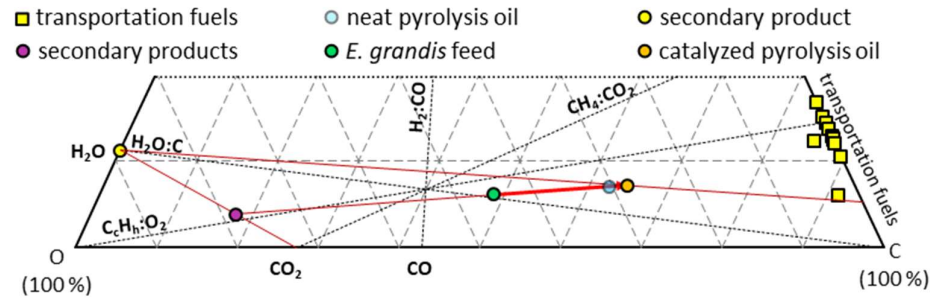

B

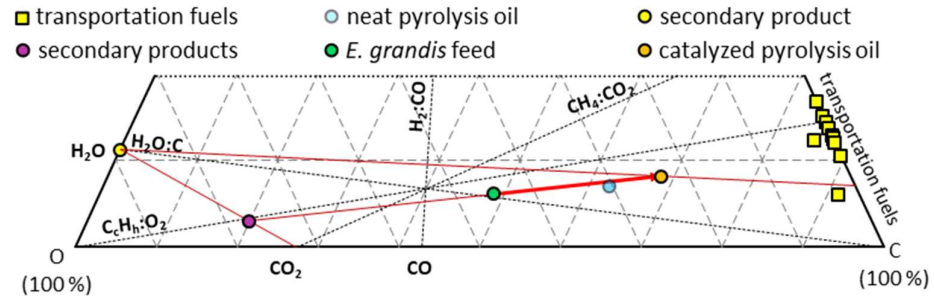

Figure 39: Ternary plot of zsm-5-catalysed pyrolysis oil at 500 °C (**A**) and 300 °C (**B**) in association with neat pyrolysis oil and the *E. grandis* feed

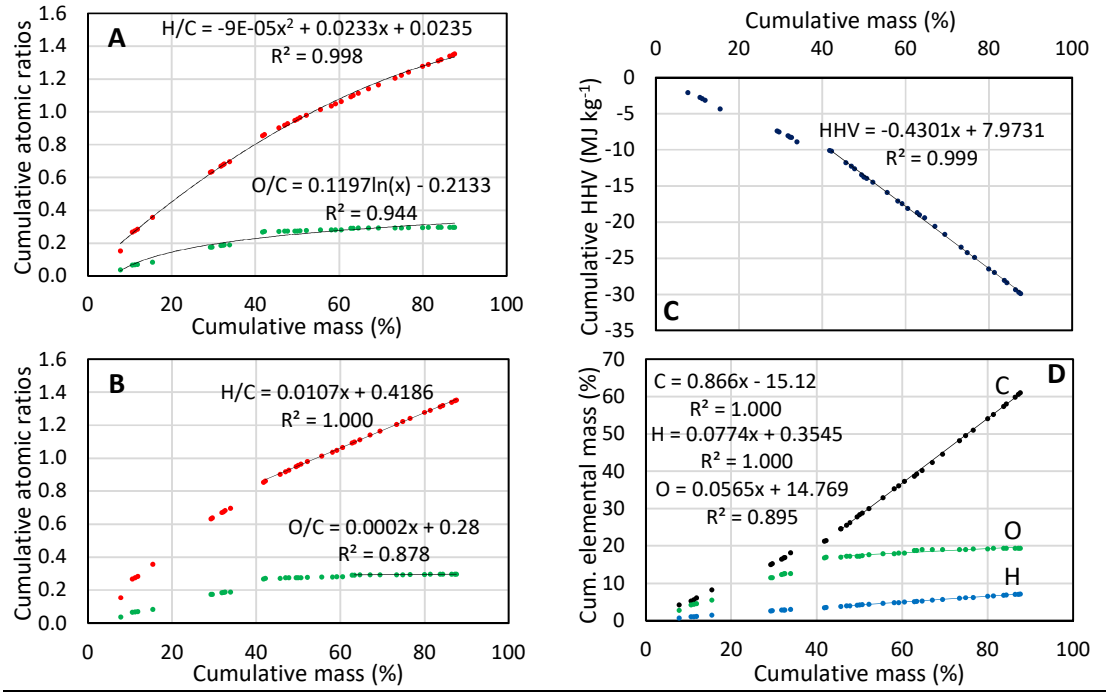

Figure 40: Plot of cumulative atomic ratios (A & B), cumulative higher heating values (C), and cumulative mass percentages (D) against the cumulative mass percentage for zsm-5 zeolite-catalysed pyrolysis oil produced via py-GC/MS at 300 °C.

Based on a mass balance of Figure 39A & B, the equivalent deoxygenation selectivity CO_2/H_2O increases from $65.4/34.6 = 1.9$ (which is the same for neat pyrolysis oil) to $73.2/26.8 = 2.7$ and suggests that zsm-5 catalysis at 300 °C favours the removal of oxygen from pyrolysis oil via the decarboxylation route rather than via dehydration. At 300 °C, the by-products have an equivalent mass of $10.8\ kg_{H_2O}/100\ kg_{E.\ grandis}$ and $29.6\ kg_{CO_2}/100\ kg_{E.\ grandis}$ and a maximum pyrolysis oil yield of $59.6\ kg_{H_2O}/100\ kg_{E.\ grandis}$. In comparison, pyrolysis with zsm-5 at 500 °C comparatively has an equivalence in by-products of $11.7\ kg_{H_2O}/100\ kg_{E.\ grandis}$ and $22.2\ kg_{CO_2}/100\ kg_{E.\ grandis}$ with a maximum pyrolysis oil yield of $66.1\ kg_{H_2O}/100\ kg_{E.\ grandis}$ observed, as the M1213 presents much lower trends with respect to oxygen.

The cumulative data for the last two catalysts, namely C2013 and M1213 are shown in Figure 41 and Figure 42. The data trends for C2013 are very similar to those of bentonite-catalysed pyrolysis oil. Atomic ratios of $H/C = 1.48$ and $O/C = 0.33$ are estimated, with the elemental masses estimated to be between 64.1 % and 69.9 % for carbon, 7.9 % and 8.4 % for

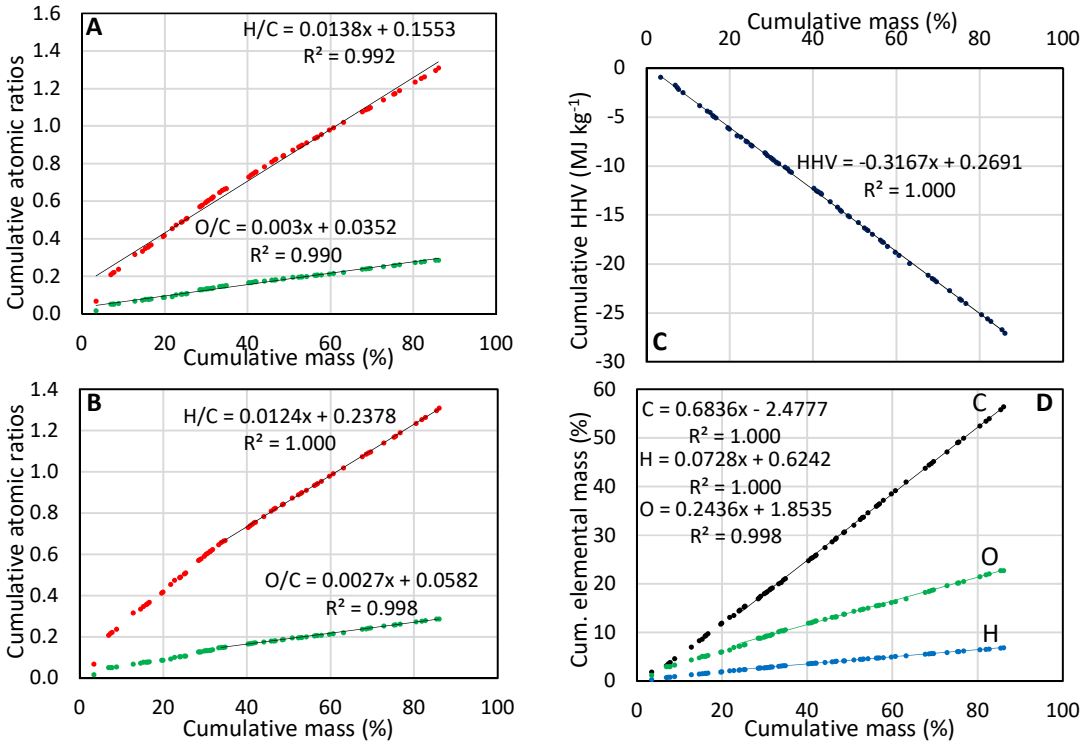

Figure 41: Plot of cumulative atomic ratios (A & B), cumulative higher heating values (C), and cumulative mass percentages (D) against the cumulative mass percentage for C2013-catalysed pyrolysis oil produced via py-GC/MS at 500 °C.

hydrogen, and 21.7 % and 28.0 % for oxygen, with an HHV of around $-31.3\ \mathrm{MJ\ kg^{-1}}$. When the C2013 data (Figure 41B & D) are compared with the M1213, an immediate difference in the cumulative O/C ratio and oxygen mass percentage (Figure 42B & D) is observed, as the M1213 presents much lower trends with respect to oxygen.

Also, the trends are also much more linear for the M1213 data compared to the C2013 data. This suggests that the activity of M1213 on upgrading the pyrolysis oil components is not isolated to a portion of components, but is active over the full range of components. Compared to all the other data sets, C2013 has the highest estimations for carbon (between 74.5 % and 76.2 %) and hydrogen (between 9.2 % and 9.4 %), and the lowest estimation for oxygen (between 12.3 % and 16.0 %). Based on these results, the HHV is also the highest predicted, with an average estimation of $-39.1\ \mathrm{MJ\ kg^{-1}}$, based on calculated values of $-39.0\ \mathrm{MJ\ kg^{-1}}$ (atomic ratios estimation), $-40.1\ \mathrm{MJ\ kg^{-1}}$ (cumulative HHV estimation), and $-37.4\ \mathrm{MJ\ kg^{-1}}$ (elemental masses estimation). The equivalent deoxygenation selectivity

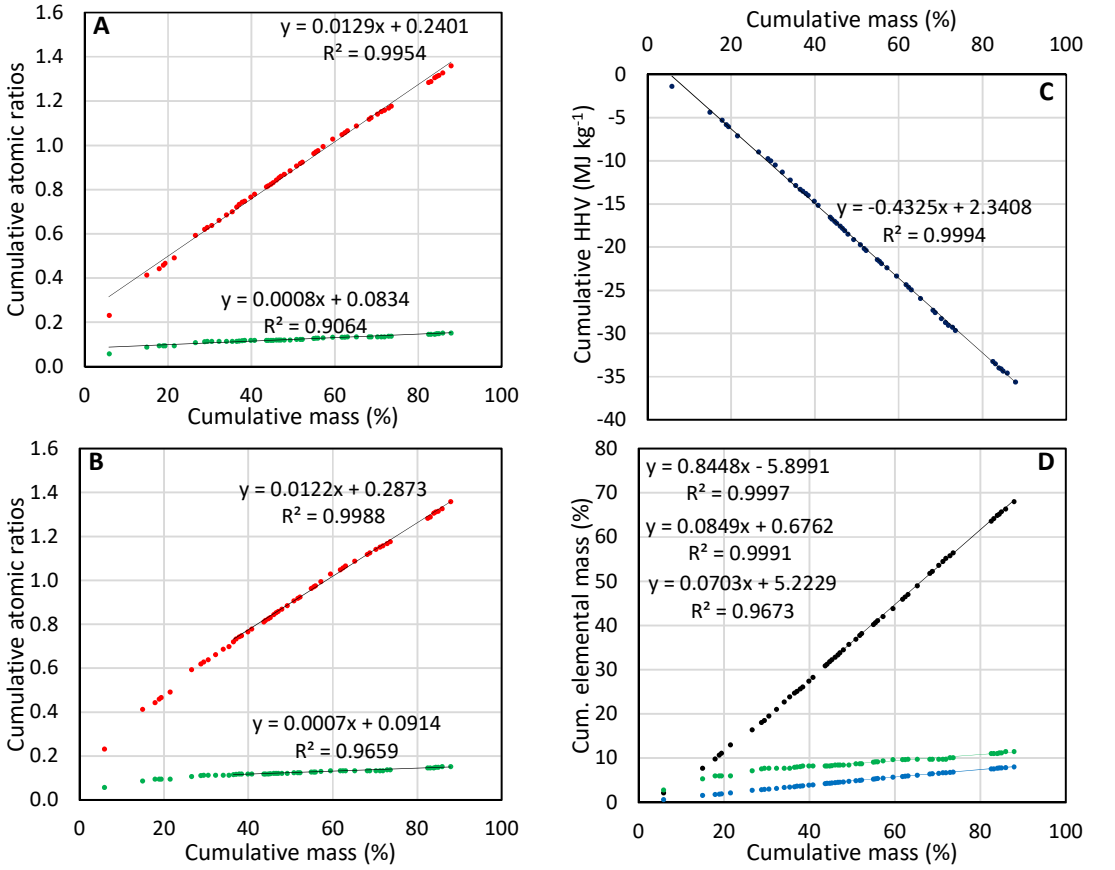

Figure 42: Plot of cumulative atomic ratios (A & B), cumulative higher heating values (C), and cumulative mass percentages (D) against the cumulative mass percentage for M1213-catalysed pyrolysis oil produced via py-GC/MS at 500 °C.

H_2O:CO_2 is also the lowest compared to the other catalysed- and non-catalysed pyrolysis oil data, at $CO_2/H_2O = 85.3/14.7 = 5.8$, while C2013 has an equivalent selectivity of $CO_2/H_2O = 3.0$ (Figure 43A). The composition of the resulting M1213-catalyzed pyrolysis oil is also much closer to that of typical transportation fuels as it achieves a much higher change in energy quality, one that is more or less similar to that of coal tar fuel relative to *E. grandis* (Figure 44). Theoretically, as much as 47.7 % of the M1213 catalysed pyrolysis oil could be produced, but due to side reactions, this yield is expected to be much lower. Therefore, more work on the bench and pilot scale is required. Regardless, if further refinement of the M1213 pyrolysis oil were to be carried out, any of the main routes could be used. Achieving further deoxygenation via the decarbonylation route would produce a transportation fuel close to that of the distillate range, while decarboxylation and dehydration would produce a product closer in composition to residual fuel oils and crude oils (see Figure 43B, green shading). In all

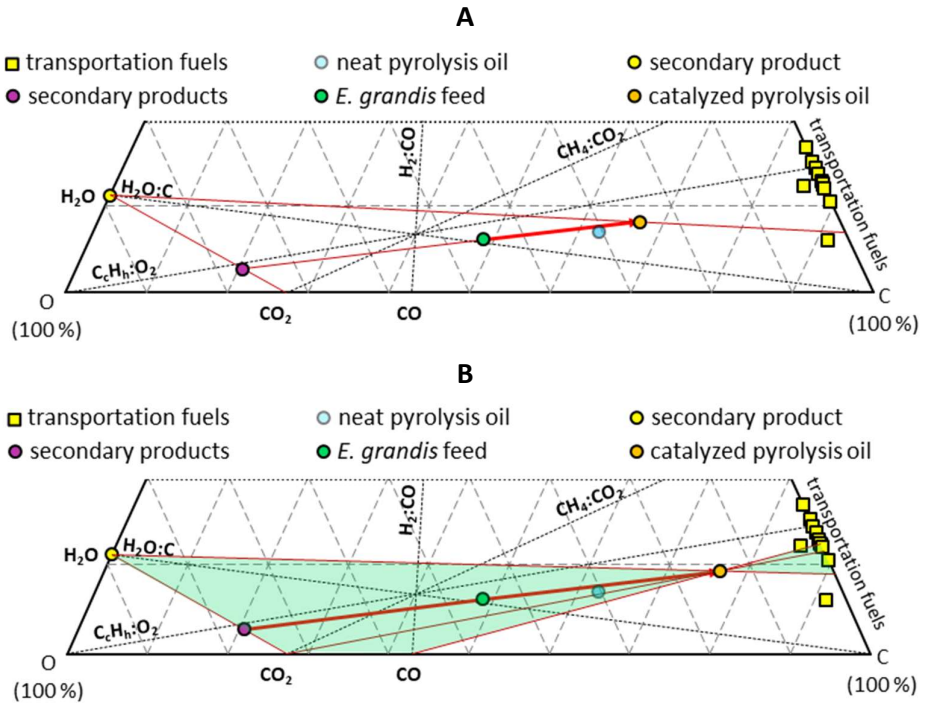

Figure 43: Ternary plot of C2013-catalysed (**A**) and M1213-catalysed (**B**) pyrolysis oils in association with neat pyrolysis oil and the *E. grandis* feed

cases of catalytic upgrading evaluated here, it seems inevitable that additional refining would be required to alter the raw pyrolysis oil into a more useful fuel, while ensuring that other physical properties pertaining to transportation fuel are also considered. Herein lies the limitation of such an analytical approach as presented in this chapter.

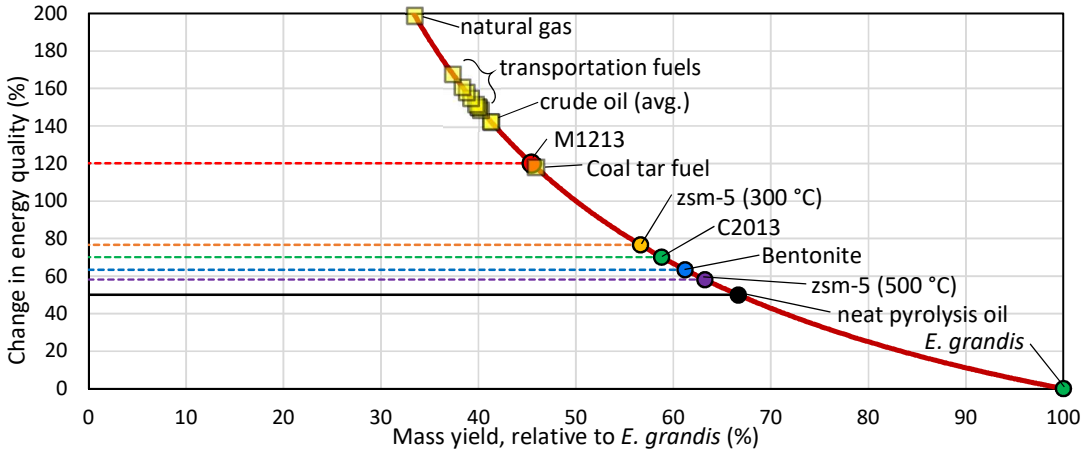

Figure 44: Change in energy quality against mass yield for all pyrolysis oils produced using py-GC/MS, compared to conventional transportation fuels and crude oil

It would be inappropriate to use estimations of elemental compositions and calorific values alone to rate pyrolysis oils in totality, and further work is required on the bench-scale to validate these results and test other important physical properties. While it may be possible to develop a similar analytical technique to estimate boiling ranges, flash points, specific gravities, and viscosities, this would be an overreach of such techniques.

4.7. Summary

Catalytic upgradation of fast pyrolysis processes for the valorisation of biomass feedstocks to energy products is a major theme of research. The complexity of pyrolysis oils and the plethora of reaction mechanisms governing their genesis reflects this. The power of the analytical technique of pyrolysis-GC/MS has attracted many researchers in the field to use it as a convenient tool for investigating pyrolysis in more depth, and to use it further in the screening of various biomass feedstocks and catalysts. The add-on ability to perform evolved gas analysis (EGA-MS) to define the thermal desorption zone, and the flexibility in scanning a wide range of temperatures under various residence times and atmospheres are some of the considerable plus points of this tool. Moreover, these may be achieved while using only the smallest quantities of sample. The reliability of the pyrolysis-GC/MS analysis technique is taken advance of in this work with the development of a set of novel methods that may be used to estimate other properties of pyrolysis oils. In the theoretical derivation, these methods are shown to achieve reasonable accuracy even when only $20\ \%$ of the GC/MS data is utilized in predicting the elemental composition and calorific values for pyrolysis oils, and this result is further confirmed in the application of these techniques to data obtained from the literature. During this validation, the indirect methods performed surprisingly well as most of the data sets obtained from the literature reported only limited peak identification, with only minor discrepancies present. Pyrolysis oil data obtained for the pyrolysis of *E. grandis* was generated using py-GC/MS. These data were used to compare the catalytic activity of potential catalysts with each other and with uncatalyzed pyrolysis oil. The potential catalysts, namely bentonite, zsm-5 zeolite, oxide C2013 and oxide M1213, were compared with respect to their abilities to improve the calorific value of pyrolysis oil and reduce the presence of oxygen. The comparisons between uncatalyzed (neat) pyrolysis oil and catalysed

pyrolysis oils took the order of neat pyrolysis oil (-27.6 MJ kg^{-1} and 30.4 % oxygen) < zsm-5-catalysed pyrolysis oil at 500 °C (-29.1 MJ kg^{-1} and 28.2 % oxygen) < bentonite-catalysed pyrolysis oil (-30.1 MJ kg^{-1} and 28.1 % oxygen) < C2013-catalysed pyrolysis oil (-31.3 MJ kg^{-1} and 24.9 % oxygen) < zsm-5-catalysed pyrolysis oil at 300 °C (-32.5 MJ kg^{-1} and 23.5 % oxygen) < M1213-catalysed pyrolysis oil (-39.1 MJ kg^{-1} and 14.2 % oxygen).

By plotting these data onto a ternary plot, the main route(s) of deoxygenation that resulted in the pyrolysis oils could be estimated on an equivalence basis of CO_2 and H_2O. In principle, even though the actual syngas and biochar compositions would be unknown when using the technique of py-GC/MS (e.g. if hydrogen is not measurable), these by-products can be approximated by an equivalent amount of CO_2 and H_2O instead. By applying this simplification, a deoxygenation selectivity equivalent to CO_2/H_2O can be expressed for comparative purposes. Here M1213-catalyzed pyrolysis oil achieved the highest ratio of 5.8, compared to the next highest ratio of 3.0 for C2013-catalyzed pyrolysis oil, with the lowest value of 1.9 being produced for both bentonite- and zsm-5-catalyzed pyrolysis oils produced at 500 °C. These techniques, of course, have their limitations in providing all the information necessary for the proper development of alternative transportation fuels, but are powerful tools for the initial phase of R&D towards the advancement of pyrolysis technologies.

Chapter 5: Conclusions and recommendations

5.1. Conclusions

A lot is owed to the heavy-weight scientists, physicists, chemists, and engineers who helped to formulate the modern theory of classical thermodynamics and, in doing so, also transformed the once very rudimentary phlogiston theory of combustion hypothesized in the 1600s by Becher (Bowler & Morus, 2005) into an advanced science. The discovery of oxygen by Lavoisier helped pave the way to a better (albeit obsolete) explanation of combustion based on the calorific theory. Eventually the modern principle of conservation of energy led to a proper, accurate description of combustion. Many attempts have previously been made to correlate the properties of particular fuels, starting from elemental composition and proximate analyses, and progressing to the magnitude of exothermicity of the combustion reaction. Yet only as recently as 2015, with the work of Schmidt-Rohr (Schmidt-Rohr, 2015), has anyone come closer to explaining the reason as to why combustion in oxygen proceeds exothermally. Schmidt-Rohr correctly identifies oxygen as the main culprit; he relates the moles of oxygen combusted to the higher heating value (also on a mole basis) as

$$\Delta_{\mathrm{c}} H^{\circ}{}_{m}\big|_{\mathrm{LHV}} = -418\, n_{\mathrm{O}_2}$$

and cites oxygen's weak bonds as the cause of exothermicity. Concerning the first hypothesis of this thesis, it is demonstrated that the cause of exothermicity is not simply the weaker bonds characteristic of diatomic oxygen, but the changes in energy undergone by all the elements during combustion. By applying the fundamental principles of thermodynamics and treating bond enthalpies as state variables, a new thermodynamic equation for redox reactions (which govern combustion processes) is derived as

$$\Delta_{\mathrm{c}} h^{\circ}\big|_{\mathrm{HHV}} = \Delta_{\mathrm{c}} D_H(\mathrm{fuel}) + \Delta_{\mathrm{c}} D_H(\mathrm{O}_2) - \Delta_{\mathrm{c}} D_H(\mathrm{H}\cdots\mathrm{O}) + \Delta_{RS} h^{\circ}$$

for the higher heating value. Careful assumptions and analysis of known fuels undergoing combustion are used to simplify the general thermodynamic equation of combustion to

$$\Delta_c h^\circ\big|_{\mathrm{HHV}} = \frac{-13.87}{\omega_{\mathrm{O}_2}^{-1} - 1} = -13.87\, m_{\mathrm{O}_2}$$

which estimates the higher heating value as a strong function of oxygen consumed during the combustion process. This important result is crucial in the formulation and testing the remaining hypotheses.

Ternary plots have been demonstrated to be useful in visualizing how biomass as feedstocks relate and compare to various fuels. The categorization of the main upgradation pathways relating to dehydration/carbonization ($\mathrm{H_2O} \leftrightarrow \mathrm{C}$), decarboxylation/methanogenesis ($\mathrm{CH_4} \leftrightarrow \mathrm{CO_2}$) and decarbonylation/hydrogenization ($\mathrm{H_2} \leftrightarrow \mathrm{CO}$) was used to assess the *prima face* objectives of upgrading technologies, namely to reduce oxygenate presence in pyrolysis oils, to maximise mass yields (based on either total yields or carbon yields), and to maximize energy yields. Biofuels are postulated herein to be energy products first and foremost, and from this viewpoint a new definition is proposed with the derivation of an equation that describes the change of energy quality ΔE_{Q} for any fuel or potential fuel:

$$\Delta E_{\mathrm{Q}} = \frac{m_{\mathrm{O}_2}\big|_{\mathrm{product}}}{m_{\mathrm{O}_2}\big|_{\mathrm{feed}}} - 1$$

The implication of this equation is simple: any improvement in energy quality of a combustible species must be accompanied by an increase in oxygen consumed by the product, relative to the feedstock that was used in its manufacture. Further analysis of this equation using more than 16 million data points resulted in the discovery of a boundary limit in the change in energy quality, given by the equation

$$\Delta E_Q = \frac{m_i}{m_f} - 1$$

This equation led to the realization that an increase in energy quality of any combustible material must be accompanied by a decrease in redundant mass (i.e. energy-deficient mass removed through upgradation, such as $\mathrm{CO_2}$ or $\mathrm{H_2O}$). Furthermore, it was found that as $m_f \to 0$, ΔE_Q approaches infinity:

$$\lim_{m_f \to 0} \Delta E_Q = \lim_{m_f \to 0} \frac{m_i}{m_f} - 1 \to \infty$$

and where no upgradation takes place (in other words, $m_v = 0$ and $m_f = m_i$), no change in energy quality occurs:

$$\Delta E_Q\big|_{m_f = m_i} = \frac{m_i}{m_f}\bigg|_{m_f = m_i} - 1 = 0$$

These results are in direct conflict with the *prima facie* objectives of maximizing the mass yields of biofuels. The objective of achieving favourable carbon yields is likewise demonstrated to be a poor metric to use for evaluating the outcomes of biofuel synthesis. About $99.9\ \%$ of the possible 16 million fuel compositions investigated have been shown to have a limited change in energy quality of $116\ \%$ when this metric is applied. This indicates that maximizing carbon yields could limit the change in energy quality to just $116\ \%$, which is much lower than what could be achieved if this mass-based metric were not adopted.

The volatility of pyrolysis and combustion products is an advantageous consequence that makes the enhancement of pyrolytic processes possible through the use of the powerful analytical technique of GC/MS. For this reason, pyrolysis-GC/MS is often employed in biomass and/or catalyst screening. A new set of methods for evaluating the performance of catalysts for catalytic fast pyrolysis has therefore been developed. These methods rely on a cumulative approach with respect to mass-based quantities and require only part of the total components comprising the pyrolysis oil to be characterized. As the cumulative calorific values and the elemental masses follow some linearity when plotted as a function of the cumulative mass, an accurate estimation of the elemental composition and heat of combustion of the pyrolysis oil may be obtained. To estimate the atomic ratios of pyrolysis oils using the py-GC/MS method, the following equations may be used:

$$\sum_{i=1}^{j} \frac{v_{\mathrm{H}_i}}{v_{\mathrm{C}_i}} \omega_i = \frac{v_{\mathrm{H}}}{v_{\mathrm{C}}}\bigg|_{\text{pyro.oil}} \sum_{i=1}^{j} \omega_i + \epsilon \qquad \text{and} \qquad \sum_{i=1}^{j} \frac{v_{\mathrm{O}_i}}{v_{\mathrm{C}_i}} \omega_i = \frac{v_{\mathrm{O}}}{v_{\mathrm{C}}}\bigg|_{\text{pyro.oil}} \sum_{i=1}^{j} \omega_i + \epsilon$$

The atomic ratios may then be used to determine the heating value and/or elemental masses, or these may be determined directly with the following equations, respectively:

$$\sum_{i=1}^{j} \Delta_{\mathrm{c}} h^{\circ}\big|_{\mathrm{HHV},i} \omega_i = \Delta_{\mathrm{c}} h^{\circ}\big|_{\mathrm{HHV}} \sum_{i=1}^{j} \omega_i + \epsilon \quad \text{and} \qquad \sum_{i=1}^{j} \left(\omega_{A_i} m_i\right) = \sum_{i=1}^{j} m_i \left(\omega_A + \sum_{i=j}^{n} \omega_{A_i}\right)$$

Following the successful demonstration and validation of these methods using 19 sets of data from the literature, these four equations were further used in the evaluation of four catalysts in the upgradation of pyrolysis oil produced from *E. grandis*. In this evaluation, the catalysts were compared according to their abilities to improve the heating value of pyrolysis oil and to decrease the presence of oxygen. The best performing catalyst on both accounts was M1213, which improved the HHV from $-18.4\ \mathrm{MJ\ kg^{-1}}$ for *E. grandis* to $-39.1\ \mathrm{MJ\ kg^{-1}}$ and decreased the oxygen content in pyrolysis oil from $30.4\ \%$ (for neat pyrolysis oil) to $14.2\ \%$. This is a $68.3\ \%$ reduction in the oxygen content originally present in the feedstock ($44.8\ \%$). The major routes of deoxygenation were reported on an equivalence basis of water and carbon dioxide with the aid of a ternary plot—reported as a mass-percentage-based selectivity of $\mathrm{CO_2/H_2O}$. M1213 achieved the highest selectivity towards deoxygenation with an equivalent deoxygenation selectivity of $\mathrm{CO_2/H_2O} = 5.8$—much higher than for neat pyrolysis oil, which achieved the lowest selectivity of 1.9.

5.2. Recommendations

It may be said that the contributions made in this thesis to the theory of combustion are by no means limited to this field of science. Indeed, any system comprising matter and energy that undergoes thermodynamic changes where redox reactions are concerned may similarly be analysed and explained in this way. Such a phenomenon may very well impact the development of all energy systems, especially concerning energy storage and utilization. Are battery-powered technologies for use in the aviation industry better at managing the required energy demands than methane for instance? Scientists Kim et al. recently published their research presenting a complex hydride lithium that functions as an all-solid-state battery with a realizable energy density of just over $2\ 500\ \mathrm{Wh\ kg^{-1}}$, or rather $9\ \mathrm{MJ\ kg^{-1}}$—roughly half of the typical energy density of woody biomass (Kim, et al., 2019). Clearly, the answer to

the proposed question, for now at least, is an affirmative ‘no’: never mind methane, even woody biomass currently outcompetes a marketable class of batteries with the highest energy densities developed to date! It is therefore strongly recommended that the thermodynamic explanation in this thesis applied to the theory of combustion should be further expanded to other energy systems undergoing similar chemical changes that take place during combustion. One field that would benefit the most is electrochemistry.

References

Acıkgoz, C., Onay, O. & Kockar, O., 2004. Fast pyrolysis of linseed: product yields and compositions. *Journal of Analytical and Applied Pyrolysis,* 71(2), pp. 417-429.

Akhtar, J. & Amin, N., 2012. A review on operating parameters for optimum liquid oil yield in biomass pyrolysis. *Renewable and Sustainable Energy Reviews,* 16(7), pp. 5101-5109.

Amaya, A., Píriz, J., Tancredi, N. & Cordero, T., 2007. Activated charbon pellets from eucalyptus char and tar TG studies. *Journal of Thermal Analysis and Calorimetry,* 89(3), pp. 987-991.

Ateş, F. & Işikdağ, M. A., 2008. Evaluation of the role of the pyrolysis temperature in straw biomass samples and characterization of the oils by GC/MS. *Energy & Fuels,* 22(3), pp. 1936-1943.

Basu, P., 2010. *Biomass Gasification and Pyrolysis.* Cambridge: Academic Press.

BCC, 1998. *Improved analytical techniques for coal characterisation,* Cheltenham: s.n.

Beckman, D. et al., 1990. *Techno-economic assessment of selected biomass liquefaction process, Report No. 697,* Espoo: VTT.

Behrenfeld, M. et al., 2001. Biospheric primary production during an ENSO transition. *Science,* 291(5513), pp. 2594-2597.

Beis, S., Onay, Ö. & Koçkar, Ö., 2002. Fixed-bed pyrolysis of safflower seed: influence of pyrolysis parameters on product yields and compositions. *Renewable Energy,* 26(1), pp. 21-32.

Boateng, A. A., Daugaard, D. E., Goldberg, N. M. & Hicks, K. B., 2007. Bench-scale fluidized-bed pyrolysis of switchgrass for bio-oil production. *Industrial & Engineering Chemistry Research,* 46(7), pp. 1891-1897.

Boie, W., 1953. Fuel technology calculations. *Energietechnik,* Volume 3, pp. 309-316.

Bowler, P. & Morus, I., 2005. *Making modern Science: A Historical Survey.* Chicago: University of Chicago Press.

Bridgwater, A. & Bridge, S., 1991. A Review of Biomass Pyrolysis and Pyrolysis Technologies. In: A. Bridgwater & G. Grassi, eds. *Biomass Pyrolysis Liquids Upgrading and Utilization.* Berlin: Springer, Dordrecht, pp. 11-92.

Bridgwater, A. & Grassi, G., 1991. *Biomass Pyrolysis Liquids Upgrading and Utilization.* Berlin: Spinrger Dordrecht.

Bridgwater, A. V., 2012. Review of fast pyrolysis of biomass and product upgrading. *Biomass & Bioenergy,* Volume 38, pp. 68-94.

British Coal Corporation, 1998. *Improved analytical techniques for coal characterisation,* Cheltenham: Directorate-General Energy.

Brown, C., 2000. *The global outlook for future wood supply from forest plantations,* Rome, Italy: Food and Agricultural Organisation of the United Nations.

Carrier, M. et al., 2014. Inherent process variations between fast pyrolysis technologies: A case study on Eucalyptus grandis. *Fuel Processing Technology,* 131(2014), pp. 389-395.

Çengel, Y. A. & Boles, M. A., 1994. *Thermodynamics: An Engineering Approach.* New York City: McGraw-Hill.

Chakraborty, S., Aggarwal, V., Mukherjee, D. & Andras, K., 2012. Biomass to biofuel: a review on production technology. *Asia-Pacific Journal of Chemical Engineering,* 7(s3), pp. s254-s262.

Chang, Y. C., 1979. Estimating heat of combustion for waste material. *Pollution Engineering,* p. 29.

Channiwala, S. A. & Parikh, P. P., 2002. A unified correlation for estimating HHV of solid, liquid and gaseous fuels. *Fuel,* Volume 81, pp. 1051-1063.

Chiaramonti, D. et al., 2003. Development of emulsions from biomass pyrolysis liquid and diesel and their use in engines - part 1: emulsion production. *Biomass and Bioenergy,* 25(1), pp. 85-99.

Chisti, Y., 2007. Biodiesel from microalgae. *Biotechnology Advances,* 25(2007), pp. 294-306.

Cizdziel, J. & Chen, W.-Y., 2010. GC/MS for Combustion and Pyrolysis Research. In: M. Lackner, F. Winter & A. Agarwai, eds. *Handbook of Combustion.* s.l.:s.n., pp. 51-74.

Collard, F.-X. & Blin, J., 2014. A review on pyrolysis of biomass constituents: Mechanisms and composition of the products obtained from the conversion of cellulose, hemicellulose and lignin. *Renewable and Sustainable Energy Reviews,* 38(2014), pp. 594-608.

Constable, D., Curzons, A. & Cunningham, V., 2002. Metrics to 'green' chemistry - which are the best?. *The Royal Society of Chemistry,* 4(2002), pp. 521-527.

Czernik, S. & Bridgwater, A., 2007. Overview of applications of biomass fast pyrolysis oil. *Energy Fuels,* 18(2), pp. 590-598.

Dayton, D. C., 2017. *Catalytic deoxygenation of biomass pyrolysis vapours to improve bio-oil stability,* Research Triangle Park: RTI International.

de Jong, W., 2014. Biomass Composition, Properties, and Characterization. In: *Biomass as a Sustainable Energy Source for the Future.* s.l.:American Institute of Chemical Engineers, Inc..

de Soete, G. G., 1975. *Overall reaction rates of NO and N2 from fuel nitrogen.* s.l., Symposium (International) on Combustion, pp. 1093-1102.

Demirbas, A., 1997. Calculation of higher heating values of biomass fuels. *Fuel,* 76(5), pp. 431-434.

Demirbas, A., 2008. Relationships proximate analysis results and higher heating values of lignites. *Energy Sources,* 30(20), pp. 1876-1883.

Demirbas, A., 2008. Relationships proximate analysis results and higher heating values of lignites. *Energy Sources,* 30(20), pp. 1876-1883.

Demirbas, A., Gullu, D., Caglar, A. & Akdeniz, F., 1997. Estimation of calorific values pf fuel from lignocellulosics. *Energy Source A,* Volume 19, pp. 765-770.

D'Huart, K., 1930. Die Warme. *Chemical Abstracts,* Volume 53, pp. 313-317.

Dickerson, T. & Soria, J., 2013. Catalytic fast pyrolysis: a review. *Energies,* 6(1), pp. 514-538.

Diebold, J. P. & Czernik, S., 1997. Additives to lower and stabalize the viscosity of pyrolysis oils during storgae. *Energy & Fuels,* 11(5), pp. 1081-1091.

Directorate: Mineral Economics, 2005. *Operating and developing coal mines in the Republic of South Africa,* Pretoria: Department of Minerals and Energy.

Domalski, E. S., 1972. Selected values of heats of combustion and heats of formation of organic compounds containing the elements C, H, N, O, P, And S. *Journal of Physical and Chemical Reference Data,* 1(2), pp. 221-277.

Doornbosch, R. & Steenblik, R., 2007. *Biofuels: is the cure worse than the disease?,* Paris, France: OECD Round Table on Sustainable Development.

Ek, M., Gellerstedt, G. & Henriksson, G., 2009. *Pulping Chemistry and Technology.* Berlin: de Gruyter.

Elliott, D., 2007. Historical developments in hydroprocessing bio-oils. *Energy Fuels,* 21(3), pp. 1792-1815.

Evans, J. & Turnbull, J., 2004. *Plantation forestry in the tropics, the role silviculture and use of planted forests for industrial, social, environmental and agroforestry purposes.* 3rd ed. Cape Town, South Africa: Oxford University Press.

Field, C., Campbell, J. & Lobell, D., 2007. Biomass energy: the scale of the potential resource. *Trends in Ecology and Evolution,* 23(2), pp. 65-72.

Garcia, R., Pizarro, C., Lavin, A. G. & Bueno, J. L., 2014. Spanish biofuels heating value estimation. Part I: Ultimate analysis data. *Fuel,* 117(Pt B), pp. 1130-1138.

Giebelhaus, A. W., 2004. History of Oil Industry. In: C. J. Cleveland, ed. *Encyclopedia of Energy.* Boston: Elsivier Science, pp. 649-660.

Grabolski, M. S., McCormick, R. L., Alleman, T. L. & Herring, A. M., 2003. *The effect of biodiesel compositionon engine emissions from a DDC series 60 diesel engine,* Golden: s.n.

Grabosky, M. & Bain, R., 1981. *Properties of biomass relevant to gasification.* New Jersey, Noyes Data Corporation, pp. 41-69.

Grummel, E. S. & Davis, I. A., 1933. *Fuel,* Volume 12, pp. 199-203.

Grummel, E. S. & Davis, I. A., 1933. *Colliery Guardian,* Volume 146, pp. 1154-1155.

Gumz, W., 1938. *Feuerungstech,* Volume 26, pp. 322-323.

Hang, P. & Brindley, G., 1970. Methylene blue absorption by clay minerals. Determination of surface areas and cation exchange capacities (clay organic studies xviii). *Clays and Clay Minerals,* 18(1970), pp. 203-212.

Harrison, D., Higgins, I. & Watkinson, R., 1980. *Hydrocarbons in biotechnology: proceedings of a meeting.* s.l., Heyden.

Hassan, M. H. & Kalam, M. A., 2013. An overview of biofuel as a renewable energy source: development and challenges. *Procedia Engineering,* Volume 56, pp. 39-53.

Heidari, A. et al., 2014. Effect of process conditions on product yield and composition of fast pyrolysis of Eucalyptus grandis in fluidized bed reactor. *Journal of Industrial and Engineering Chemistry,* 20(4), pp. 2594-2602.

IGT, 1978. *Coal Conversion Systems Technical Data Book, DOE Contract EX 76-C-01-2286.* Springfield: VA: NTIS.

Ikura, M., 2003. Emulsification of pyrolysis derived bio-oil in diesel fuel. *Biomass & Bioenergy,* 24(3), pp. 221-232.

Ingram, L. et al., 2008. Pyrolysis of wood and bark in an auger reactor: physical properties and chemical analysis of the produced bio-oils. *Energy & Fuels,* 2008(22), pp. 614-625.

Jahirul, M., Rasul, M. & Chowdhury, A. A. N., 2012. Biofuel production through biomass pyrolysis - A technical review. *Energies,* 5(12), pp. 4952-5001.

Jenkins, B. & Ebeling, J. M., 1985. *Correlation of physical and chemical properties of terrestrial biomass with conversion.* s.l., IX IGT, p. 371.

Jenkins, B. M., Baxter, L. L., Miles Jnr, T. R. & Miles, T. R., 1998. Combustion properties of biomass. *Fuel Processing Technology,* 54(1-3), pp. 17-46.

Kaipainen, T., Liski, J., Pussinen, A. & Karjalainen, T., 2004. Managing carbon sinks by changing rotation length in European forests. *Environmental Sciences & Policy,* 7(3), pp. 205-219.

Khan, M. Z. A. & Abu-Gharah, Z. H., 1991. New approach for estimating energy content of municipal solid waste. *Journal of Environmental Engineering,* 117(3), pp. 376-380.

Kim, S. et al., 2019. A complex hydride lithium superionic conductor for high-energy-density all-solid-state lithium metal batteries. *Nature Communications,* 10(1), pp. 1-9.

Klass, D., 1998. *Biomass for renewable energy, fuels, and chemicals.* Amsterdam, Netherlands: Academic Press.

Krutof, A. & Hawboldt, K., 2016. Blends of pyrolysis oil, petroleum, and other bio-based fuels: A review. *Renewable and Sustainable Energy Reviews,* 59(2016), pp. 406-419.

Lackner, M., 2011. Combustion. In: *Ullmann's Encyclopedia of Industrial Chemistry.* New York: John Wiley & Sons.

Lapkin, A. & Constable, D. eds., 2008. In: *Green Chemistry Metrics: Measuring and Monitoring Sustainable Processes.* New York: Wiley.

Lin, B.-F., Huang, J.-H. & Huang, D.-Y., 2009. Experimental study of the effects of vegetable oil methyl ester on DI diesel engine performance characteristics and pollutant emissions. *Fuel,* 88(9), pp. 1779-1785.

Liou, K. N., 2002. Chemical Composition. In: *Introduction to Atmospheric Radiation; 2nd Edition.* s.l.:Elsivier.

Liska, A. & Cassman, K., 2008. Towards standardization of life-cycle metrics for biofuels: greenhouse gas emissions mitigation and net energy yield. *Journal of Biobased Materials and Bioenergy,* 2(3), pp. 187-203.

Liu, C. et al., 2014. Catalytic fast pyrolysis of lignocellulosic biomass. *Chemical Society Reviews,* 43(22), pp. 7594-7623.

Li, X. et al., 2011. Simultaneous catalytic esterification of carboxylic acids and acetisation of aldehydes in a fast pyrolysis bio-oil from mallee biomass. *Fuel,* 90(7), pp. 2530-2537.

Li, X. et al., 2012. Catalytic fast pyrolysis of Kraft lignin with HSM-5 zeolite for producing aromatic hydrocarbons. *Frontiers of Environmental Science & Engineering,* 6(3), pp. 295-303.

Louw, J., Schwarz, C. & Burger, A., 2016. Supercritical water gasification of Eucalyptus grandis and related pyrolysis char: Effect of feedstock composition. *Bioresource Technology,* 216(2016), pp. 1030-1039.

Lu, Q. et al., 2011. Influence of pyrolysis temperature and time on the cellulose fast pyrolysis products: Analytical py-GC/MC study. *Journal of Analytical and Applied Pyrolysis,* 92(2), pp. 430-438.

Lu, Q., Zhang, J. & Zhu, X., 2008. Corrosion properties of bio-oil and its emulsions with diesel. *Chinese Science Bulletin,* 53(23), pp. 3726-3734.

Lu, Q., Zhang, Z.-F., Dong, C.-Q. & Zhu, X.-F., 2010. Catalytic upgrading of biomass fast pyrolysis vapors with nano metal oxides: an analytical py-GC/MS study. *Energies,* 3(11), pp. 1805-1820.

Lu, Q. et al., 2013. Catalytic fast pyrolysis of biomass impregnated with K3PO4 to produce phenolic compounds: Analytical py-GC/MS study. *Journal of Analytical and Applied Pyrolysis,* 104(2013), pp. 139-145.

Makarieva, A. M. & Gorshkov, V. G., 2010. The biotic pump: condensation, atmospheric dynamics and climate. *International Journal of Water,* 59(4), pp. 365-385.

May, P. M. et al., 2018. Goodbye to S2- in aqueous solution. *Chemical Communications,* 54(16), pp. 1980-1983.

McElrone, A. J., Choat, B., Gambetta, G. A. & Broderson, C. R., 2013. Water uptake and transport in vascular plants. *Nature Education Knowledge,* 4(5), p. 6.

Meier, R. D. & Pereira, F. H., 1999. Determination of tree to tree variation in syringyl/guaiacyl ratio of Eucalyptus globulus wood lignin by analytical pyrolysis. *Journal of Analytical and Applied Pyrolysis,* 48(1999), pp. 121-128.

Miller, B. G., 2004. *Coal Energy Systems (Sustainable World).* 1st ed. Cambridge: Academic Press.

Mohan, D., Pittman, C. & Steele, P., 2006. Pyrolysis of wood/biomass for bio-oil: a critical review. *Energy Fuels,* 20(3), pp. 848-889.

Montoya, J. et al., 2015. Bio-oil production from Columbian bagasse by fast pyrolysis in a fluidized bed: An experimental study. *Journal of Analytical and Applied Pyrolysis,* 112(2015), pp. 379-387.

Moran, S., Dhafr, N. & Ahmad, M., 2017. Chemical Plants: Performance Measurement of Processes. In: B. Elvers, ed. *Ullmann's Encyclopedia of Industrial Chemistry.* Weinheim: Wiley-VCH Verlag GmbH & Co. KGaA, pp. 1-18.

Mortensen, P. et al., 2011. A review of catalytic upgrading of bio-oil to engine fuels. *Applied Catalysis A: General,* 407(1-2), pp. 1-19.

Mott, R. A. & Spooner, C. E., 1940. The calorific value of carbon in coal: the Dulong relationship. *Fuel,* 19(10-11), pp. 226-251.

Mullen, C. A. et al., 2010. Bio-oil and bio-char production from corn cobs and stover by fast pyrolysis. *Biomass and Bioenergy,* 34(1), pp. 67-74.

Mullen, C. A. et al., 2009. Analysis and comparison of bio-oil produced by fast pyrolysis from three barley biomass/byproduct streams. *Energy & Fuels,* 24(1), pp. 699-706.

Mullen, C. & Boateng, A., 2008. Chemical composition of bio-oils produced by fast pyrolysis of two energy crops. *Energy & Fuels,* 22(3), pp. 2104-2109.

Mullen, C. & Boateng, A., 2010. Catalytic pyrolysis-GC/MS of lignin from several sources. *Fuel Processing Technology,* 91(11), pp. 1446-1458.

Musinguzi, W., Okure, M., Wang, L. & Sebbit, A., 2012. Thermal characterization of Uganda's Acacia hockii, Combretum molle, Eucalyptus grandis and Terminalia glaucescens for gasification. *Biomass and Bioenergy,* 46(2012), pp. 402-408.

Myburg, A. et al., 2014. Sequencing of the Eucalyptus genome. *Nature,* 510(7505), pp. 356-362.

Naqvi, S. R. et al., 2015. The role of zeolite structure and acidity in catalytic deoxygenation of biomass pyrolysis vapours. *Energy Procedia,* 75(2015), pp. 793-800.

Niessen, W. R., 2010. *Combustion and Incineration Processes: Applications in Environmental Engineering.* 4th ed. Boca Raton: CSC Press.

NIST, n.d. *the NIST WebBook.* [Online]
Available at: https://webbook.nist.gov/cgi/cbook.cgi?ID=C7440440&Type=JANAFG&Plot=on
[Accessed 30 December 2018].

Oasmaa, A. & Czernik, S., 1999. Fuel oil quality of biomass pyrolysis oils-state of the art for the end users. *Energy & Fuels,* 13(1999), pp. 914-921.

Oasmaa, A., Elliott, D. C. & Korhonen, J., 2010. Acidity of biomass fast pyrolysis bio-oils. *Energy & Fuels,* Volume 24, pp. 6548-6554.

Oasmaa, A., Kuoppala, E. S. J.-F., Gust, S. & Solantausta, Y., 2004. Fast Pyrolysis of forestry residue and pine. 4. Improvement of the product quality by solvent addition. *Energy & Fuels,* 18(5), pp. 1578-1583.

Oasmaa, A., Kuoppala, E. & Solantausta, Y., 2003. Fast pyrolysis of forestry residue. 2. Physiochemical composition of product liquid. *Energy & Fuels,* 17(2), pp. 433-443.

Ohra-Aho, T. & Linnekoski, J., 2015. Catalytic pyrolysis of lignin by using analytical pyrolysis-GC-MS. *Journal of Analytical and Applied Pyrolysis,* 113(2015), pp. 186-192.

Panwar, N., Pawar, A. & Salvi, B., 2019. Comprehensive review on production and utilization of biochar. *SN Applied Sciences,* 1(2), pp. 1-19.

Park, H. J. et al., 2011. Catalytic vapor cracking for improvement of bio-oil. *Catalysis Surveys from Asia,* 15(3), pp. 161-180.

Patwardhan, P. R., Brown, R. C. & Shanks, B. H., 2011. Product distribution from the fast pyrolysis of hemicellulose. *ChemSusChem,* 4(5), pp. 636-643.

Pereira, B. et al., 2013. Influence of chemical composition of eucalyptus wood on gravimetric yield and charcoal properties. *BioResources,* 8(3), pp. 4574-4592.

Perry, R. H. & Green, D. W., 2007. *Perry's Chemical Engineers' Handbook.* 8th ed. New York: McGraw-Hill International Editions.

Portin, A. & Lehtonen, P., 2012. *Strategic review on the future of forest plantations,* Helsinki, Finland: Indufor Oy, for the Forest Stewardship Council.

Puértolas, B., Imtiaz, Q., Müller, C. R. & Pérez-Ramírez, J., 2016. Platform chemicals via Zeolite-catalyzed fast pyrolysis of glucose. *ChemCatChem,* 9(9), pp. 1579-1582.

Puig-Arnavat, M. et al., 2019. Pyrolysis and gasification of lignocellulosic biomass. In: J. Bastidas-Oyanedel & J. Schmidt, eds. *Biorefinery.* New York City: Springer, Cham, pp. 79-110.

Rahman, M. M., Liu, R. & Cai, J., 2018. Catalytic fast pyrolysis of biomass over zeolites for high quality bio-oil - A review. *Fuel Processing Technology,* 180(2018), pp. 32-46.

Reed, R., 2014. 19 Liquid Fossil Fuels from Petroleum. In: M. Kutz, ed. *Mechanical Engineers' Handbook.* Hoboken: Wiley & Sons Inc., pp. 1-19.

Schmidt-Rohr, K., 2015. Why combustions are always exothermic, yielding about 418 kJ per mole O2. *Journal of Chemical Education,* 92(12), pp. 2094-2099.

Schmitt, N. et al., 2019. Thermo-chemical conversion of biomass and upgrading to biofuel: the thermo-catalytic reforming process - A review. *Biofuels, Bioproducts & Biorefining,* 13(2019), pp. 822-837.

Schobert, H., 2013. *Chemistry of Fossil Fuels and Biofuels.* Cambridge: Cambridge University Press.

Scholze, B., 2002. *Long-term stability, catalytic upgrading, and application of pyrolysis oils - Improving the properties of a potential substitute for fossil fuels.* Hamburg: s.n.

Schuster, F., 1934. *Brennstoff-Chemie,* Volume 25, pp. 45-46.

Serrano-Ruiz, J. & Dumesic, J., 2012. Catalytic Production of Liquid Hydrocarbon Transportation Fuels. In: L. Guczi & Erdőhelyi, eds. *Catalysis fro Alternative Energy Generation.* New York: Springer Science+Business Media, pp. 29-56.

Seyler, C. A., 1938. *Petrology and the classification of coal: Parts I and II.* s.l., Proceedings of the South Wales Institute of Engineers, pp. 254-327.

Sharifzadeh, M. et al., 2019. The multi-scale challenges of biomass fast pyrolysis and bio-oil upgradinh: review of the state of the art and future research directions. *Progress in Energy and Combustion Sciences,* 71(2019), pp. 1-80.

Shortall, O. & Millar, K., 2012. The ethics of using agricultural land to produce biomass: using energy like it grows on trees. In: T. Potthast & S. Meisch, eds. *Climate Change and Sustainable Development: Ethical Perspective on Land Use and Food Production.* Wageningen, Netherlands: Wageningen Academic Publishers.

Si, Z. et al., 2017. An overview on catalytic hydrodeoxygenation of pyrolysis oil and its model compounds. *Catalysts,* 7(6), pp. 169-191.

Sparkman, O., Penton, Z. & Kitson, F., 2011. *Introduction and History.* Cambridge, MA: Academic Press.

Steuer, W., 1926. *Brennstoff-Chemie,* Volume 7, pp. 344-347.

Stoikos, T., 1991. Upgrading of Biomass Pyrolysis Liquids to High-Value Chemicals and Fuel Additives. In: A. Bridgwater & G. Grassi, eds. *Biomass Pyrolysis Liquids Upgrading and Utilization.* Berlin: Springer, Dordrecht, pp. 227-241.

Strache, H. & Lant, R., 1924. *Kohlenchemie.* Leipzig: Akademische Verlagsgesellschaft.

Sumegi, L., 1939. *Magyar Mernok Epiteszegylet Kozlonye,* Volume 73, pp. 345-346.

Theodore, L., Ricci, F. & van Vilet, T., 2009. Thermodynamics for the Practicing Engineer. In: *Fuel Options.* Hoboken: Wiley & Sons Inc., pp. 365-375.

Tillman, D. A., 1978. *Wood as an Energy Resource.* 1st ed. Cambridge: Academic Press.

Ugalde, L. & Pérez, O., 2001. *Mean annual volume increments of selected industrial forest plantation species,* Rome, Italy: Food and Agricultural Organisation of the United Nations.

Uzun, B. & Pütün, E., 2006. Composition of products obtained via fast pyrolysis temperature. *Journal of Analytical and Applied Pyrolysis,* 79(1-2), pp. 147-153.

van Eck, N. & Waltman, L., 2019. *CitNetExplorer.* [Online]
Available at: https://www.citnetexplorer.nl/
[Accessed June 2019].

van Eck, N. & Waltman, L., 2019. *VOSviewer.* [Online]
Available at: https://www.vosviewer.com
[Accessed June 2019].

Venderbosch, R., 2015. A critical view on catalytic pyrolysis of biomass. *ChemSusChem,* 8(8), pp. 1306-1316.

Vondracek, R., 1934. *Brennstoff-Chemie,* Volume 8, pp. 22-23.

Wasiak, A. & Orynycz, O., 2017. Energy Efficiency of a biofuel production system. *Management and Production Engineering Review,* 8(1), pp. 60-68.

Whitmarsh, J. G. & Govindjee, 1999. Chapter 2: The Basic Photosynthetic Process. In: G. Singhal, et al. eds. *Concepts in Photobiology: Photosynthesis and Photomorphogenesis.* Boston: Kluwer Academic Publishers, p. 13.

Wildschut, J., Melián-Cabrera, I. & Heeres, H., 2010. Catalyst studies on the hydrotreatment of fast pyrolysis oil. *Applied Catalysis B: Environmental,* 99(1-2), pp. 298-306.

Wilson, D. L., 1972. Prediction of heat of combustion of solid wastes from ultimate analysis. *Environmental Science & Technology,* 6(13), pp. 1119-1121.

Wright, M., Brown, R. & Boateng, A., 2008. Distributed processing of biomass to bio-oil for subsequent production of Fischer-Tropsch liquids. *Biofuels, Bioproducts and Biorefining,* 2(3), pp. 229-238.

Wright, M., Daugaard, D., Satrio, J. & Brown, R., 2010. Techno-economic analysis of biomass fast pyroylsis to transportation fuels. *Fuel,* 89(2010), pp. s2-s10.

Yildiz, G., Ronsse, F. & Prins, W., 2017. Catalytic Fast Pyrolysis Over Zeolites. In: R. C. Brown & K. Wang, eds. *Fast Pyrolysis of Biomass: Advances in Science and Technology.* London: The Royal Society of Chemistry, pp. 200-230.

Yildiz, G., Ronsse, F., van Duren, R. & Prins, W., 2016. Challenges in the design and operation of processes for catalytic fast pyrolysis of woody biomass. *Sustainable Energy Reviews,* 57(2016), pp. 1596-1610.

Yuan, Y., Hansen, A. & Zhang, Q., 2004. The specific gravity of biodiesel fuels and their blends with diesel fuel. *Agricultural Engineering International: CIGR Journal,* Volume VI, pp. 1-111.

Yue, D., You, F. & Snyder, S. W., 2014. Biomass-to-bioenergy and biofuel supply chain optimization: overview, key issues and challenges. *Computers & Chemical Engineering,* Volume 66, pp. 36-56.

Zhang, B., Zhong, Z., Ding, K. & Song, Z., 2015. Production of aromatic hydrocarbons from catalytic co-pyrolysis of biomass and high density polyethylene: an analytical py-GC/MS study. *Fuel,* 139(2015), pp. 622-628.

Zhang, Q., Chang, J., Wang, T. & Xu, Y., 2007. Review of biomass pyrolysis oil properties and upgrading research. *Energy Conservation and Management,* Volume 48, pp. 87-92.

Zhang, S., Yan, Y., Li, T. & Ren, Z., 2005. Upgrading of liquid fuel from the pyrolysis of biomass. *Bioresource Technology,* 96(5), pp. 545-550.

Zheng, A. et al., 2014. Effect of crystal size ZSM-5 on the aromatic yield and selectivity from catalytic fast pyrolysis of biomass. *Journal of molecular catalysis A: Chemical,* 383-384(2014), pp. 23-30.

Zheng, J.-L., 2008. Pyrolysis oil from fast pyrolysis of maize stalk. *Journal of Analytical and Applied Pyrolysis,* 2008(83), pp. 205-212.

Zheng, J., Yi, W. & Wang, N., 2007. Bio-oil production from cotton stalk. *Energy Conversion and Management,* 49(6), pp. 1724-1730.

Zhu, X. & Venderbosch, R., 2005. A correlation between stoichiometrical ratio of fuel and its higher heating valuw. *Fuel,* Volume 81, pp. 1001-1063.

Research outputs

Publications

Type	Description	Date	Status
Paper	Grobler, ABL, Heydenrych, MD, Swart, SD, Boateng, AA, Merckel, RD 2019. Scalable fluidized bed reactor system for fast pyrolysis of woody biomass. *South African Journal of Chemical Engineering*.	2019	Submitted
Paper	Beckinghausen, A, Reynders, J, Merckel, RD, Schwede, S 2019. Comparison of biochar enhancements for ammonia ($NH_4 - N$) sorption from concentrated wastewater applications. Paper to be presented at the *11th Conference on Applied Energy*, 12–15 August, 2019, Västerås, Sweden.	2020	Submitted
Paper	Merckel, RD, Labuschagne, FJWJ, Heydenrych, MD 2020. Energy metrics of fuel juxtaposed with mass yield metrics. *Renewable Energy*.		Submitted
Paper	Merckel, RD, Heydenrych, MD, Labuschagne, FJWJ, 2019. Oxygen consumption as the definitive factor in predicting heat of combustion. *Applied Energy*, 235(2019), pp. 1041-1047.	2019	Published
Paper	Merckel, RD, Heydenrych, MD, 2017. Mass-fraction of oxygen as a predictor of HHV of gaseous, liquid and solid fuels, *Energy Procedia*, 142(2017), pp. 4124-4130.	2017	Published
Patent	Heydenrych, M, del Fabbro, O, Focke, W, Labuschagne, F, Merckel, R, 2016. Oxygenate reduction catalyst and process, *WO 2017/063004 A4*, assigned to the University of Pretoria, South Africa		Published

Publications to be submitted

Type	Description
Paper	Merckel, RD, Heydenrych, MD, Labuschagne, FJWJ, 20XX. Estimation of pyrolysis oil energy quality, composition and catalytic activity by cumulative atomic ratios using py-GC/MS, *Journal of Analytical and Applied Pyrolysis*.

Conferences

Type	Description	Date
Paper presented	IBC2019 conference, Johannesburg, South Africa	2019
Poster presented	TCS2018 symposium, Auburn, USA.	2018
Paper presented	9th ICAE2017, Cardiff, Wales.	2017
Paper presented	IFSA conference, Johannesburg, South Africa.	2017
Paper presented	TAPPSA conference, Durban, South Africa.	2016

Appendix

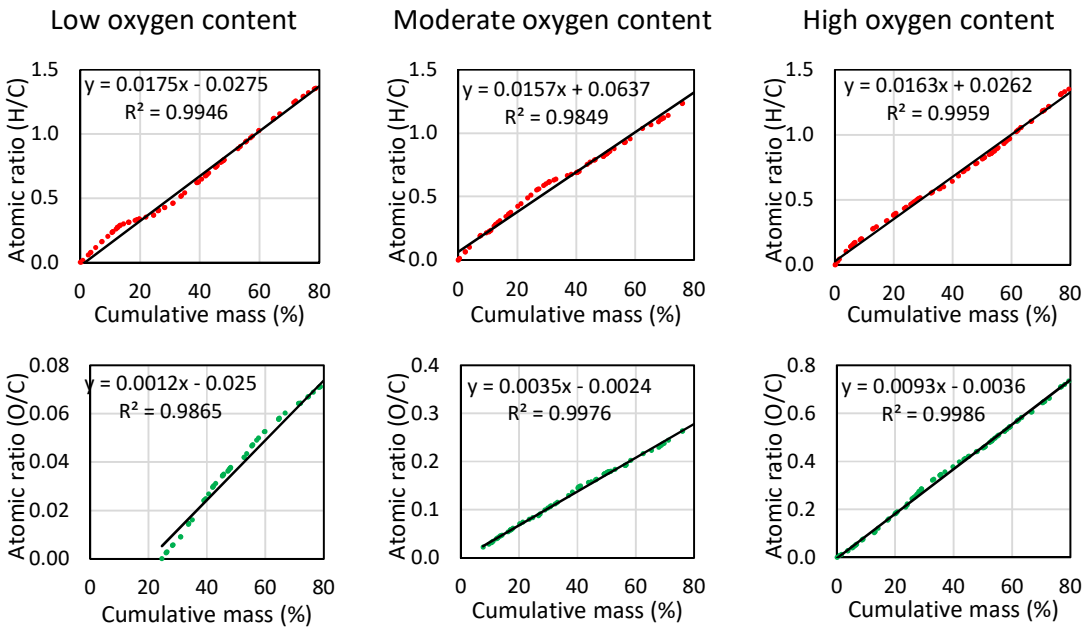

Figure A1: Plot of cumulative H/C and O/C ratio fractions against the respective cumulative mass fractions for three sets of model data for low, moderate, and high oxygen-containing compounds for 80 % of randomly selected data points foe pseudo-GC/MS data sets

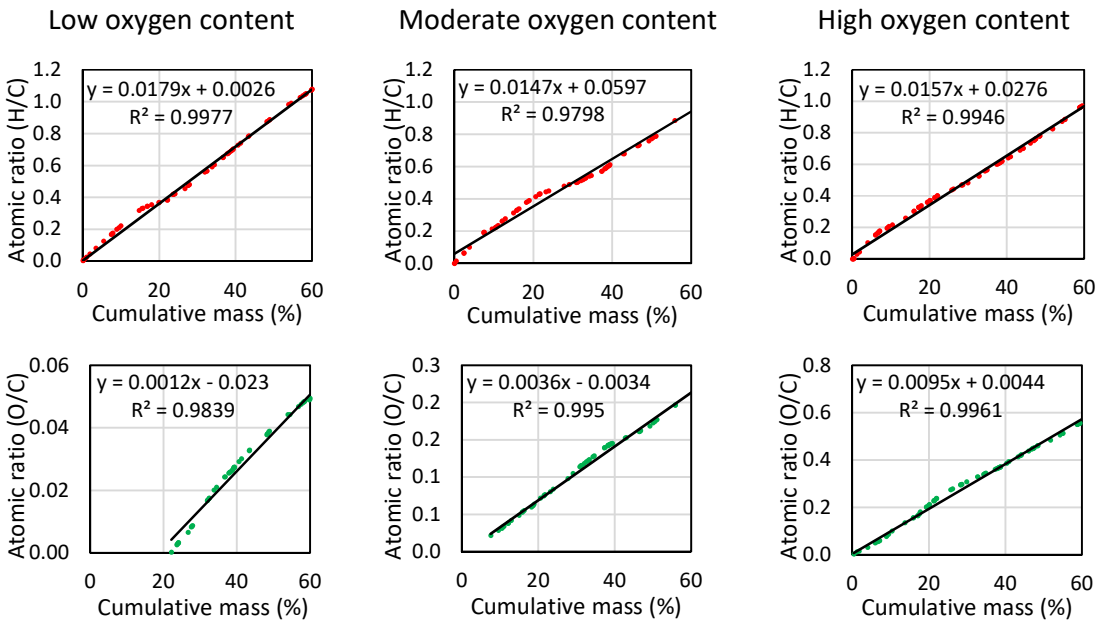

Figure A2: Plot of cumulative H/C and O/C ratio fractions against the respective cumulative mass fractions for three sets of model data for low, moderate, and high oxygen-containing compounds for 60 % of randomly selected data points foe pseudo-GC/MS data sets

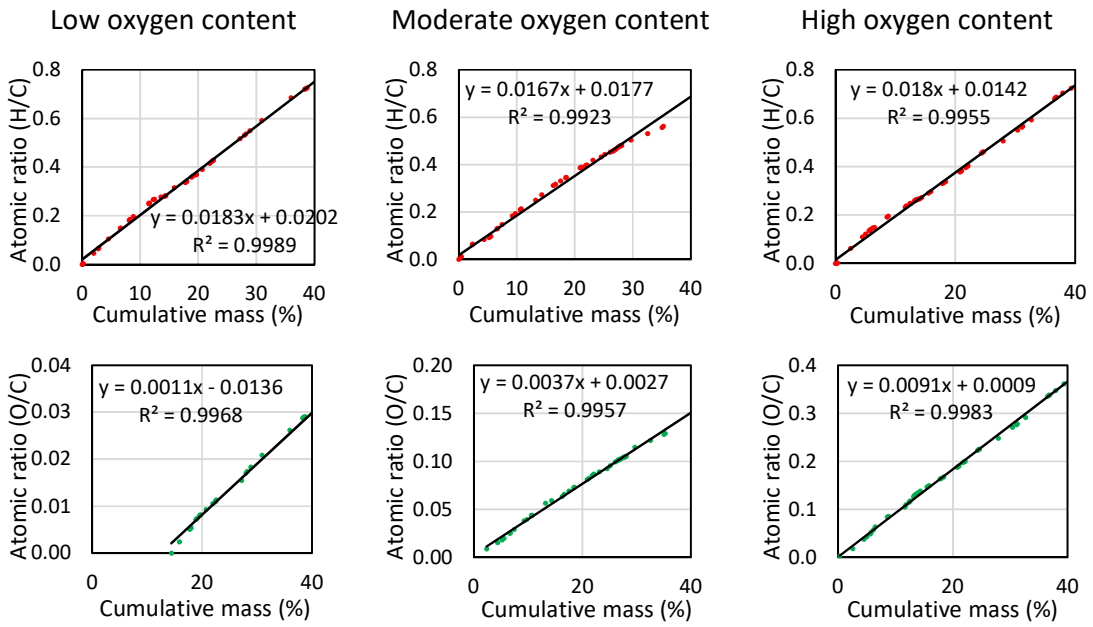

Figure A3: Plot of cumulative H/C and O/C ratio fractions against the respective cumulative mass fractions for three sets of model data for low, moderate, and high oxygen-containing compounds for 40 % of randomly selected data points foe pseudo-GC/MS data sets

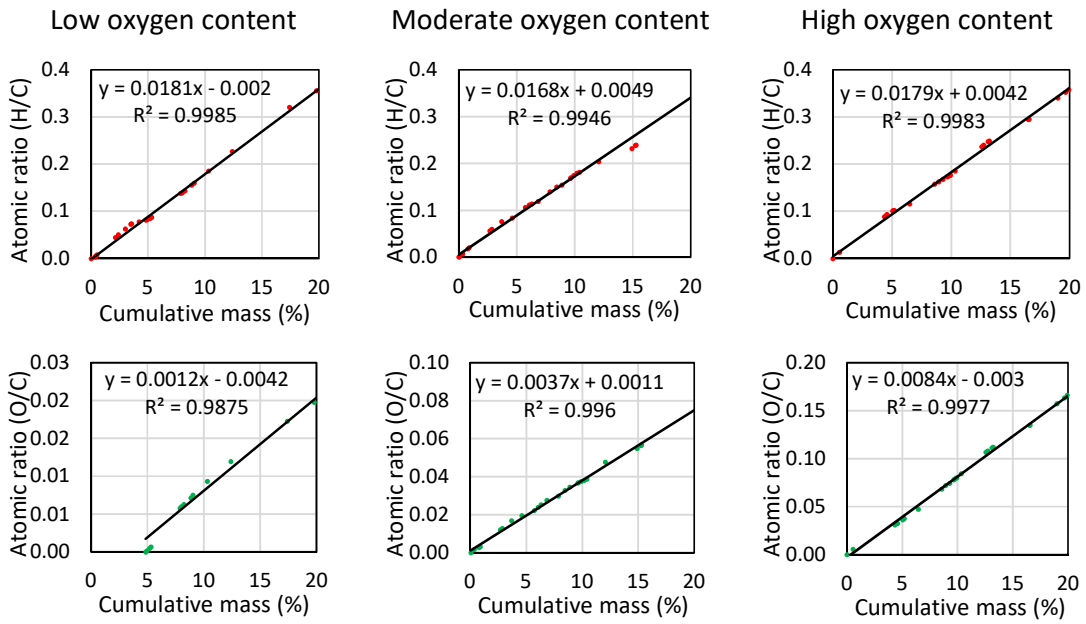

Figure A4: Plot of cumulative H/C and O/C ratio fractions against the respective cumulative mass fractions for three sets of model data for low, moderate, and high oxygen-containing compounds for 20 % of randomly selected data points foe pseudo-GC/MS data sets

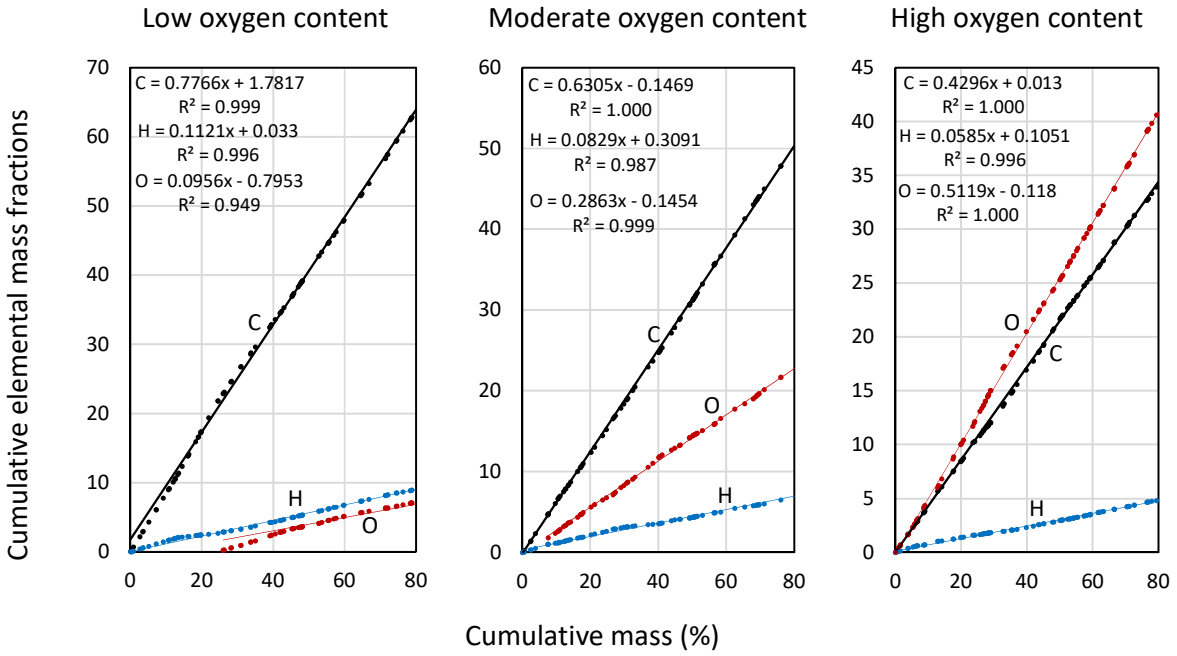

Figure A5: Plot of cumulative elemental mass fractions against the respective cumulative mass fractions for three sets of model data for low, moderate, and high oxygen-containing compounds using 80 % of the data

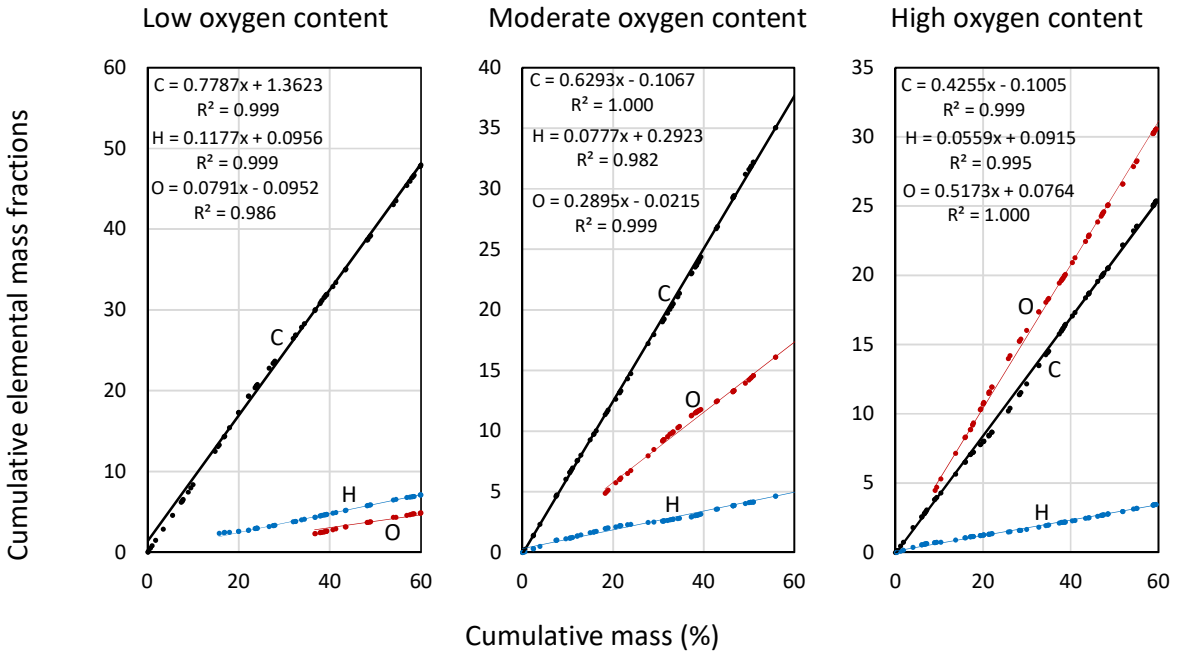

Figure A6: Plot of cumulative elemental mass fractions against the respective cumulative mass fractions for three sets of model data for low, moderate, and high oxygen-containing compounds using 60 % of the data

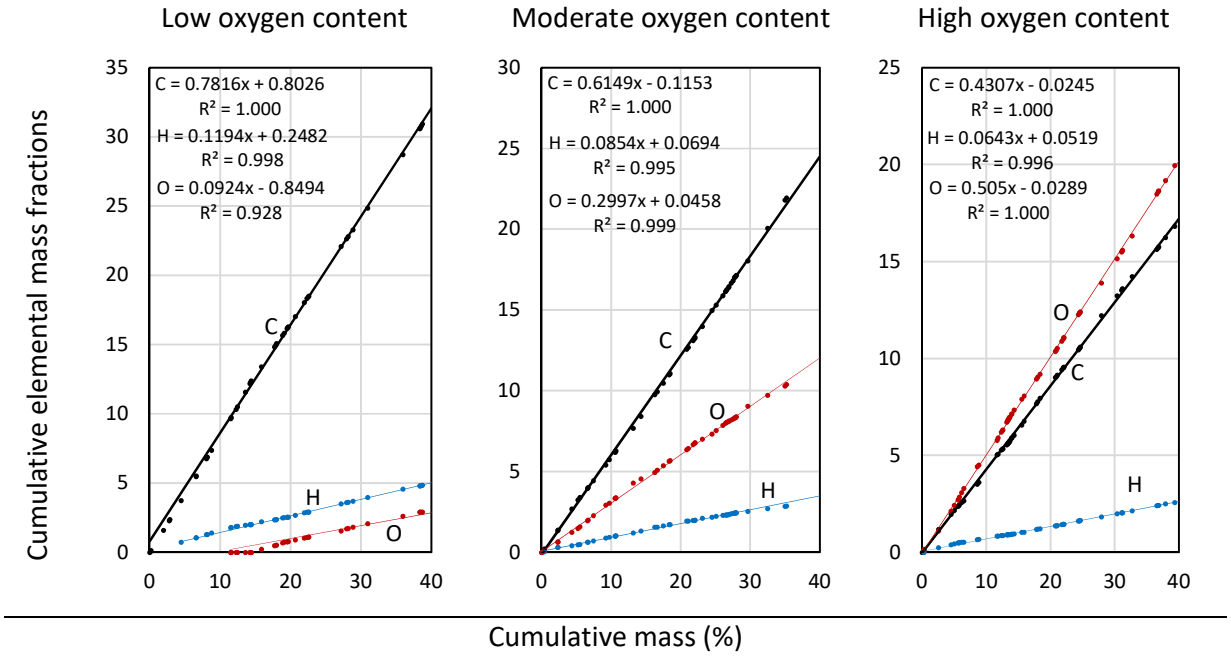

Figure A7: Plot of cumulative elemental mass fractions against the respective cumulative mass fractions for three sets of model data for low, moderate, and high oxygen-containing compounds using 40 % of the data

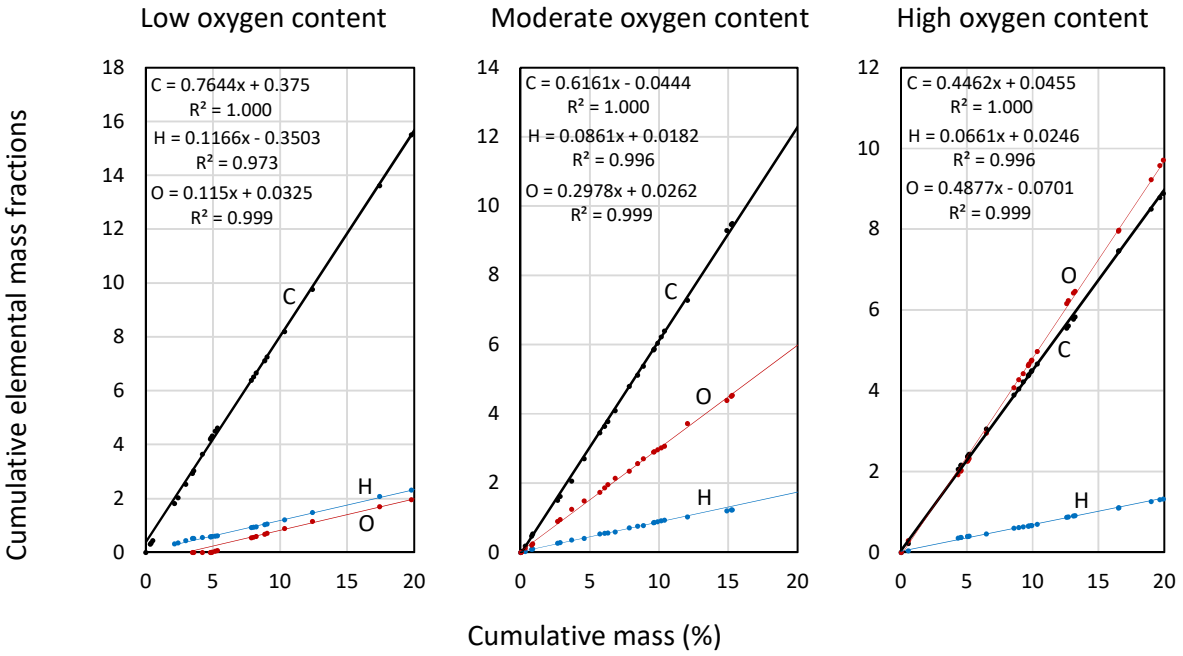

Figure A8: Plot of cumulative elemental mass fractions against the respective cumulative mass fractions for three sets of model data for low, moderate, and high oxygen-containing compounds using 20 % of the data

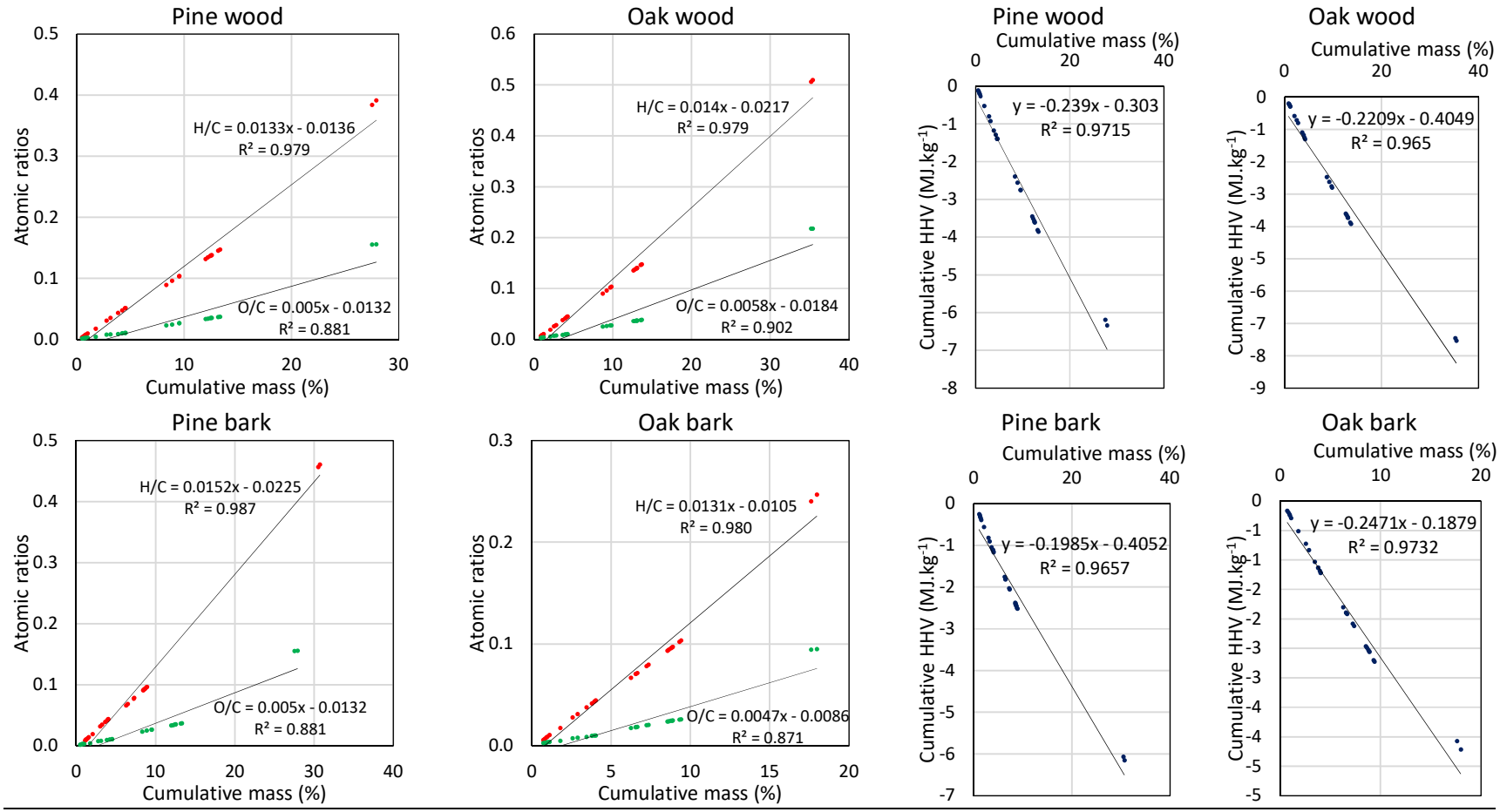

Figure A9: (Ingram, et al., 2008) Cumulative atomic ratios and higher heating values as a function of the cumulative mass percentages

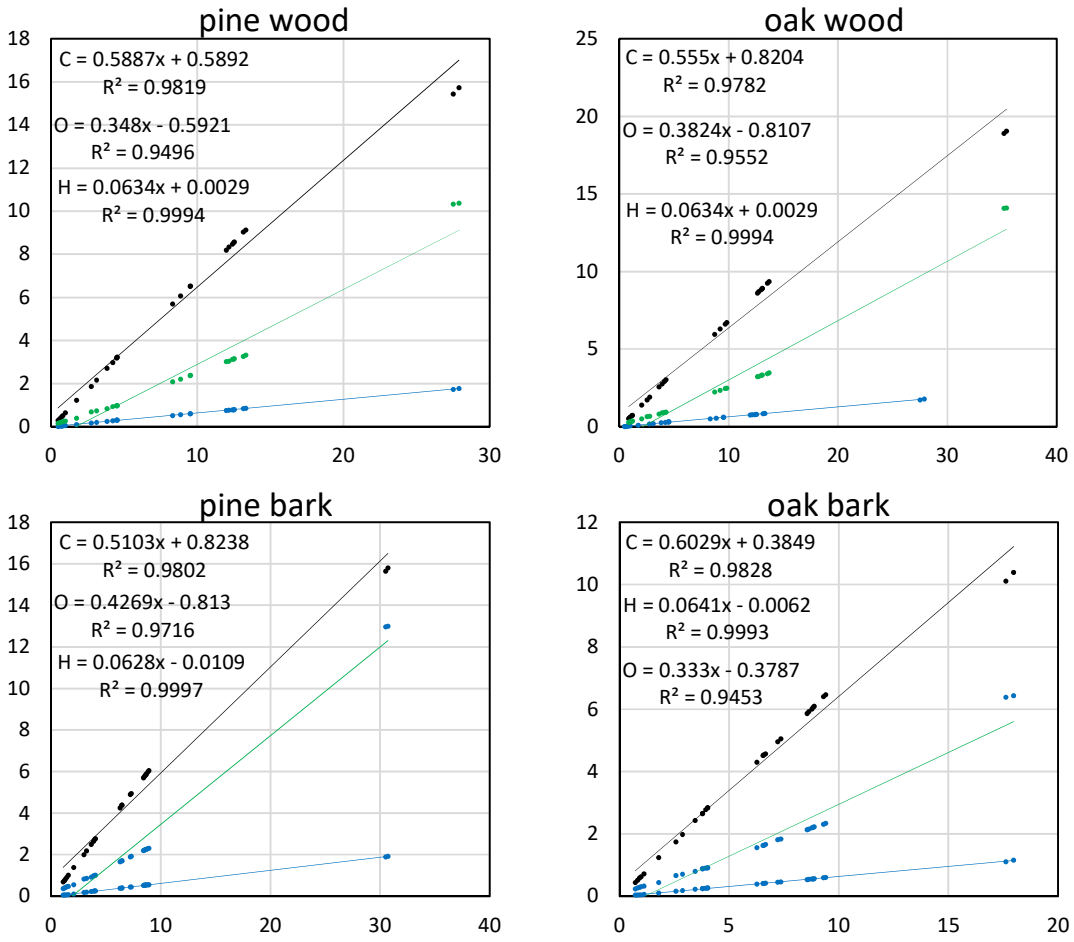

Figure A10: (Ingram, et al., 2008) Cumulative elemental masses as a function of the cumulative mass percentages

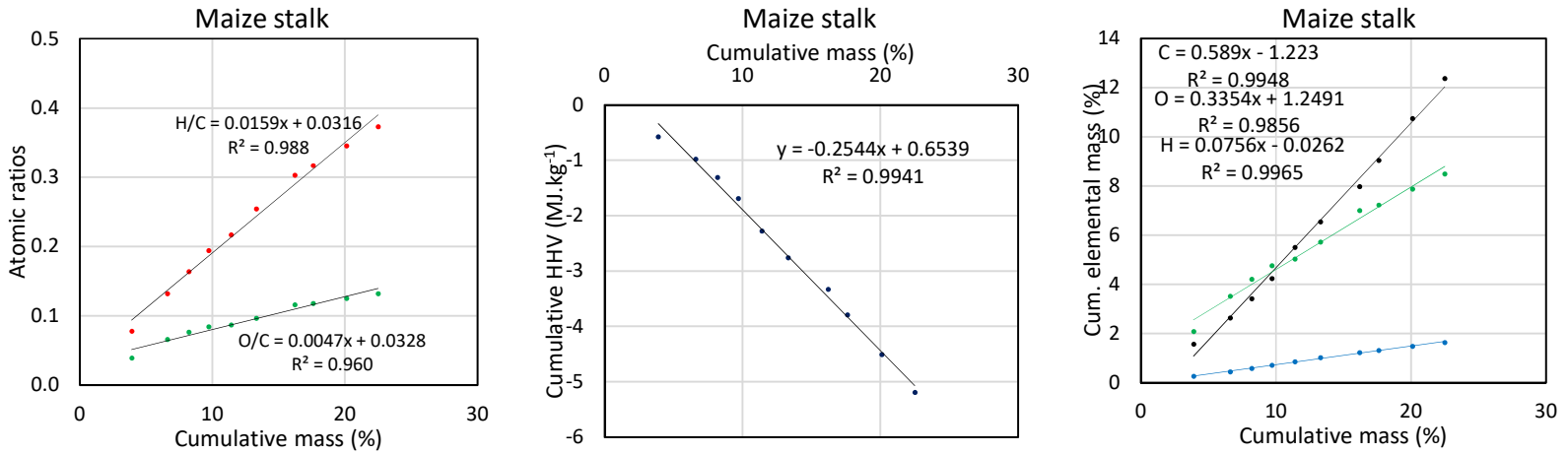

Figure A11: (Zheng, 2008) Cumulative atomic ratios and higher heating values as a function of the cumulative mass percentages

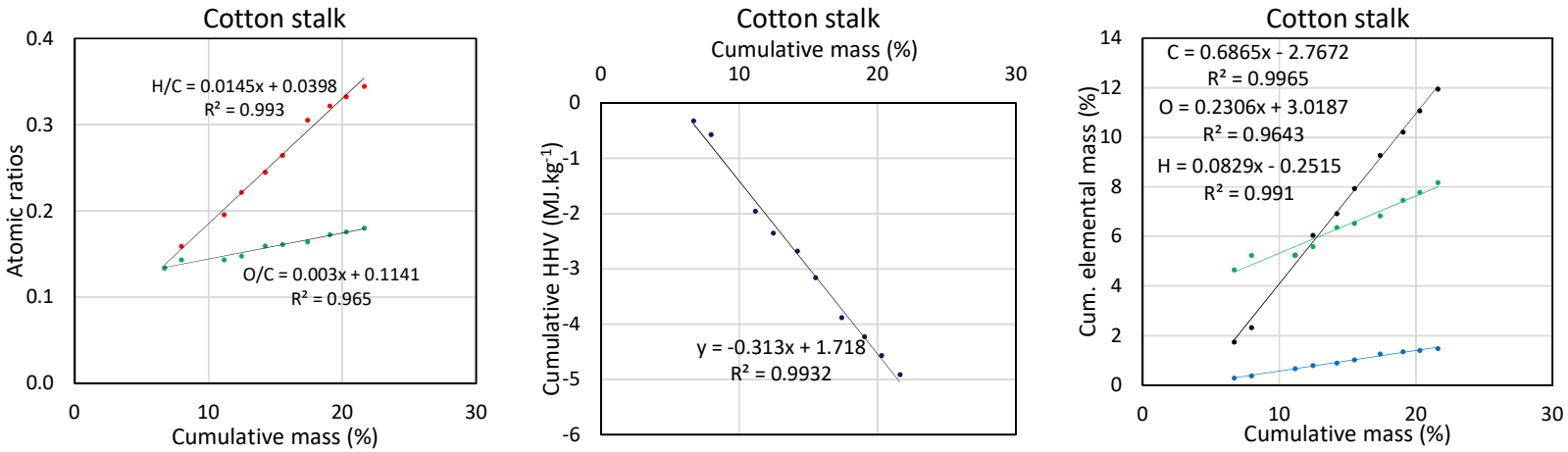

Figure A12: (Zheng, et al., 2007) Cumulative atomic ratios and higher heating values as a function of the cumulative mass percentages

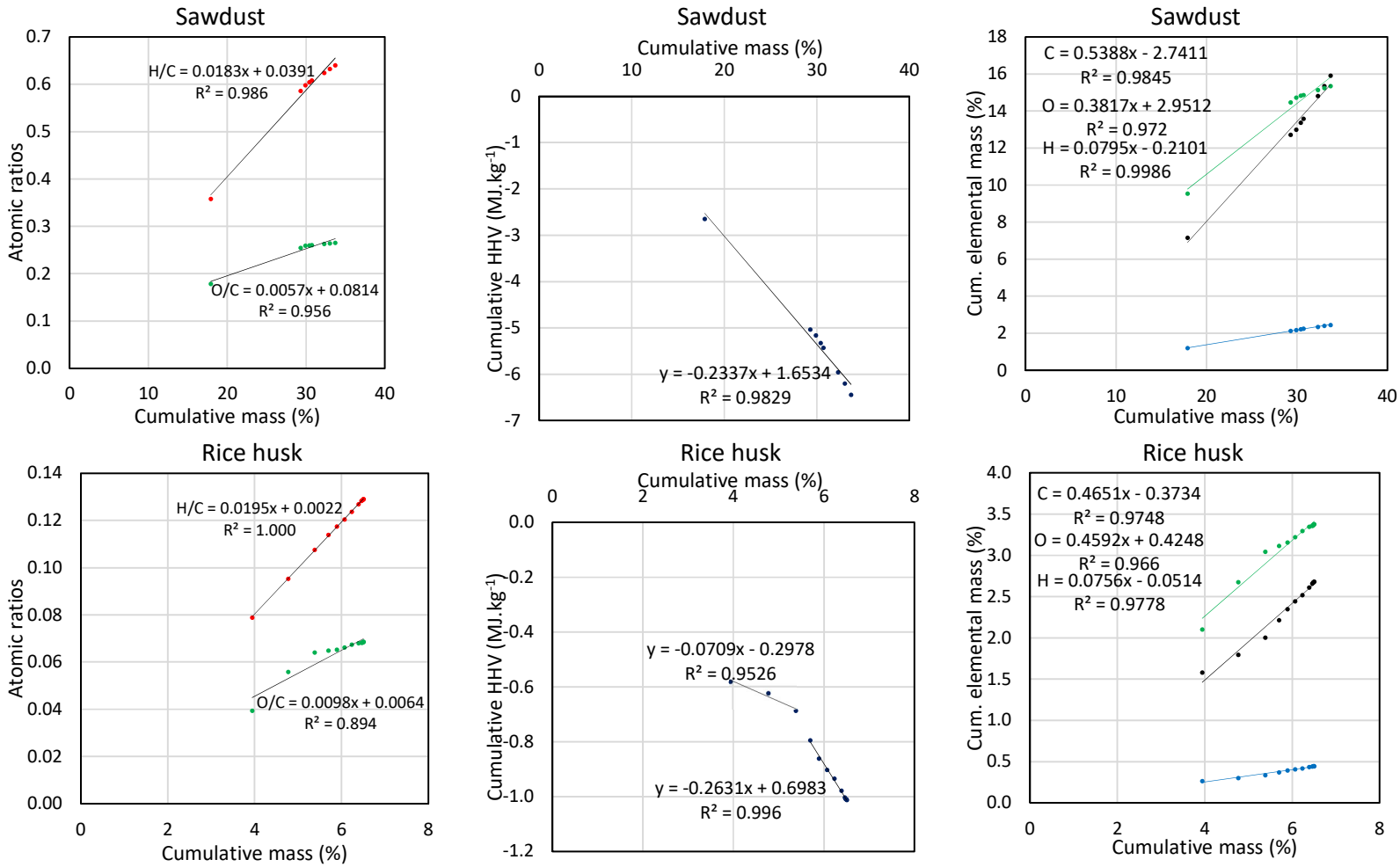

Figure A13: (Lu, et al., 2008) Cumulative atomic ratios and higher heating values as a function of the cumulative mass percentages

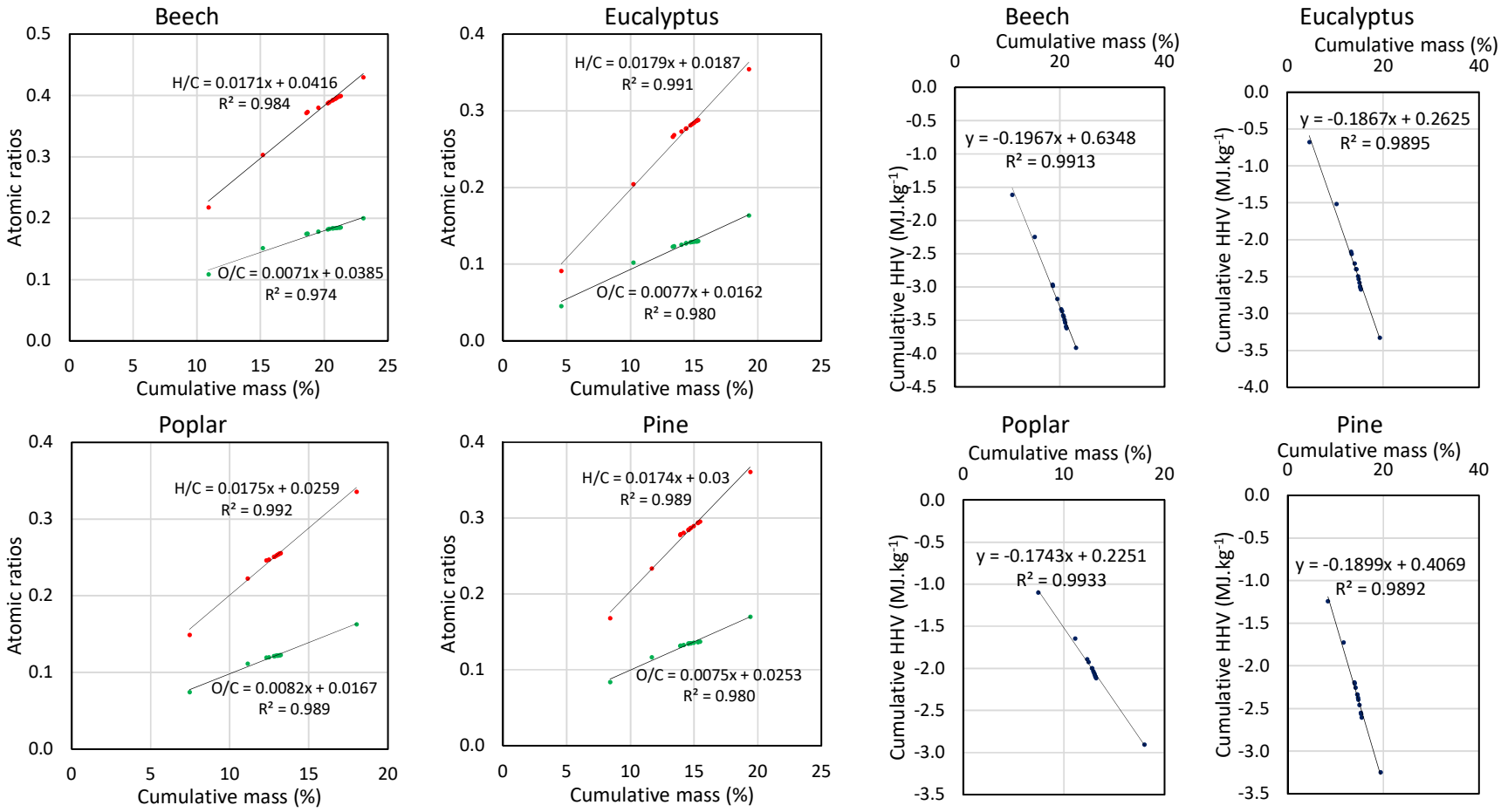

Figure A14: (Scholze, 2002) Cumulative atomic ratios and higher heating values as a function of the cumulative mass percentages

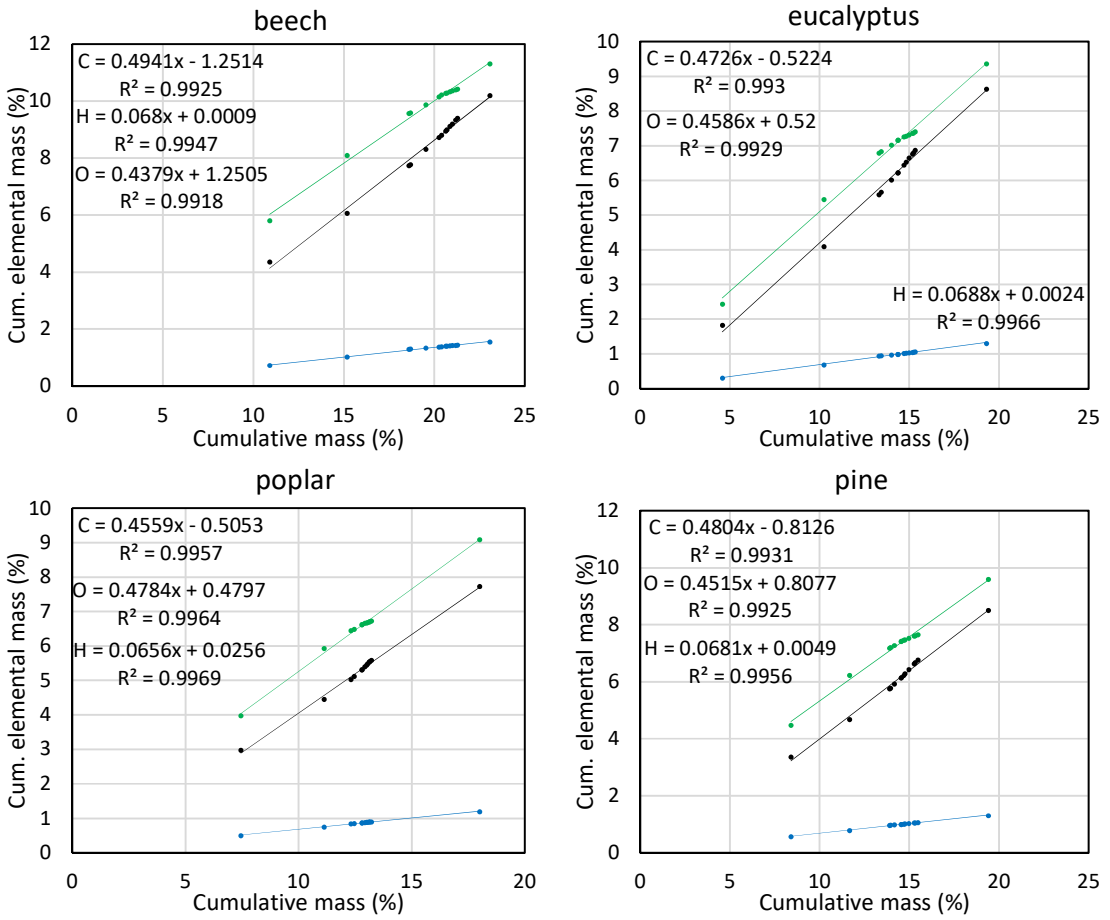

Figure A15: (Scholze, 2002) Cumulative elemental masses as a function of the cumulative mass percentages

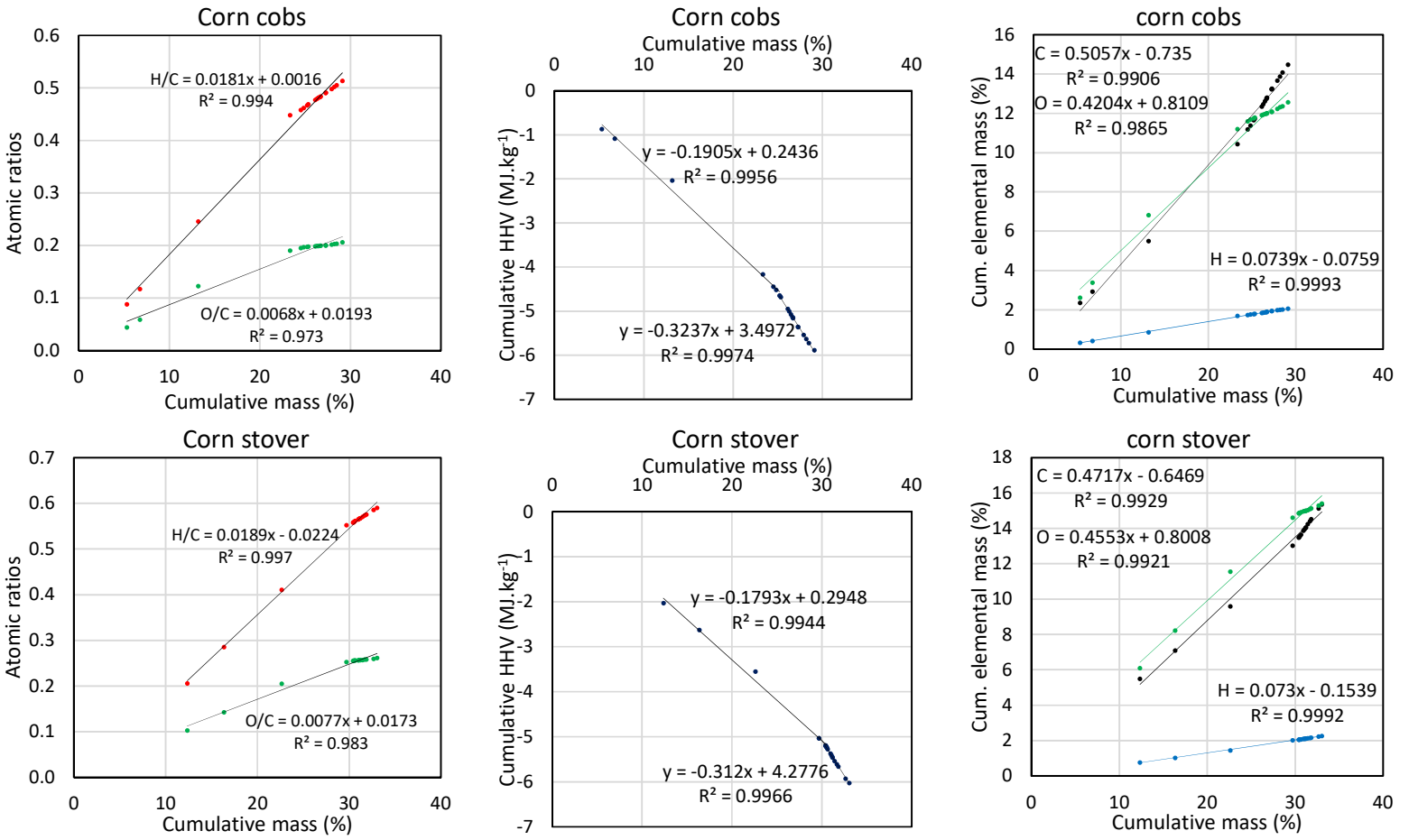

Figure A16: (Mullen, et al., 2010) Cumulative atomic ratios and higher heating values as a function of the cumulative mass percentages

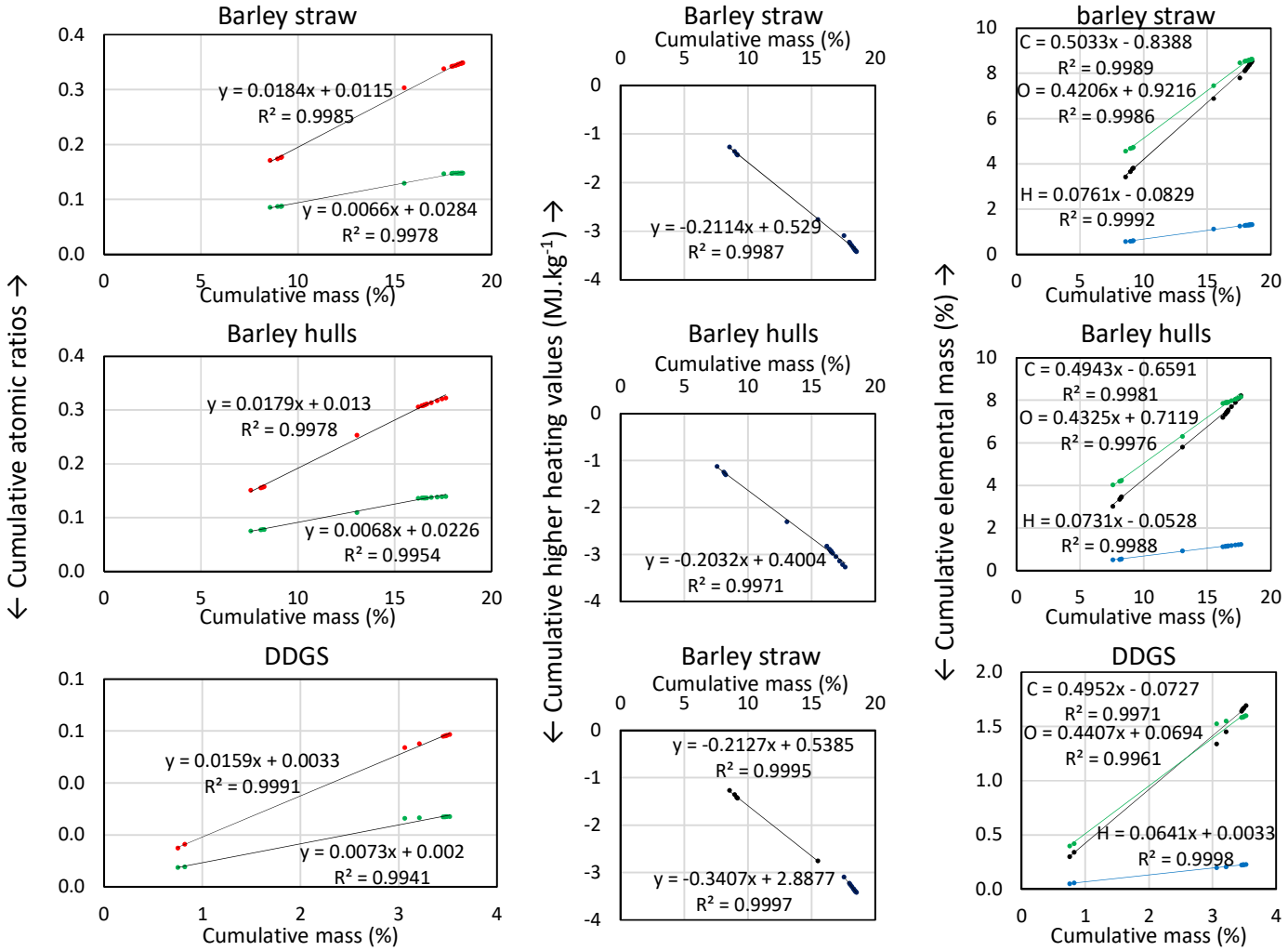

Figure A17: (Mullen, et al., 2010) Cumulative atomic ratios and HHV as a function of the cum. mass percentages

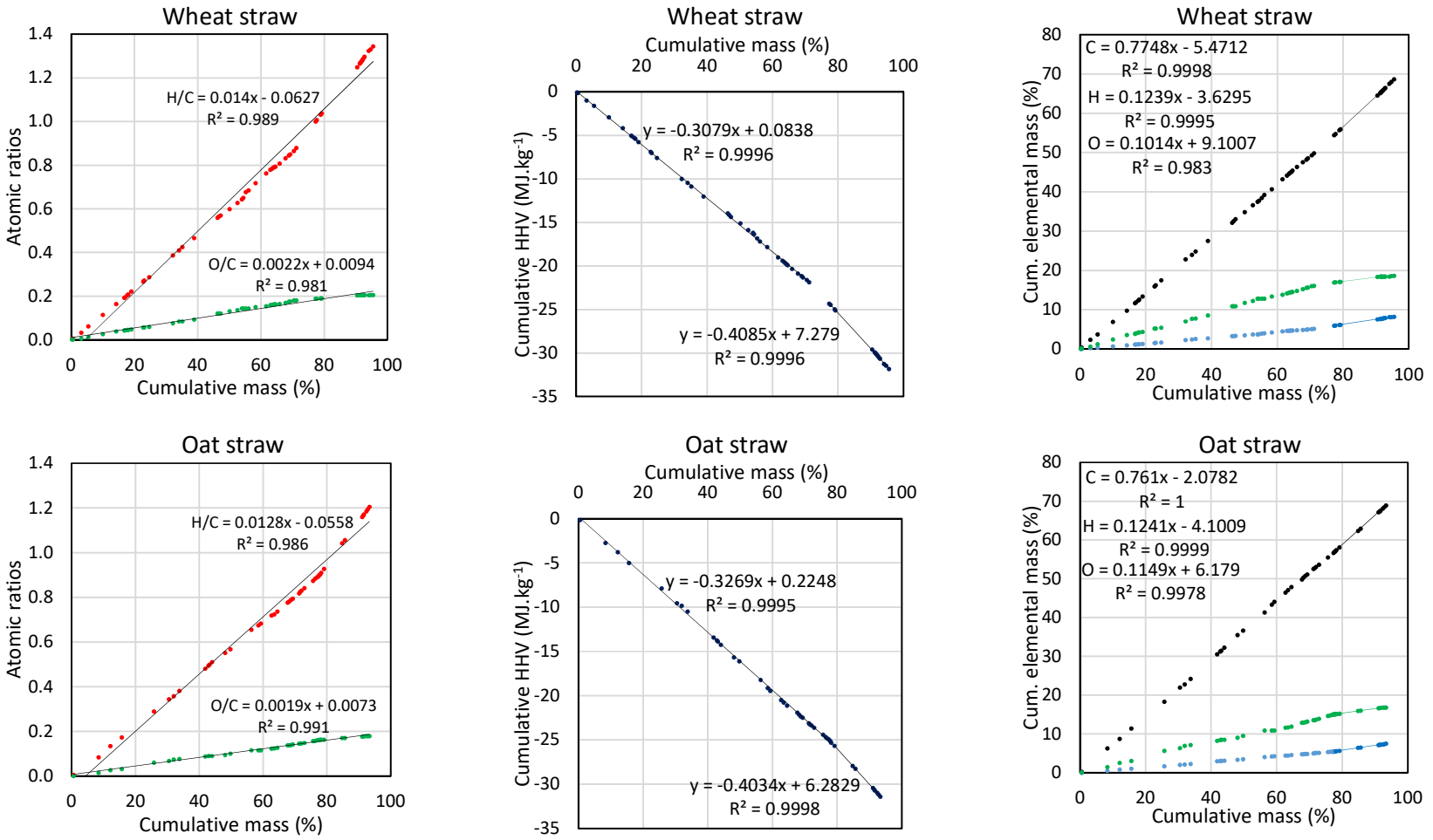

Figure A18: (Ateş & Işikdağ, 2008) Cumulative atomic ratios and higher heating values as a function of the cumulative mass percentages